uOttawa

L'Université canadienne
Canada's university

Reproduced with permission of the copyright owner. Further reproduction prohibited without permission.

FACULTÉ DES ÉTUDES SUPÉRIEURES ET POSTOCTORALES

uOttawa

L'Université canadienne
Canada's university

FACULTY OF GRADUATE AND POSDOCTORAL STUDIES

Ziyi Zhang

AUTEUR DE LA THÈSE / AUTHOR OF THESIS

Ph.D. (Physics)

GRADE / DEGREE

Department of Physics

FACULTÉ, ÉCOLE, DÉPARTEMENT / FACULTY, SCHOOL, DEPARTMENT

Polarization Effects in Optical Fiber Communication and Distributed Vibration Sensing Systems

TITRE DE LA THÈSE / TITLE OF THESIS

Xiaoyi Bao

DIRECTEUR (DIRECTRICE) DE LA THÈSE / THESIS SUPERVISOR

Liang Chen

CO-DIRECTEUR (CO-DIRECTRICE) DE LA THÈSE / THESIS CO-SUPERVISOR

EXAMINATEURS (EXAMINATRICES) DE LA THÈSE / THESIS EXAMINERS

John Armitage

Nicolas Jaeger

Andrej Czajkowski

Sylvain Raymond

Gary W. Slater

Le Doyen de la Faculté des études supérieures et postdoctorales / Dean of the Faculty of Graduate and Postdoctoral Studies

Reproduced with permission of the copyright owner. Further reproduction prohibited without permission.

Polarization Effects in Optical Fiber Communication and Distributed Vibration Sensing Systems

by

Ziyi Zhang

Thesis submitted to the
Faculty of Graduate and Postdoctoral Studies
In partial fulfillment of the requirements for the Degree of

Doctor of Philosophy

Ottawa-Carleton Institute for Physics
University of Ottawa
Ottawa, Canada

© Ziyi Zhang, Ottawa, Canada, 2009

Reproduced with permission of the copyright owner. Further reproduction prohibited without permission.

Library and Archives Canada

Published Heritage Branch

395 Wellington Street
Ottawa ON K1A 0N4
Canada

Bibliothèque et Archives Canada

Direction du Patrimoine de l'édition

395, rue Wellington
Ottawa ON K1A 0N4
Canada

Your file Votre référence
ISBN: 978-0-494-51808-3
Our file Notre référence
ISBN: 978-0-494-51808-3

NOTICE:
The author has granted a non-exclusive license allowing Library and Archives Canada to reproduce, publish, archive, preserve, conserve, communicate to the public by telecommunication or on the Internet, loan, distribute and sell theses worldwide, for commercial or non-commercial purposes, in microform, paper, electronic and/or any other formats.

The author retains copyright ownership and moral rights in this thesis. Neither the thesis nor substantial extracts from it may be printed or otherwise reproduced without the author's permission.

AVIS:
L'auteur a accordé une licence non exclusive permettant à la Bibliothèque et Archives Canada de reproduire, publier, archiver, sauvegarder, conserver, transmettre au public par télécommunication ou par l'Internet, prêter, distribuer et vendre des thèses partout dans le monde, à des fins commerciales ou autres, sur support microforme, papier, électronique et/ou autres formats.

L'auteur conserve la propriété du droit d'auteur et des droits moraux qui protège cette thèse. Ni la thèse ni des extraits substantiels de celle-ci ne doivent être imprimés ou autrement reproduits sans son autorisation.

In compliance with the Canadian Privacy Act some supporting forms may have been removed from this thesis.

While these forms may be included in the document page count, their removal does not represent any loss of content from the thesis.

Conformément à la loi canadienne sur la protection de la vie privée, quelques formulaires secondaires ont été enlevés de cette thèse.

Bien que ces formulaires aient inclus dans la pagination, il n'y aura aucun contenu manquant.

Canada

Reproduced with permission of the copyright owner. Further reproduction prohibited without permission.

To my parents and grandparents

Reproduced with permission of the copyright owner. Further reproduction prohibited without permission.

Abstract

This thesis includes studies of polarization effects in two main research areas of optical fiber technology: optical fiber communication systems and optical fiber sensors. Polarization of light in optical fiber is sensitive to environmental disturbances. On the negative side, this results in complex measurement processes and errors in communication systems caused by dynamic polarization mode dispersion (PMD) and polarization dependent loss (PDL). On the positive side though, it also results in the possibility of developing a distributed optical fiber vibration sensor.

For the purpose of fast polarization measurement for high bit-rate communication systems, a new PDL vector method was proposed based on the equation of motion in Stokes space. It is capable of providing accurate PDL measurements while requiring less measurement steps compared with other available techniques.

We had performed a PMD field test, and found the fastest PMD change in submarine fibers under the Caribbean Sea. With long measurement duration (>24h) on one pair of fiber, correlations between polarization effects and tides were reported for the first time. A histogram of the differential group delay (DGD) data and an auto-correlation function of state of polarization (SOP) and DGD were validated by theoretical fittings. The average and fastest drift time for both SOP and DGD was found to be ~3min and less than 15s, respectively.

Polarization effects were then utilized as a sensing parameter to detect and locate external disturbances along the optical fiber. A system based on polarization optical time domain reflectometry (Polarization-OTDR) technique was developed in order to pinpoint the disturbances as well as to give events' frequency information. For the first time, a fully distributed optical fiber vibration sensor has been demonstrated in a 1km fiber link with 10m spatial resolution and 5kHz maximum detectable frequency. Moreover, by our proposed spectrum analysis, multiple simultaneous events with the same frequency components can be identified.

Reproduced with permission of the copyright owner. Further reproduction prohibited without permission.

This work contains no material which has been accepted for the award of any other degree or diploma in any University or other tertiary institution and, to the best of my knowledge and belief, contains no material previously published or written by another person, except where due reference has been made in the text.

I give consent to this copy of my thesis, when deposited in the University Library, being available for loan and photocopying.

SIGNED: .....

DATE: .....

Supervisors: Dr. Xiaoyi Bao and Dr. Liang Chen

Reproduced with permission of the copyright owner. Further reproduction prohibited without permission.

Acknowledgements

I am heartily grateful to my enthusiastic supervisors Dr. Xiaoyi Bao and Dr. Liang Chen, for their guidance in my graduate study. For years, their comprehensive knowledge, invaluable experience, and insight as well as their kindness have taught and inspired me to challenge useful but difficult research topics one after another. It is under their guidance and influence I have gradually learnt how to become a scientific researcher.

Many thanks to my friends and colleagues in fiber optics group at University of Ottawa during this work. Special thanks to Dr. Qinrong Yu, Dr. Shiquan Yang, David Waddy, and Dr. Evgueni A. Ponomarev for their kind help and encouragement at the beginning of my graduate study. I would also like to thank Dr. Wenhai Li for his many valuable suggestions on developing the distributed optical fiber vibration system; and to Ryan Bolen and Jesse Leeson, for their thoughtful discussions with me and their help on proofreading my thesis.

Also I need to acknowledge the following people for their generous help in several field tests: Mr. John Stears (Caribbean Crossing), Dr. Colin D. Rennie (University of Ottawa), Dr. Andrew Cornett (NRC of Canada), Dr. Sherif El-Gamal (University of Sherbrooke) and Dr. Pingyu Zhu (Hunan University of Sci. & Tech., China).

I am deeply indebted to my parents and grandparents for their support and encouragement to pursue my graduate study, as well as their enduring love and understanding. To them I dedicate this thesis.

I cannot end without thanking my husband Wei Xu, on whose constant inspiration, deep love and support I have relied throughout all the time. My hearty appreciation goes to him.

Reproduced with permission of the copyright owner. Further reproduction prohibited without permission.

Contents

Abstract iii

Acknowledgements v

List of Figures viii

List of Tables x

List of Acronyms xi

1 Introduction 1

1.1 Polarization effects in optical fiber communication system....2
1.2 Optical fiber vibration sensor....5
1.3 Thesis outline (sandwich thesis format)....8

2 Theory of polarization in optical fiber 11

2.1 Basics of PMD and PDL....11
2.1.1 Birefringence in single-mode fibers....11
2.1.2 Principal state of polarization and differential group delay....15
2.1.3 Polarization dependent loss....17
2.2 Mathematical description of polarization....18
2.2.1 Jones vector....18
2.2.2 Stokes parameters....20
2.3 Measurement techniques....23
2.3.1 Measurement of PMD and SOP....23
2.3.2 Measurements of PDL....29

3 Principles of optical fiber vibration/acoustic sensor 30

3.1 Applications of vibration/acoustic sensor....30
3.1.1 Structural health monitoring....31
3.1.2 Intrusion sensing....32
3.1.3 Conventional vibration sensors....33
3.2 Optical fiber vibration/acoustic sensor....34
3.2.1 Point sensors....34
3.2.2 Distributed sensors....36

Reproduced with permission of the copyright owner. Further reproduction prohibited without permission.

3.3 Optical time domain reflectometry (OTDR).....40
3.3.1 Rayleigh backscattering in the fiber.....41
3.3.2 Fundamentals of OTDR operation.....44
3.3.3 Performance parameters.....47
3.4 Polarization-OTDR.....48

4 Polarization dependent loss vector measurement in a system with polarization mode dispersion 55

5 Fast state of polarization and PMD drift in submarine fibers 62

6 Time evolution of PMD due to tides and sun radiation on submarine fibers 70

7 Continuous and damped vibration detection based on fiber polarization diversity detection sensor by Rayleigh backscattering 77

8 Distributed optical fiber vibration sensor based on spectrum analysis of Polarization-OTDR 86

9 Application of polarization based optical fiber sensor 97

9.1 Water wave frequency test.....100
9.2 Highway pavement vibration test.....105
9.3 Lab tests on cantilever beam mode frequencies.....109

10 Conclusion 127

10.1 Thesis outcomes.....127
10.2 Future work.....129

Bibliography 132

Curriculum Vita 139

Reproduced with permission of the copyright owner. Further reproduction prohibited without permission.

List of Figures

Note: Figures in each journal paper remain self-contained.

Figure 2.1 Pulse broadening due to birefringence inside optical fiber.....12

Figure 2.2 (a) State of polarization evolves along the fiber, s and f denotes slow and fast axis, respectively; (b) slow and fast axes at the x, y plane.....14

Figure 2.3 Birefringence axes and magnitudes change randomly along the fiber.....15

Figure 2.4 Maxwellian probability density of DGD for a fiber having 1-ps mean DGD [Nelson 2004].....17

Figure 2.5 An elliptical polarization described by Jones vector.....19

Figure 2.6 Normalized Stokes vectors on Poincar é sphere can represent all possible polarization states [Agilent 2002].....21

Figure 2.7 Output SOP with respect to frequency is a circular trace on Poincaré sphere.....22

Figure 2.8 (a) A typical test setup of interferometric method for measuring DGD; Sample interferogram envelope for (b) a non-mode coupled device and (c) a mode-coupled device [Williams 2004].....24

Figure 2.9 HP 8509B polarization analyzer: (a) block diagram, (b) setup for SOP measurements, (c) setup for PMD measurements, external tunable source needs to sweep the wavelength of light with a suitable step size.....28

Figure 3.1 Image of the piezoelectric accelerometer (Brüel & Kjær 4513).....34

Figure 3.2 A Fiber Bragg Grating structure, with refractive index profile and spectral response.....35

Reproduced with permission of the copyright owner. Further reproduction prohibited without permission.

Figure 3.3 A typical observed spectrum of light scattering. Frequency and intensity axis are not scaled to reproduce accurately the peaks heights and frequencies [Boyd 2003]....37

Figure 3.4 Energy level diagrams for (a) Raman Stokes scattering and (b) Raman anti-Stokes scattering....39

Figure 3.5 Schematic diagram of a conventional OTDR....45

Figure 3.6 A typical OTDR trace [Derickson 1998]....46

Figure 3.7 Basic arrangement for Polarization-OTDR system [Roger 2005]....49

Figure 3.8 Another Polarization-OTDR arrangement [Ellison 1998]....50

Figure 3.9 Schematic relations between the direction of the polarizer and the backscattered electric fields....51

Figure 3.10 Polarization-OTDR trace: (a) for broad pulses; (b) for short pulses [Nakazawa 1983]....53

Figure 5.1 Schematic configuration of PMD and PDL test using Adaptif A2000....63

Figure 5.2 Map of Bahamas: two pairs of submarine fibers were between Eleuthera and Nassau while the third one was from Eleuthera to Abaco....64

Figure 6.1 Ocean wave spectrum [Kampion 1997]....71

Figure 8.1 A picture of the transceiver module....88

Figure 9.1 A picture of all the equipments using the transmission sensor setup....97

Reproduced with permission of the copyright owner. Further reproduction prohibited without permission.

List of Tables

Table 2.1 Comparison of HP 8509B and Adaptif 2000 polarization analyzers.....27

Table 5.1 PMD and PDL test results of three submarine fibers.....65

Reproduced with permission of the copyright owner. Further reproduction prohibited without permission.

List of Acronyms

AOM	Acousto-Optical Modulator
APD	Avalanche Photodiode
BER	Bit Error Rate
CW	Continuous Wave
DFB laser	Distributed Feedback Laser
DGD	Differential Group Delay
DOFS	Distributed Optical Fiber Sensors
DOP	Degree of Polarization
EOM	Electro-Optical Modulator
ER	Extinction Ratio
FBG	Fiber Bragg Gratings
FUT	Fiber Under Test
JME	Jones Matrix Eigenanalysis
MMM	Müeller matrix method
NEP	Noise Equivalent Power
OFDR	Optical Frequency Domain Reflectometry
OFS	Optical Fiber Sensors
OFVS	Optical Fiber Vibration Sensor
OTDR	Optical Time Domain Reflectometry

Reproduced with permission of the copyright owner. Further reproduction prohibited without permission.

PDF	Probability Density Function
PDL	Polarization Dependent Loss
PMD	Polarization Mode Dispersion
PSP	Principal States of Polarization
RMS	Root Mean Square
SBS	Stimulated Brillouin Scattering
SHM	Structural Health Monitoring
SMF	Single Mode Fiber
SNR	Signal to Noise Ratio
SOP	State of Polarization
SRS	Stimulated Raman Scattering

Reproduced with permission of the copyright owner. Further reproduction prohibited without permission.

Chapter 1

Introduction

Over the past decade optical fiber technology has emerged as an active research area through numerous communication and sensing applications. For communication purpose, optical fibers serve as a channel to transport the optical signal from transmitter to receiver; while for sensing applications, the role of optical fiber is to serve either a sensing medium or as a means of connecting a remote sensor to the signal process unit. The advantages of optical fiber include small size, lightweight, low loss, and resistance to corrosion - thereby implying that they can be installed in remote locations to transmit the signal. Also, due to its dielectric nature optical fiber is less prone to electrical interference and can withstand higher temperatures than its metallic counterparts: this allows it to work better under the harsh environments.

Light propagating inside optical fiber has the following four basic properties: intensity, frequency, phase and polarization. In the communication systems, the modulation formats of the optical signal at the transmission end are designed based on one of these four properties. In the sensing systems though, information about the measurand is primarily conveyed by a change in either intensity, frequency, phase, polarization or a combination of the above.

This thesis focuses on the polarization effects in both optical fiber communication and vibration sensing systems. Polarization effects are very sensitive to the environmental

Reproduced with permission of the copyright owner. Further reproduction prohibited without permission.

disturbances, such as temperature, wind, pressure, etc. On the one hand, it adds complexity on measuring the signal degradation in high speed communication systems and makes it difficult to mitigate the polarization effects; on the other hand, however, polarization can be exploited to construct a dynamic sensor to detect vibration or acoustic emission events.

This introductory chapter is to provide the background material and briefing of the research work. Section 1.1 focuses on the polarization effects in an optical fiber communication system while section 1.2 introduces the optical fiber vibration sensor. Section 1.3 gives the thesis outline.

1.1 Polarization effects in an optical fiber communication system

The impairments of an optical fiber communication system operating at low bit rates (<2.5Gbits/s) include fiber loss, chromatic dispersion and nonlinear effects (stimulated light scattering, nonlinear phase modulation and four-wave mixing) [Agrawal 2002]. With the development of higher speed communication systems (>10Gbits/s), the polarization mode dispersion (PMD) and polarization dependent loss (PDL) become additional limitations and a major source of concern for the system's performance [Huttner 2000, Gordon 2000].

PMD has its origins in optical birefringence: a difference in the phase velocities of the two orthogonally polarized components of the fundamental fiber mode. In conventional single mode fibers (SMF), birefringence is not a constant but changes randomly in both

Reproduced with permission of the copyright owner. Further reproduction prohibited without permission.

magnitude and direction along the fiber. PMD is described by principal states of polarization (PSP) and differential group delay (DGD); DGD is the group delay difference between two PSPs - the slow and fast modes [Gordon 2000]. Both PSP and DGD are wavelength and time dependent; the average of DGD over time or frequency is called PMD [Gisin 1992]. Polarization dependent loss (PDL) refers to energy loss that is dependent on the polarization state: one mode suffers more loss than the other. PDL is defined as the difference between the maximum and minimum transmission intensities in decibels through the system with respect to all the possible states of polarization (SOP). PMD alone causes pulse broadening while PDL alone causes power fluctuation. As PMD and PDL usually co-exist in optical fiber communication systems, the interaction of PMD and PDL creates complicated effects, for example, the two PSPs are not mutually orthogonal [Gisin 1997, Huttner 2000]. Thus the lightwaves propagating along the two PSPs may interfere and produce anomalously large pulse broadening, which in turn increases system's bit error rate (BER) [Huttner 2000, Lu 2001].

Since environmental changes including temperature and stress cause the PMD in fiber to vary stochastically in time, PMD is considered to be particularly difficult to manage or compensate. Various techniques for PMD measurement are available, which fall into both the time domain as well as the frequency domain categories [Williams 2004]. Detailed description and comparison of different approaches will be given in Chapter 2. However, previous techniques have either assumed that the system has no PDL or requires a complete knowledge of both the input and output SOP for three independent polarizations [Heffner 1992a]. Chen et al [Chen 2004] introduced a generalized Poincaré sphere method based on the equation of motion to measure the PMD with PDL in the

Reproduced with permission of the copyright owner. Further reproduction prohibited without permission.

system, which requires only three output SOPs and their derivatives. A new PDL measurement method based on equation of motion is then proposed and verified by both numerical simulation and experiment in Chapter 4. This method is compatible with the well known Jones Matrix method and shows a faster response speed due to its least measurement steps requirement. The testing speed of PMD and PDL is critical for studying the environmental effects on the fiber and designing the mitigation scheme for communication systems.

The field tests regarding the time evolution of polarization effects has been studied mostly in buried fibers and aerial fibers. Previous experiments showed that in buried fibers SOP drift is relatively slow (on the order of hours or days), and PMD fluctuation is due to temperature [Cameron 1998, Karlsson 2000, Allen 2003]. In aerial fibers SOP drift is relatively fast (on the order of microseconds in winter [Waddy 2001]), and PMD fluctuation is due to temperature, wind or even power line current variations since aerial fibers are often cabled together with power lines [Wuttke 2003]. Although another type of fiber, submarine fiber, is widely used in global telecommunication networks, very little work on the polarization effects in it has been conducted. This is due to the fact that submarine fibers are usually installed in remote areas, which makes it hard to get access to. In this thesis, for the first time we performed a long-term field test of polarization effects on four >200km submarine fibers at high speeds (15s interval) to quantify SOP drift and correlate the PMD fluctuations with the exposed environmental conditions. Chapter 5 reports the temporal drift of SOP and PMD; while Chapter 6 discusses the statistical distribution and behavior of both PSP and DGD, and most importantly the PMD fluctuation is found mainly caused by the water currents induced tension on

Reproduced with permission of the copyright owner. Further reproduction prohibited without permission.

submarine fibers. The obtained results would not only provide valuable information for PMD compensators in submarine cable systems, but also suggest the possibility to utilize polarization effects to monitor external conditions. Eventually this leads to the development of a polarization based optical fiber sensor which becomes the second part of this thesis.

1.2 Optical fiber vibration sensor

In parallel with the development of the optical fiber communication systems, optical fiber sensors (OFS) have also undergone tremendous growth and advancement, where many components and multiplexing techniques associated with the communication industry can be adopted. Based on the advantages of optical fiber as mentioned before, OFS is well suited in some particular environments and has the ability to provide information in a distributed manner.

An OFS is basically composed of a light source, an optical fiber serving as a sensing element, and a detector. The principle of operation is that the measurand modulates some parameter of the optical fiber (intensity, frequency, phase, polarization, etc.) which gives rise to a change in the characteristics of the optical signal received at the detector. OFS has been studied and applied to monitor a variety of quantities such as temperature, strain, pressure, displacement, rotation, vibration, acoustics, as well as chemical, biomedical and electrical variables [Udd 1991, Yu 2002]. Various OFS have been developed in the laboratory and later proved successful for many field applications. To name a few commercialized OFS techniques: optical fiber gyroscope [Bergh 1981], which provides extremely precise rotational rate information and is widely used in surveying,

Reproduced with permission of the copyright owner. Further reproduction prohibited without permission.

stabilization and inertial navigation tasks; fiber Bragg gratings (FBG) [Berkoff 1996], which are finding uses in instrumentation applications in oil and gas wells to measure external pressure, temperature, seismic vibrations and inline flow measurement; optical time domain reflectometry (OTDR) [Barnoski 1976], which has become an indispensable tool for checking the connections of optical networks. A modified type of OTDR, so called Polarization-OTDR, was then proposed as a first distributed optical fiber sensor [Rogers 1981].

According to the spatial distribution of the quantity to be measured, OFS can be divided into two categories: point and distributed sensors. A point sensor takes the measurements at a particular location. This is the way in which most OFS operate, for example - interferometric type sensors, FBG sensors and microstructure fiber sensors (like photonic-crystal fiber, which usually contains a lattice of air holes in the silica fiber). Although a large number of point sensors can be assembled in series or in matrices to achieve so called quasi-distributed sensor, unless the sensor heads are in vicinity of local effects, they fail to detect the signal. Accordingly, there is a clearly need for a technique that is able to provide a continuous reading of the measurand as a function of position along the sensing fiber - a process which is termed distributed sensing. In this way a distributed sensor can substitute thousands of point sensors. The mechanisms of distributed sensors are based on backscattered light inside the optical fiber including Rayleigh, Brillouin and Raman scattering. They can provide information either with centimeter spatial resolution in a km long fiber link [Kee 2000] or with sub-millimeter resolution in a few meters short range [Soller 2005] depending on different sensing configurations. Distributed sensors are particularly needed for the applications of

Reproduced with permission of the copyright owner. Further reproduction prohibited without permission.

structural health monitoring and homeland security whereby sensing over an extended distance. Our target applications and an overview of available point and distributed sensors will be given in Chapter 3.

Previous research regarding distributed sensors over km long fiber mostly focused on static measurements, i.e. no time-varying or slowly time-varying signals, such as, temperature or static strain. Due to the extremely weak backscattered signal and signal fluctuations induced by polarization effects, taking an average of a large number of waveforms is unavoidable in order to average out polarization dependency and to get high signal to noise ratio (SNR). Thus, the testing speed has been sacrificed in such developed sensors and only the time-averaged information would be provided instead of real-time dynamic signals. However, for structural impact/vibration monitoring or intrusion detection of a large facility, the sensor system should respond fast enough to catch those dynamic events up to kHz in addition to the location information. In this thesis we propose to utilize changes in the state of polarization in the transmission or backscattered direction of light to realize an optical fiber vibration sensor (OFVS). Experimental configuration and test results will be compared to a conventional sensor in Chapter 7. In Chapter 8, for the first time to the best of our knowledge, a fully distributed OFVS has been successfully demonstrated based on a Polarization-OTDR system in the lab. It has the ability to detect vibration disturbances up to 5kHz in a 1km fiber with 10m spatial resolution. Moreover, by a novel spectrum analysis multiple dynamic events occurring simultaneously with different or even the same frequency can be identified.

The transmission setup, which works as a point sensor giving vibration frequency without location information, has been verified by both lab and field tests. Detailed test

Reproduced with permission of the copyright owner. Further reproduction prohibited without permission.

conditions, processes and results will be shown in Chapter 9. We plan to take the backscattered setup (i.e. Polarization-OTDR) out to do field tests for intrusion sensing or impact detection on a large structure in the near future.

1.3 Thesis outline

This thesis adopts the *sandwich thesis* format, containing eight published or submitted papers from Chapter 4 to Chapter 9. An introduction part has been provided in the beginning of Chapter 4 through Chapter 9 to link the different chapters together. And each paper is presented exactly in its published or submitted format. Figures and references remain self-contained, within each journal paper.

Chapter 2 provides the theory of PMD and PDL in optical fiber communication system, including their definition and two mathematical descriptions of polarization. We also discuss and compare some current available measurement methods.

Chapter 3 introduces some optical fiber vibration sensors in either a point or distributed manner. These are mainly applied on structural health monitoring or for intrusion sensing. The basic configuration of Polarization-OTDR and its working principle will also be presented.

Chapter 4 describes a new PDL vector measurement method based on the PDL vector equation of motion, which has been verified by numerical simulation and experiment.

Chapter 5 and Chapter 6 study the polarization effects in a submarine fiber communication system based on the long-term field test results: Chapter 5 primarily focuses on measuring the fast SOP and PMD drifts while Chapter 6 correlates PMD time evolution to the environmental effects - especially the tidal waves undersea.

Reproduced with permission of the copyright owner. Further reproduction prohibited without permission.

Chapter 7 proposes to use polarization change of Rayleigh backscattering to measure continuous and damped vibration. A series of experiments have been conducted and compared with a conventional sensor. The Polarization-OTDR setup has been successfully developed in Chapter 8 to achieve a fully distributed vibration sensor.

Chapter 9 gives three application examples of the polarization-based vibration sensor: 1) to measure water wave frequencies for both regular and irregular waves; 2) to study the impact on the highway pavement slabs during vehicles passing; 3) to examine the mass loading effects on mode frequencies of a lightweight cantilever bar.

Finally, Chapter 10 concludes all the work we have done and suggests some possible future directions.

The eight papers are listed as follows:

[Chap 4] Liang Chen, **Ziyi Zhang** and Xiaoyi Bao, "Polarization dependent loss vector measurement in a system with polarization mode dispersion," *Optical Fiber Technology,* 12, 251-254 (2006)

[Chap 5] Ziyi Zhang, Xiaoyi Bao, Qinrong Yu and Liang Chen, "Fast state of polarization and PMD drift in submarine fibers," *Photonics Technology Letters, IEEE,* 18, 1034 –1036 (2006)

[Chap 6] Ziyi Zhang, Xiaoyi Bao, Qinrong Yu and Liang Chen, "Time evolution of PMD due to tides and sun radiation on submarine fibers," *Optical Fiber Technology,* 13, 62-66 (2007)

Reproduced with permission of the copyright owner. Further reproduction prohibited without permission.

[Chap 7] Ziyi Zhang and Xiaoyi Bao, "Continuous and Damped Vibration Detection Based on Fiber Diversity Detection Sensor by Rayleigh Backscattering," *Journal of Lightwave Technology, IEEE,* 26, 852-838 (2008)

[Chap 8] Ziyi Zhang and Xiaoyi Bao, "Distributed optical fiber vibration sensor based on spectrum analysis of Polarization-OTDR system," *Optics Express* 16, 10240-10247 (2008)

[Chap 9.1] Ziyi Zhang, Xiaoyi Bao, Colin D. Rennie, Ioan Nistor, Andrew Cornett, "Water Wave Frequency Detection by Optical Fiber Sensor," *Optics Communications,* 281, 6011-6015 (2008)

[Chap 9.2] Ziyi Zhang, Samuel LeBlanc and Xiaoyi Bao, "Concrete pavement vibration monitoring due to the car passing using optical fiber sensor," 19th International Conference on Optical Fiber Sensors, *Proc. SPIE* 7004, 70041U (2008)

[Chap 9.3] Ziyi Zhang, Pingyu Zhu and Xiaoyi Bao, "Measurement of the cantilever bending and torsion mode frequency by optical fiber sensor and accelerometer," submitted to *Optical Engineering*

Reproduced with permission of the copyright owner. Further reproduction prohibited without permission.

Chapter 2

Theory of polarization in optical fiber

This chapter covers several important concepts to the understanding of polarization effects in optical fiber. Section 2.1 introduces basics of PMD and PDL, including birefringence in the fiber, principal state of polarization, differential group delay and statistics of PMD. Section 2.2 gives two mathematical descriptions of polarization, namely Jones vector and Stokes parameters. And section 2.3 lists and discusses some commonly used measurement techniques for PMD and PDL.

2.1 Basics of PMD and PDL

2.1.1 Birefringence in single-mode fiber

A lightwave propagating in optical fiber is composed of many discrete modes. An optical mode refers to a specific solution of the wave equations that satisfies the appropriate boundary conditions and has the property that its spatial distribution does not change with propagation [Agrawal 2002]. SMF refers to a type of fiber that can only support one fundamental transmission mode, i.e. HE_{11} mode. Because the small differences in core and cladding refractive indexes, we can make approximations for modes in the SMF as plane waves.

Reproduced with permission of the copyright owner. Further reproduction prohibited without permission.

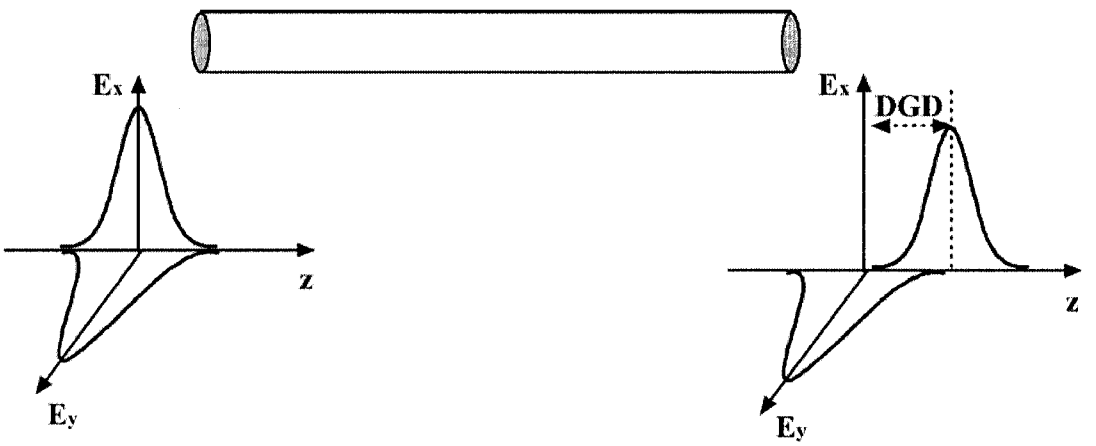

Figure 2.1 Pulse broadening due to birefringence inside optical fiber.

In an ideal SMF, with the circularly symmetric fiber core, the fiber supports two orthogonally polarized components that have the same mode index. As a result, the propagation constant β is independent of polarization modes. β is related to the refractive index n by $\beta = \frac{n\omega}{c}$, where c is the speed of light in vacuum and ω is the angular frequency of the light. n is a function of fiber geometry as well as the material properties of the core and cladding. In practice, fiber core is not perfectly circular due to many facts, including imperfection in the manufacturing process and external stress during the fiber cabling or laying. Because of the asymmetry the two polarization components travel with different phase velocities ($n_x \neq n_y, n_x$ and n_y are the effective refractive indices when the polarization component is along the x and y direction, respectively), so called "birefringence" inside optical fiber. Fig. 2.1 illustrates the time-domain effect of birefringence inside a portion of optical fiber. One pulse launched into the fiber with equal power on the x and y axes; at the output end, it becomes broadened

Reproduced with permission of the copyright owner. Further reproduction prohibited without permission.

since two polarized components have different traveling times due to different refractive indexes. In the case of large birefringence, two output pulses would be observed. As a result, the impact of the polarization mode delay increases with the data rates in the optical fiber communication system.

Another consequence of birefringence is the SOP of the light rotates in Stokes space around the birefringence axes - the slow and fast axes, as shown in Fig. 2.2 (a). Here, the slow and fast axis refers to the direction at the transverse plane with the minimum and maximum group velocity, respectively. Fig. 2.2 (b) depicts the slow and fast axes with respect to x and y on the transverse plane. Linearly polarized light may evolve to circular or elliptical polarization and eventually turns back to the input polarization state at some point of the fiber. The parameter "beat length", $L_b = \lambda/\Delta n = \lambda/(n_s - n_f)$, is used to describe the propagation distance over which the polarization rotates through full cycle, or in other words, the electric field in the slow axis is delayed by one wavelength relative to that in the fast axis. For standard SMFs the beat length has the value of ~10m [Galtarossa 2000].

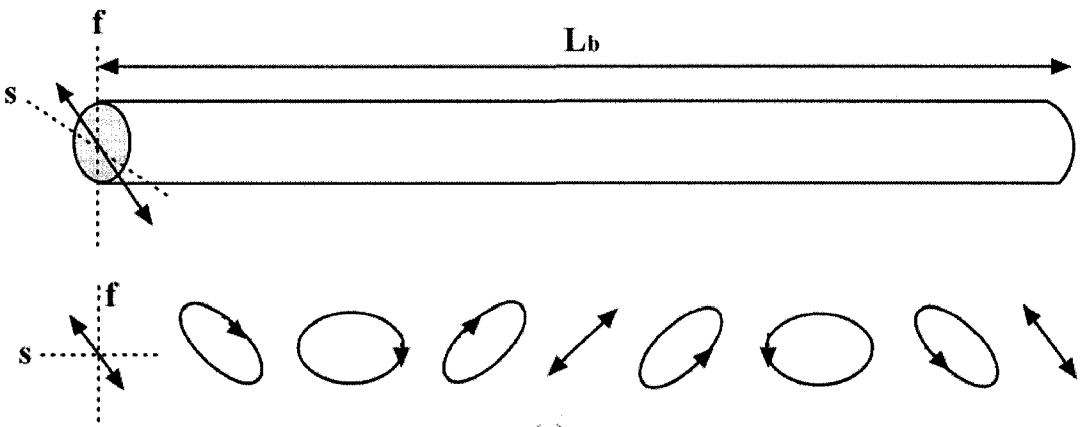

(a)

Reproduced with permission of the copyright owner. Further reproduction prohibited without permission.

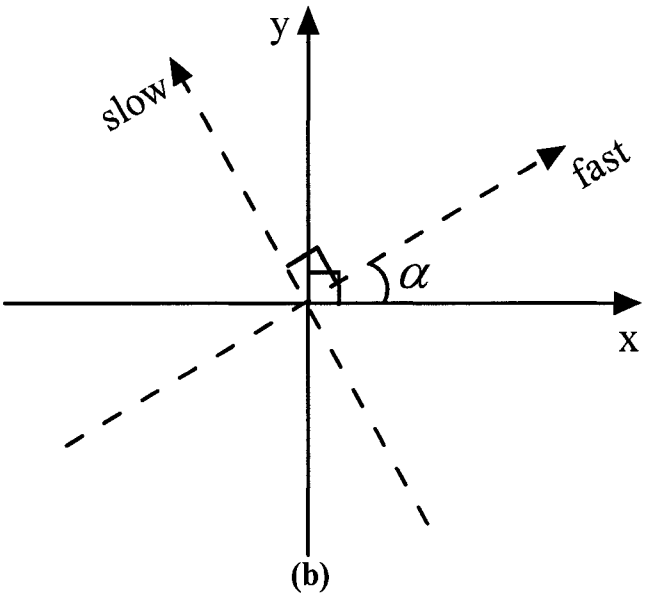

Figure 2.2 (a) State of polarization evolves along the fiber, s and f denotes slow and fast axis, respectively; **(b)** slow and fast axes at the x, y plane.

In a short section of fiber (several meters in length), the birefringence can be considered uniform; while for long fibers with over hundreds of meters length, the birefringence axes and magnitude ($\Delta n = n_s - n_f$) randomly vary along the fiber length, as depicted in Fig. 2.3. This results in polarization mode coupling wherein the fast and slow polarization modes from one segment each decomposes into both the fast and slow modes of the next segment [Kogelnik 2002]. The length of each segment is not a constant, but varies along the fiber. Therefore, the concatenation of birefringence sections as in Fig. 2.3 is often adopted as the modeling method of polarization effect in long fibers. How fast the birefringence axes are evolving gives the other important parameter, coupling length (h), which usually can categorize a fiber into the short or long length regime. A precise definition involves the spatial correlations of the birefringence vector: $\vec{\beta}(z)$ [Huttner 1999].

Reproduced with permission of the copyright owner. Further reproduction prohibited without permission.

$$\frac{1}{\mathrm{L}}\int_0^L \vec{\beta}(z)\cdot\vec{\beta}(z+\Delta)dz = \overline{\beta}^2 \exp\left(-2\frac{|\Delta|}{h}\right) \tag{2.1}$$

where $\overline{\beta}$ is the root mean square (RMS) average of the birefringence over the length L, and can be obtained by letting $\Delta = 0$ in (2.1). Loosely speaking, h refers to the distance after which the birefringence axis has changed significantly. For standard fibers, the coupling length is in the range of 5~500m [Huttner 1999].

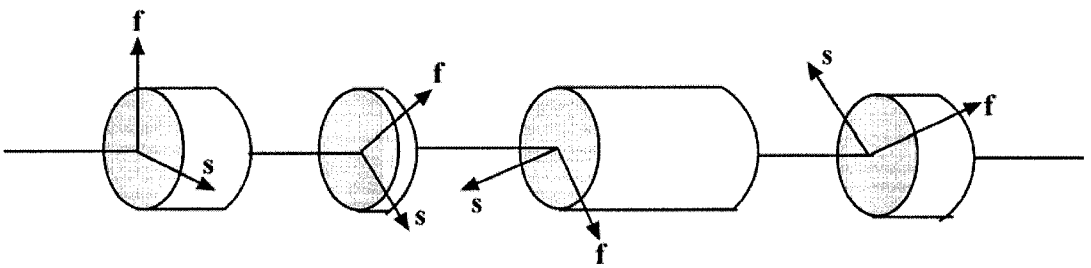

Figure 2.3 Birefringence axes and magnitudes change randomly along the fiber.

2.1.2 Principal state of polarization and differential group delay

The variations of the birefringence axes and environmental effects on the birefringence in long fibers complicate the description and analysis of PMD. The concept of principal state of polarization (PSP), proposed by Poole and Wagner, is in common use for the characterization of PMD. In absence of PDL, for any length of fiber there exists for every wavelength an orthogonal pair of input polarization states, whose output states are independent of the wavelength to first order [Poole 1986]. If $\vec{s}$ denotes the output SOP in Stokes space, then $\frac{d\vec{s}}{d\omega} = 0$. Detailed mathematical descriptions can be found in the section 2.2.2, equation (2.10). This special pair of input states is called PSP: the state with minimum group delay refers to fast PSP while the other with maximum group delay

Reproduced with permission of the copyright owner. Further reproduction prohibited without permission.

refers to slow PSP. The differential group delay (DGD) is defined as the difference in signal arrival times of the fast and slow PSPs, usually on the order of picoseconds (ps). The importance of understanding PSPs in time-domain picture is if the input pulse is aligned with either of the PSPs, then the resulting output pulse shape is undistorted to first order of optical wavelength or frequency.

Using the concept of PSP, PMD can be characterized by the PMD vector $\vec{\Omega}$ [Poole 1988]: DGD, $\Delta\tau$, represents its magnitude while its direction points to the slow PSP $\hat{p}$.

$$\vec{\Omega} = \Delta\tau \hat{p} \tag{2.2}$$

For a highly-mode-coupled fiber (fiber length >> coupling length), both the PSP and DGD vary with wavelength. Also, at a given frequency, PSP and DGD fluctuate stochastically with time due to environmental perturbations. Therefore, a single PMD measurement at any particular wavelength and time cannot represent a system's PMD impairment. Instead, a statistical description of PMD is required in order to assess its long term system impacts. In optical fiber communication systems, the impact of PMD includes the degradation of the outage probability [Poole 1997] and system Q factor [Beltrame 2000] due to the pulse broadening as well as the decrease of the pulse peak power. It has been shown that the probability density function (PDF) of the DGD in a fiber follows a Maxwell function for both wavelength and time ensembles [Gisin 1991a, Curti 1990].

$$p(\Delta\tau) = \sqrt{\frac{2}{\pi}} \frac{\Delta\tau^2}{\sigma^3} e^{\left(\frac{-\Delta\tau^2}{2\sigma^2}\right)} \tag{2.3}$$

where $\Delta\tau(\lambda, t)$ is the DGD at one particular wavelength and time. While the mean DGD

Reproduced with permission of the copyright owner. Further reproduction prohibited without permission.

is related to a coefficient σ by $<\Delta\tau>=\sigma\sqrt{8/\pi}$, which is the only parameter that determines the distribution. Fig. 2.4 gives an example of the Maxwellian PDF with 1ps mean DGD: both simulation and experimental data fit well with the theoretical calculation. Since the DGD usually drifts with time, it is difficult to obtain an accurate estimate of the mean DGD by repeatedly measuring the DGD at one wavelength. Instead, the DGD is averaged over many wavelengths and the result is assumed to be equal to the time average [Nelson 2004].

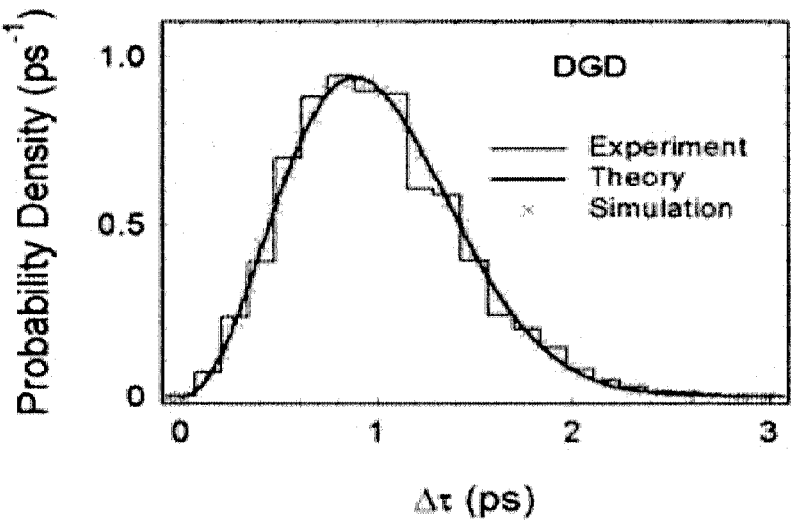

Figure 2.4 Maxwellian probability density of DGD for a fiber having 1-ps mean DGD [Nelson 2004].

2.1.3 Polarization dependent loss

Another polarization effects in the optical fiber communication system is polarization dependent loss (PDL), which refers to the ratio of the maximum and minimum output power transmitted through the system as the input polarization is varied over all possible polarization states. It is usually computed from the following equation and expressed in

Reproduced with permission of the copyright owner. Further reproduction prohibited without permission.

decibel (dB):

$$PDL(dB) = 10\log_{10}\frac{P_{\max}}{P_{\min}} \tag{2.4}$$

where $P_{\max}$ and $P_{\min}$ are the maximum and minimum transmitted power with different input polarization states. In the communication system, PDL in SMF can be ignored, but it is up to 0.4 dB in various fiber components, such as amplifiers and filters [Lu 2001].

2.2 Mathematical description of polarization

2.2.1 Jones vector

In an $x-y-z$ coordinate system with the lightwave transmitting along z direction, the polarization describes the behavior of the electric field in the x, y plane. Polarized light can be represented by a two-element column vector called "Jones vector", which gives the amplitude and phase of the orthogonal electric field components [Jones 1941]. It has the form

$$\vec{E} = \begin{pmatrix} E_x \\ E_y \end{pmatrix} = \begin{pmatrix} E_{0x}e^{j\delta_x} \\ E_{0y}e^{j\delta_y} \end{pmatrix} \tag{2.5}$$

where E_{0x} and E_{0y} are the maximum values of E_x and E_y while δ_x and δ_y represent phases. When the phase difference, $\Delta\delta = \delta_y - \delta_x$, is zero or an integer multiple of π, the light is linearly polarized; when $E_{0x} = E_{0y}$ and $\Delta\delta$ is an odd integer multiple of $\pi/2$, the light is circularly polarized. In other cases, the light has elliptical polarization as illustrated in Fig. 2.5.

Reproduced with permission of the copyright owner. Further reproduction prohibited without permission.

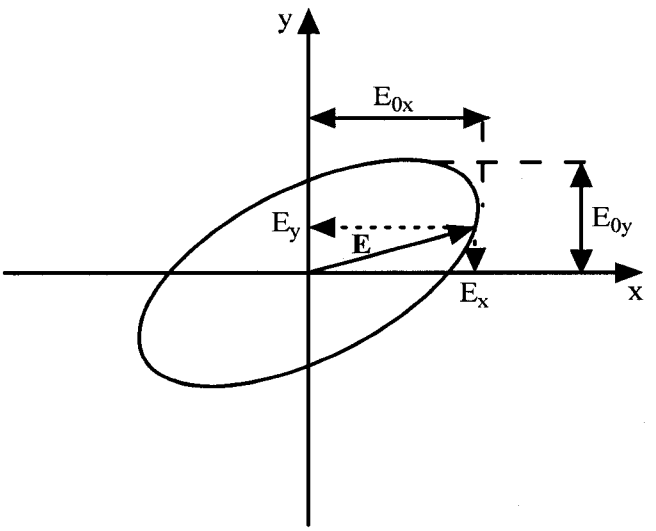

Figure 2.5 An elliptical polarization described by Jones vector.

When light passes through an optical element, like optical fiber or devices, the polarization state of light will change from the input end to the output. Such transformation of the polarization can be described using a complex two-by-two Jones matrix $U(\omega)$ [Jones 1941]. It relates the input and output Jones vector as

$$\vec{E}_{out} = T(\omega)\vec{E}_{in} = e^{-j\phi_0}U(\omega)\vec{E}_{in} \tag{2.6}$$

where the transmission matrix $T(\omega)$ is related to the Jones matrix $U(\omega)$ by the relation $T(\omega) = e^{-j\phi_0}U(\omega)$ and ϕ_0 is a phase factor common to the field on both the x and y axes from the optical element.

The Jones vector gives full information of the electric field, so it is very useful when the phase of light is of interest. However, Jones vector cannot be easily used to express partially polarized light because its phase is not a constant rather a variable. Moreover, it is not convenient to directly measure the electric field of light. So the Stokes parameters, in term of easily measured optical powers, are used as an alternative description of

Reproduced with permission of the copyright owner. Further reproduction prohibited without permission.

polarization.

2.2.2 Stokes parameters

The Stokes parameters (S_0, S_1, S_2, S_3) are a set of values that describe the polarization state of light [Shurcliff 1962]. The Stokes parameters are often combined into a vector, known as the Stokes vector. It can easily be found by measuring the power transmitted through different polarizers

$$\vec{S} = \begin{pmatrix} S_0 \\ S_1 \\ S_2 \\ S_3 \end{pmatrix} = \begin{pmatrix} P_{0^o} + P_{90^o} \\ P_{0^o} - P_{90^o} \\ P_{45^o} - P_{-45^o} \\ P_{rcp} - P_{lcp} \end{pmatrix} \tag{2.7}$$

where P_{θ^o} is the power through a θ angle of polarizer, P_{rcp} and P_{lcp} are the power through a right and left circular polarizer, respectively, S_0 is the total power of light.

The Stokes parameters take care the optical phase correlation naturally, thus it can describe partially polarized light. The degree of polarization (DOP) can be calculated as

$$DOP = \frac{\sqrt{S_1^2 + S_2^2 + S_3^2}}{S_0} \tag{2.8}$$

The locus of normalized Stokes parameters, $\vec{s} = (s_1, s_2, s_3) = (S_1/S_0, S_2/S_0, S_3/S_0)$, form a unit sphere. This is known as the Poincaré sphere [Poincaré 1892], which represents all possible polarization states. As shown in Fig 2.6, linear polarizations are along the equator of the sphere, such as horizontal linear polarization (1, 0, 0) and 45° linear polarization (0, 1, 0); circular polarizations are plotted at the poles.

Reproduced with permission of the copyright owner. Further reproduction prohibited without permission.

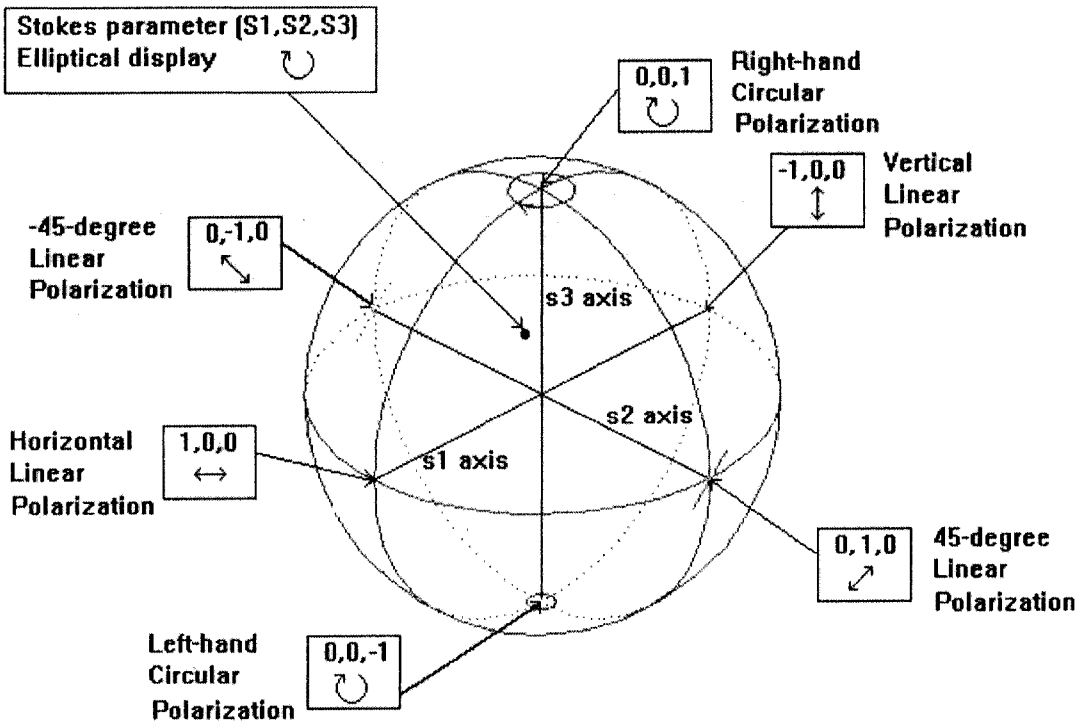

Figure 2.6 Normalized Stokes vectors on Poincaré sphere can represent all possible polarization states [Agilent 2002].

Since the Stokes parameters are observables, $S_0 \sim S_3$ often are measured directly during the experiment first and then from which Jones vectors $\vec{E} = \begin{pmatrix} E_x \\ E_y \end{pmatrix} = \begin{pmatrix} E_{0x} e^{j\delta_x} \\ E_{0y} e^{j\delta_y} \end{pmatrix}$ will be derived. These two representations are related by

$$\begin{cases} S_0 = \langle E_x E_x^* + E_y E_y^* \rangle \\ S_1 = \langle E_x E_x^* - E_y E_y^* \rangle \\ S_2 = \langle E_x E_y^* + E_x^* E_y \rangle \\ S_3 = \langle j(E_x E_y^* - E_x^* E_y) \rangle \end{cases} \tag{2.9}$$

In Stokes space, the transformation of polarization state through an optical element is described by a 4×4 Müeller matrix M.

$$\vec{S}_{out} = M(\omega)\vec{S}_{in} \tag{2.10}$$

Reproduced with permission of the copyright owner. Further reproduction prohibited without permission.

Using the Stokes parameters and the Poincaré sphere, the frequency-dependent SOP at the fiber output due to PMD can be represented. By taking the frequency derivative of equation (2.10) leads to the law of infinitesimal rotation [Poole 1997]

$$\frac{d\vec{s}}{d\omega} = \vec{\Omega} \times \vec{s} \tag{2.11}$$

where $\vec{s}$ is the output normalized Stokes parameters, PMD vector $\vec{\Omega}\times = M_{\omega}M^{T}, M^{T}$ is the transpose of M, and $M_{\omega} = \frac{dM}{d\omega}$ is the angular frequency derivative of the Müeller matrix. Equation (2.11) describes for a certain input SOP, the evolution of output SOP with respect to frequency is a circular trace on the Poincaré sphere as illustrated in Fig. 2.7.

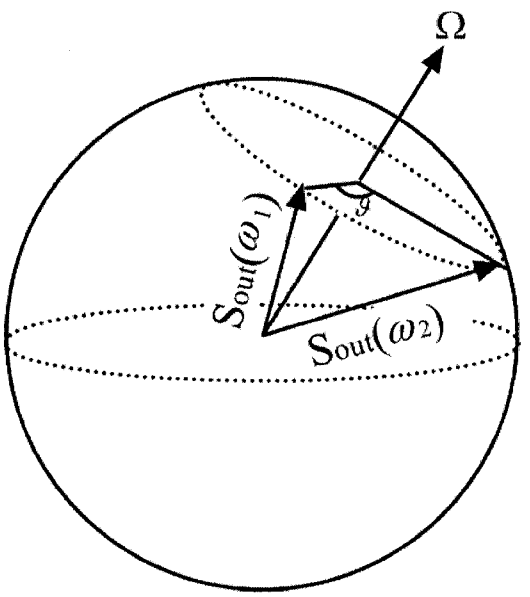

Figure 2.7 Output SOP with respect to frequency is a circular trace on Poincaré sphere.

The output SOP $\vec{s}$ precesses around $\vec{\Omega}$ when the frequency of light is varied. And the DGD, $\Delta\tau$, defined as the magnitude of $\vec{\Omega}$, determines how fast the precession is. A

Reproduced with permission of the copyright owner. Further reproduction prohibited without permission.

special case occurs, when $\vec{s}$ is aligned with $\pm\vec{\Omega}$, $\frac{d\vec{s}}{d\omega} = \vec{\Omega} \times \vec{s} = 0$. In this case, the output SOP will not change with the frequency; we recall this to be the definition of the PSP.

2.3 Measurement Techniques

2.3.1 Measurement of PMD and SOP

Over the years various techniques for the measurements of PMD have been proposed, which include interferometric method, Jones Matrix Eigenanalysis (JME), Müeller matrix method (MMM), Poincaré arc method, etc. Here, two commonly used testing techniques will be given in detail: the interferometric method, which operates in the time domain, and the JME method, which employs the frequency domain for computing the instantaneous PMD vectors as a function of frequency.

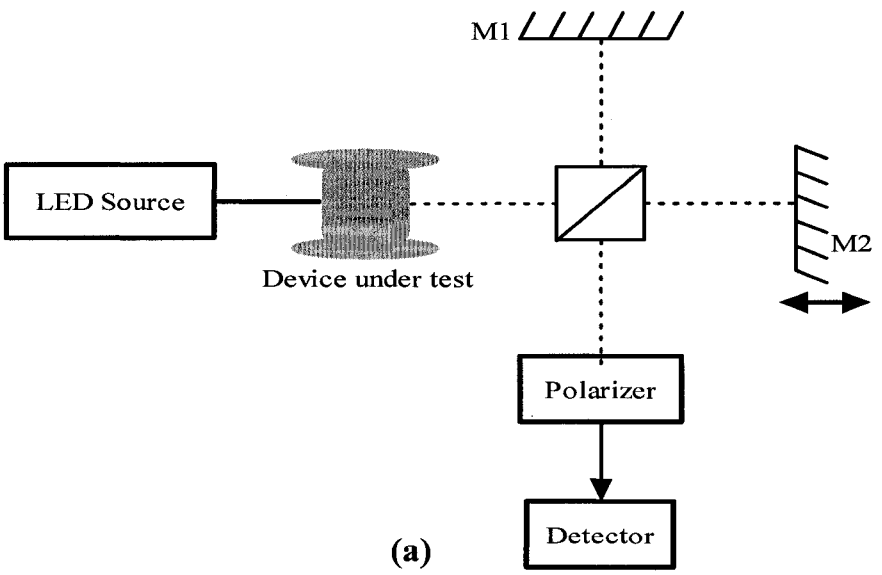

(a)

Reproduced with permission of the copyright owner. Further reproduction prohibited without permission.

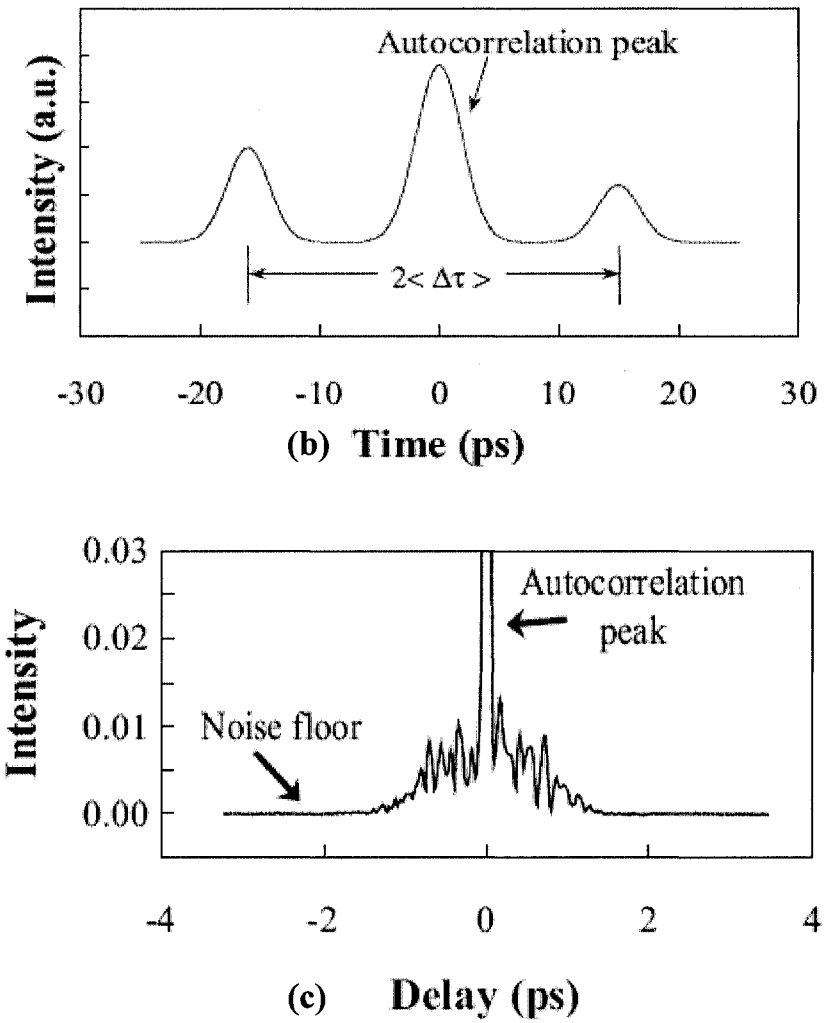

Figure 2.8 (a) A typical test setup of interferometric method for measuring DGD; Sample interferogram envelope for **(b)** a non-mode coupled device and **(c)** a mode-coupled device [Williams 2004].

Since the interferometric method allows a rapid measurement of mean DGD and does not depend on the polarization states in the fiber (which is very sensitive to environmental effects, such as temperature and strain), it is widely used in the field test [Gisin 1991b]. As a typical test setup shown in Fig. 2.8(a), the system usually contains a Michelson interferometer with one fixed arm and one scanning mirror arm. The light

Reproduced with permission of the copyright owner. Further reproduction prohibited without permission.

source is often a low-coherent LED. For a non-mode-coupled fiber (birefringence remains constant along the fiber, like polarization-maintaining fiber), when the scanning mirror moves a certain range, a fringe pattern is detected showing a central peak and two side peaks. The central peak corresponds to the equal delays from the two arms, while the side peaks are separated from the central peak by an amount $< \Delta\tau >_{\lambda}$, as illustrated in Fig. 2.8(b). For a mode-coupled fiber, the resulting fringe pattern consists of a series of peaks instead of two side peaks, as shown in Fig. 2.8(c). The RMS DGD value can be determined by the distribution of those peaks [Gisin 1994]. The interferometric method is sufficient for the application when only mean or the RMS value of the DGD is of concern, otherwise frequency domain techniques, such as the JME, will be employed. The additional information provided by the JME includes the Jones Matrix of the device under test and the PMD vector (for both magnitude and direction) resolved as a function of wavelength.

The basic principle of the JME method is to measure the Jones matrix of a device under test at two closely spaced frequencies in order to estimate the DGD of the intermediate frequency. As discussed in section 2.2.2, the output SOP with respect to frequency precesses about $\vec{\Omega}$ on the Poincaré sphere. DGD $\Delta\tau$ is defined as the precession rate, $\left|\vec{\Omega}\right| = \Delta\tau = \left|\frac{d\theta}{d\omega}\right|$, where θ is the rotation angle of output SOP about $\vec{\Omega}$ as marked in Fig. 2.7. Here the determination of $\frac{d\theta}{d\omega}$ can suffer from aliasing if $d\theta$ is greater than π for the given $\Delta\omega$. Therefore the requirement of frequency step size is expressed by

$$\Delta\tau \cdot \Delta\omega < \pi \tag{2.12}$$

Reproduced with permission of the copyright owner. Further reproduction prohibited without permission.

According to [Heffner 1992a], the Jones matrix of a device can be measured as follows: first send in a 0^{o} polarized light and the resulting response Jones vector is denoted as $\vec{h}$, then change the input polarization state to 90^{o} and 45^{o}, and the Jones vector $\vec{v}$ and $\vec{q}$ are obtained respectively. Three complex ratios are formed from x and y components of those Jones vector: $k_1 = h_x/h_y$, $k_2 = v_x/v_y$, $k_3 = q_x/q_y$. And then $k_4 = (k_3 - k_2)/(k_1 - k_3)$ is found. With a complex constant β, the Jones matrix U is expressed as

$$U = \beta \begin{bmatrix} k_1 k_4 & k_2 \\ k_4 & 1 \end{bmatrix} \tag{2.13}$$

In the case of $PDL = 0$, from equation (2.6) by taking the frequency derivative of $\vec{E}_{out}$ and eliminating $\vec{E}_{in}$, the Jones matrix eigenvector equation can be derived as

$$\frac{1}{2}\Delta\tau|p\rangle = jU_{\omega}U^{+}|p\rangle \tag{2.14}$$

where $|p\rangle$ is the Hermitian eigenstate of $jU_{\omega}U^{+}$ associated with the larger value of group delay (i.e. slow PSP), $U_{\omega} = \frac{dU}{d\omega}$ is the angular frequency derivative of the Jones Matrix, and U^{+} is the Hermitian conjugate of U. Equation (2.14) is the basis of the JME method, which allows the measurement of DGD as a function of wavelength.

The instrument used to measure PMD or SOP in this thesis employs the JME method, since it is able to provide full information of PMD vector. Experimental results from Chapter 4 were made with the HP 8509B polarization analyzer while the submarine fiber test used the Adaptif A2000 polarization analyzer. The Adaptif A2000 has the similar system setup as the HP 8509B but with a faster testing speed. Table 2.1 lists some key

Reproduced with permission of the copyright owner. Further reproduction prohibited without permission.

parameters of both HP 8509B and Adaptif 2000 test sets for comparison.

Table 2.1 Comparison of HP 8509B and Adaptif 2000 polarization analyzers

Polarization Analyzer	PMD range	PMD accuracy	PDL range	PDL accuracy	Maximum sampling rate for SOP measurement
HP 8509B	N.A.	0.3ps for $\Delta\lambda$ =0.10nm	0-3dB	0.1dB	1kHz
Adaptif A2000	0-1000ps	0.03ps+2% of PMD value	0-10dB	0.01dB+4% of PDL value	1MHz

Fig. 2.9 (a) depicts the block diagram of HP 8509B, which has three ports: external source input, optical output and optical input. At the optical input end (i.e. receiver end) the light is split into four beams and collected by four separate photodiode detectors. Then the four Stokes parameters can be calculated to show the output SOP on Poincaré sphere. As shown in Fig. 2.9 (b), SOP measurements only require the receiver end just described. However, this is not the case for polarization transfer function measurements (such as Jones matrix, PMD, and PDL) though. As illustrated in Fig. 2.9 (c), the output from the tunable laser passes through the polarization controller before being launched into the fiber under test. As the laser frequency is swept, known polarization states are launched into the fiber and the Jones matrix of the fiber are then determined as functions of frequency.

Reproduced with permission of the copyright owner. Further reproduction prohibited without permission.

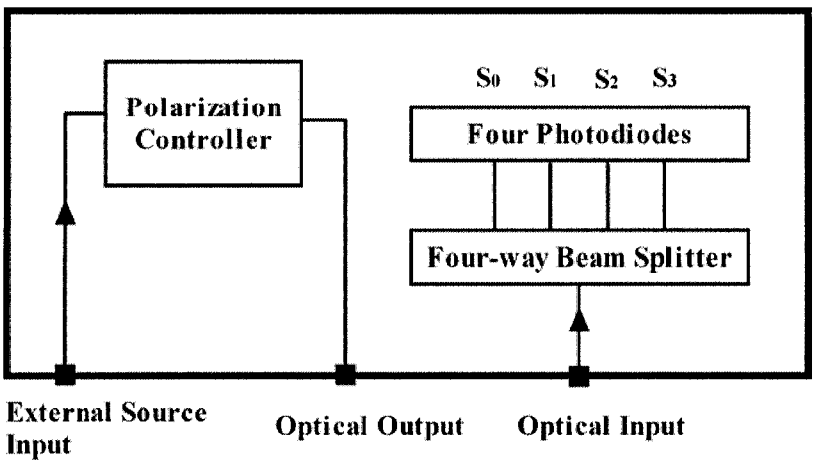

(a)

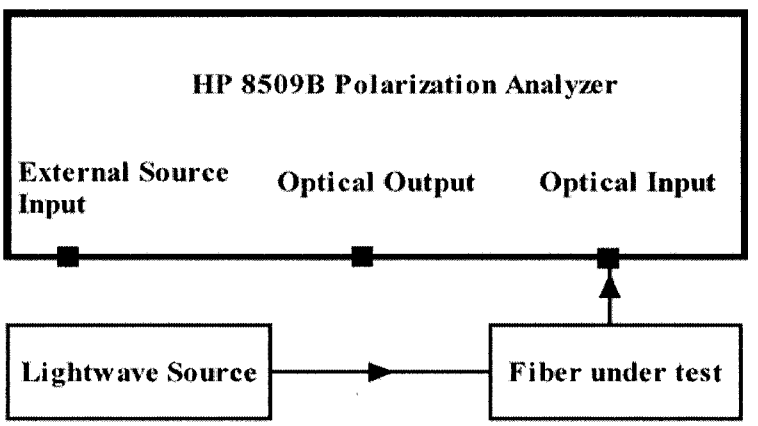

(b)

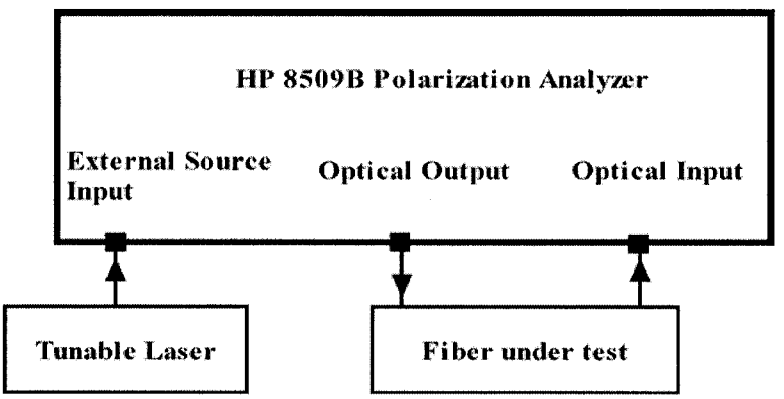

(c)

Figure 2.9 HP 8509B polarization analyzer **(a)** block diagram, **(b)** setup for SOP measurements, **(c)** setup for PMD measurements, external tunable source needs to sweep the wavelength of light with a suitable step size.

Reproduced with permission of the copyright owner. Further reproduction prohibited without permission.

2.3.2 Measurement of PDL

The measurement techniques of PDL can be classified in two categories: 1) a nondeterministic method like polarization scanning, and 2) a deterministic method like the JME or the MMM. In the case of the polarization scanning method, the maximum and minimum transmission powers are recorded through the device under test over all possible input polarization states. Then the PDL value is determined by its definition as in equation (2.4).

Both HP 8509B and Adaptif A2000 polarization analyzers employ the JME method to calculate PDL. Following the same procedure in the previous section to get the Jones matrix first, then it is shown [Heffner 1992b] that the PDL value can be calculated by two eigenvalues (ϕ_1, ϕ_2) of $T(\omega)^+ T(\omega)$

$$PDL(dB) = 10\left|\log_{10}\left(\frac{\phi_1}{\phi_2}\right)\right| \tag{2.15}$$

Reproduced with permission of the copyright owner. Further reproduction prohibited without permission.

Chapter 3

Principles of optical fiber vibration sensor

In the optical fiber communication system, test results in Chapter 5 and Chapter 6 confirm that polarization effects in fibers are closely related to the environmental disturbances. Therefore, in the area of optical fiber sensing it is natural to think about choosing polarization changes inside fibers to monitor the external conditions. Part 2 of the thesis (Chapter 7-9) presents the development and application of a fully distributed optical fiber vibration sensor based on the polarization state change of Rayleigh backscattered light.

This chapter first states the motivation of building such a vibration sensor in section 3.1 and then gives a general overview of various available point sensors and distributed sensors in section 3.2. Since our proposed sensor is based on a technique known as "Polarization-OTDR", the principle and configuration of OTDR is generally described in section 3.3. The last section focuses on some issues which are special for the Polarization-OTDR system.

3.1 Applications of vibration/acoustic sensor

There are two main target applications of the proposed distributed vibration sensor: structure health monitoring and intrusion sensing. Hence, our proposed sensor should be

Reproduced with permission of the copyright owner. Further reproduction prohibited without permission.

able to cover ~km range with frequency detection up to kHz.

3.1.1 Structural health monitoring

In recent years, structural health monitoring (SHM) has become a new field in civil, mechanical and aerospace engineering. According to Bisby, SHM can be defined as "*a non-destructive in-situ structural evaluation method that uses any of several types of sensors which are attached to, or embedded in, a structure. These sensors obtain various types of data (either continuously or periodically), which are then collected, analyzed and stored for future analysis and reference. The data can be used to assess the safety, integrity, strength, or performance of the structure, and to identify damage at its onset.*" [Bisby 2004]. The applications of SHM include large infrastructures (e.g. bridges, dams, buildings, and tunnels), oil and gas pipelines, vehicles (such as aircraft and ships), and biomedical devices. Many public civil structures are facing a problem of aging. It has been reported that 40% of the bridges in Canada are 50 years old [Bisby 2004], while the number in United States is over 50% and 42% of all bridges are structurally deficient [Stallings 2000] . Then it is crucial to determine when the structure needs to be repaired or reinforced to eliminate the risk of catastrophic structural failure. Manual inspections currently can not be conducted very often due to their costs, and accordingly the early signs of potential problems could be lost. As a result, a real-time automated monitoring system becomes extremely in demand for detecting damage in its early stage.

SHM is able to continually monitor structural physical properties such as strain, loading, vibration, cracks, etc. One remarkable advantage of distributed optical fiber sensors (DOFS) is that desired measurands can be obtained in a distributed way and

Reproduced with permission of the copyright owner. Further reproduction prohibited without permission.

spatial profiling can easily be accomplished [Alasaarela 2002]. So far the studies of DOFS have remained in the static measurements like strain and temperature. However, the structural response under impact wave has been recognized as a global damage detection method [Doebling 1996]. The vibration signal is taken as an indicator of the structural or mechanical condition with changes being recognized as structure degradation. Thus, a distributed vibration sensor needs to be developed in order to achieve the dynamic measurement over a large range for monitoring the structural health condition in real time.

3.1.2 Intrusion sensing

Perimeter security is of concern at various places such as: military bases, power plants, national boarders, airports, prisons, etc. A qualified intrusion sensor should be able to identify intrusion attempts (e.g. entering restricted areas, climbing, cutting fences), pinpoint the location in a timely way, and cover a large area as well. Thanks to its distributed ability over a long length, DOFS has its superiority over other commercially available techniques [Juarez 2005]. The optical fibers as sensing media are usually buried under the surface of the perimeter or attached to the fence. The additional fibers in the same cable may serve as communication channels.

Outdoor perimeter sensors face challenges of environmental disturbances for instances: rain, snow, wind or animals. The system must maintain its detection ability under these adverse conditions while minimizing false alarms which reduces confidence in the security system's performance. It is not quite feasible to distinguish the intrusion signal from the environmental disturbances merely by using the light intensity differences

Reproduced with permission of the copyright owner. Further reproduction prohibited without permission.

obtained from static sensors [Kapounek 2001]. Therefore we expect a distributed vibration sensor is capable of providing vibration information of various disturbances in order to identify valid alarms, by which the rate of false alarm can be significantly reduced.

3.1.3 Conventional vibration sensors

Vibration sensors usually measure acceleration of the object, so they are also widely known as an accelerometer. The first attempt of building an accelerometer involved using the resistance strain gauge [Omega Literature]. A metallic wire is bonded directly to the strained surface, and a change in the wire's resistance is proportional to the strain. However, the strain gauge accelerometers are fragile and could only produce low resonance frequencies and they also exhibited a low frequency response [Patrick 2007]. Hence, strain gauges are mainly applied to measure static strains nowadays.

Piezoelectric accelerometers are proven to be a much better alternative to the strain gauge types for dynamic measurements. The vibration force causes the seismic mass to squeeze the piezoelectric material which in-turn produces an electrical charge that is proportional to the vibratory motion. There is a build-in micro-circuit that converts the charge into voltage in order to easily interface with other standard instrumentation. Then the acceleration output can be integrated to get velocity and displacement information of the object. Since the piezoelectric accelerometer allowed for a reduction in its physical size at the manufacturing level, it has a high frequency response (up to tens of kHz) and has the ability to generate high resonant frequencies [Patrick 2007].

In this thesis, one piezoelectric type accelerometer (Brüel & Kjær model 4513) is used

Reproduced with permission of the copyright owner. Further reproduction prohibited without permission.

to compare with our proposed optical fiber sensor. The sensor head is about 10mm diameter as shown in Fig. 3.1. The sensitivity of an accelerometer is expressed in terms of voltage per unit acceleration (mV/g). With built-in preamplifiers, its sensitivity reaches 100mV/g. Its frequency response is up to 10kHz.

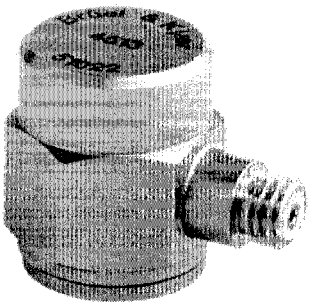

Figure 3.1 Image of the piezoelectric accelerometer (Brüel & Kjær 4513).

3.2 Optical fiber vibration/acoustic sensor

3.2.1 Point sensors

Vibration or acoustic events can be measured by a variety of optical fiber point sensors, such as fiber Bragg grating (FBG), many types of interferometer and intensity-based optical fiber sensor.

A FBG is a wavelength-dependent filter/reflector formed by introducing a periodic refractive index structure within the core of an optical fiber. The reflected optical signal is very narrow and is centered at the Bragg wavelength λ_B, which is related to the periodic unit spacing Λ and the effective refractive index n of the grating in the fiber core, $\lambda_B = 2n\Lambda$. Since the spacing varies with respect to the strain or sound pressure acting upon it, the reflected light intensity of a given wavelength changes accordingly [Berkoff 1996, Rao 1997, Hathaway 1999]. Fig. 3.2 depicts a typical FBG structure with refractive

Reproduced with permission of the copyright owner. Further reproduction prohibited without permission.

index profile and spectral response. In order to realize wide-area monitoring, an FBG acoustic sensor array that detects the acoustic field at multiple points by the time-division multiplexing (TDM) technique has been demonstrated [Yokosuka 2005].

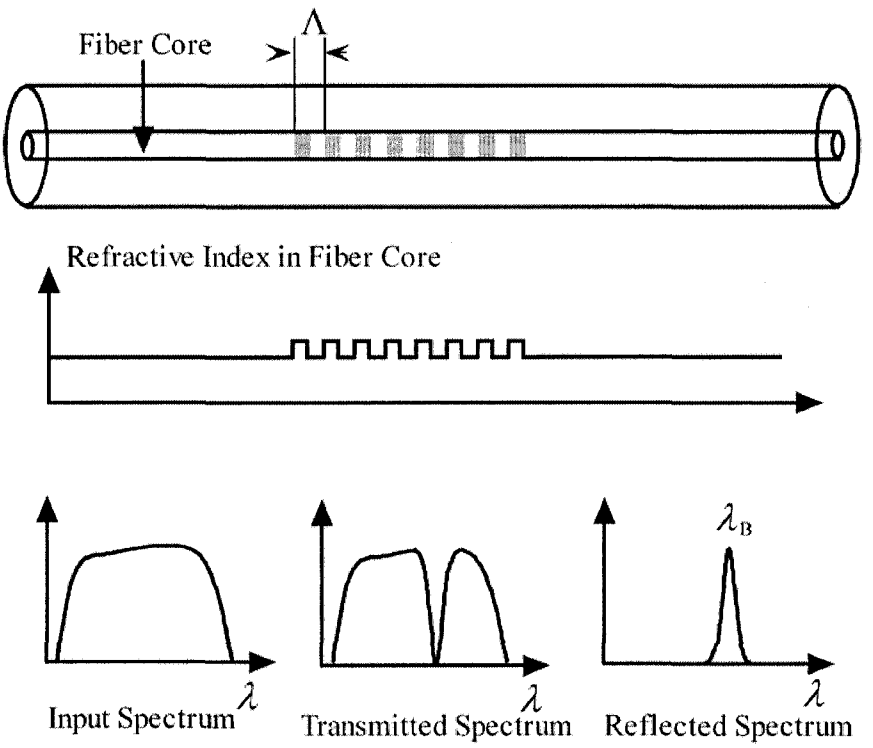

Figure 3.2 A Fiber Bragg Grating structure, with refractive index profile and spectral response.

Optical interferometers are well-known for their ability to make high precision measurement of any physical parameter that affects, directly or indirectly the optical path difference or a refractive index change in the interferometer. Laser-based interferometry has become a standard technique for distance and vibration measurement [Grattan 2000a]. A Michelson Interferometer has been adopted to do the damage detection by testing the acoustic emission in the composite material [Liu 1999]. And it has been reported [Granch 2003] that using 96 in-line Michelson interferometers based on TDM/DWDM

Reproduced with permission of the copyright owner. Further reproduction prohibited without permission.

multiplexing scheme, remotely pumped and controlled fiber-optic sensors array can be achieved for shallow water acoustic surveillance. Also, an extrinsic Fabry-Perot cavity has been implemented for micro-displacement measurement at frequencies as high as 2kHz [Gangopadhyay 1999] and fatigue testing of an F-15 aircraft [Murphy 1992]. Another type of interferometer is known as Sagnac loop, which consists of a long loop closed upon itself by a 3-dB fiber coupler. Such schemes have been studied for nondestructive characterization of material properties and testing structures for flaws [Fomitchov 2000], and underwater sound detection [Digonnet 2004].

A simple intensity-based optical fiber vibration sensor, constructed by placing two cleaved fiber ends in a capillary tube, has been proposed for structural vibrations and damage monitoring of fiber-reinforced plastics [Yang 2002]. It has the ability to detect up to 10kHz signal and to determine the impact location by placing multiple sensors on the object.

3.2.2 Distributed sensors

The most distinguished techniques for fully distributed sensing involve the use of the optical time domain reflectometry (OTDR) [Rogers 1981, Horiguchi 1989] and the optical frequency domain reflectometry (OFDR) [MacDonald 1981, Soller 2005]. The principle of operation is to measure the characteristics of various spatially-distributed scattering such as Rayleigh, Brillouin or Raman.

Light scattering occurs as a consequence of fluctuations in the optical properties of a material medium. As long as the optical properties of the medium are unaltered by the presence of the incident light, the scattering process is said to be spontaneous. Conversely,

Reproduced with permission of the copyright owner. Further reproduction prohibited without permission.

if the intensity of incident light is sufficiently large to modify the properties of the medium, then the regime becomes stimulated [Boyd 2003]. Four types of spontaneous light scattering are schematically shown in Fig 3.3: Rayleigh, Brillouin, Raman and Rayleigh wing.

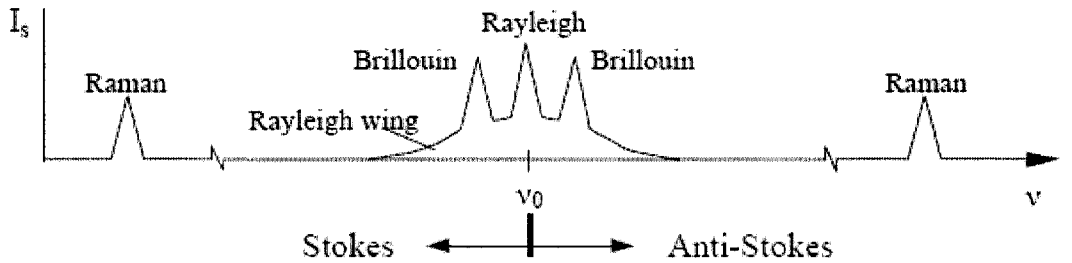

Figure 3.3 A typical observed spectrum of light scattering. Frequency and intensity axis are not scaled to reproduce accurately the peaks heights and frequencies [Boyd 2003].

The centre line without frequency shift is called Rayleigh scattering. It is a result of nonpropagating density fluctuations, which in turn causes random microscopic variations in the refractive index. Rayleigh scattering is an elastic scattering process, i.e. the frequencies of incident and scattered light are equal. The two spectral lines caused by Brillouin scattering appear on both sides of the Rayleigh peak. By definition, the line with frequency downshift is known as Stokes component, whereas the line with frequency upshift is known as anti-Stokes component. Brillouin scattering is attributed to sound waves, which are propagating pressure waves and hence refractive index waves in the medium. Alternatively, the incident light can be considered to be scattered by acoustic phonons, corresponding to the quantized mode of vibration occurring in the lattice due to sound waves. The photon-phonon interaction in silica optical fiber creates a Brillouin frequency shift ~ 11GHz for 1550nm input light. Raman scattering results from the interaction of light with molecular vibrations in the medium, or also known as optical

Reproduced with permission of the copyright owner. Further reproduction prohibited without permission.

phonons. The Raman scattered light is shifted in frequency by about 13THz for the 1550nm wavelength, about three orders of magnitude higher than that of Brillouin scattering. Both Raman and Brillouin scattering are inelastic processes due to the energy exchanges between light and phonons (acoustic or optical). The last mechanism is called Rayleigh wing scattering, which is scattering from fluctuation in the orientation of anisotropic molecules. The spectral line of Rayleigh wing is very broad due to the rapid process of molecular reorientation. Rayleigh wing scattering does not occur for molecules with isotropic polarisability tensors [Boyd 2003], which is the case for optical fibers as the silica molecule is centro-symmetric.

Here, we focus on the implications of Rayleigh, Brillouin and Raman scattering for the purpose of distributed sensing. Rayleigh backscattering is now used routinely in the optical communication system for the evaluation of installed fiber links. As the temperature dependence of Rayleigh backscattering intensity is very weak (0.015%/°C) in silicon fibers [Li 2003a], some special optical fibers need to be developed. Hartog achieved a ±1°C temperature resolution with 1m spatial resolution in a liquid-core fiber [Hartog 1983]. As for Brillouin scattering, the backscattered light experienced a frequency shift which depends linearly to the variations of temperature and strain. Such sensor has gained much attention in recent years for distributed monitoring applications: for temperature from –270°C to 800°C [Li 2003b], for static strain ranging from several με to 20,000 με [DeMerchant 2000], and for measuring temperature and static strain simultaneously [Smith 1999, Bao 2004]. Raman scattering, another nonlinear effect in fiber can also be implemented for temperature sensing purposes. The energy level diagram in Fig. 3.4 depicts the process of Raman scattering schematically. In thermal

Reproduced with permission of the copyright owner. Further reproduction prohibited without permission.

equilibrium the population of molecules at a vibrational state is much smaller than that at the ground state. In the presence of incident light, some molecules experience a transition from the ground state to the vibrational state by means of an intermediate transition associated with an excited state. This process is known as Raman Stokes scattering. While for the anti-Stokes scattering, the transition is from the vibrational state to the ground state through the excited state. Since the molecular population at the vibrational state is strongly depend on temperature, Raman scattering has far higher temperature sensitivity (0.8%/°C at the anti-Stokes band [Grattan 2000b]) than that of Rayleigh scattering. As a result, several Raman-OTDR systems have become commercially available.

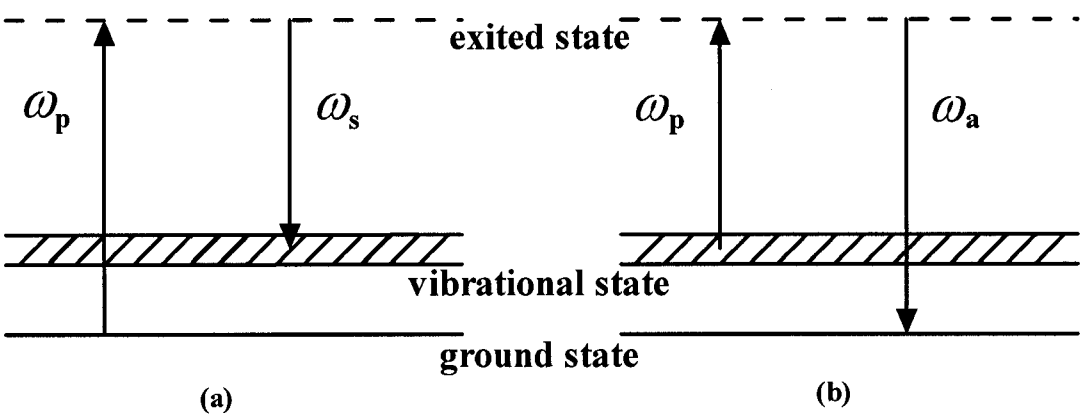

Figure 3.4 Energy level diagrams for **(a)** Raman Stokes scattering and **(b)** Raman anti-Stokes scattering.

From what precedes, up to now, the study of fully distributed sensors remains largely to static measurements, limited by the testing speed. This is due to the weak backscattering signals in OTDR systems or the frequency scanning speed of the tunable laser in OFDR systems. Recently, Bao *et al.* proposed a dynamic Brillouin fiber sensor to

Reproduced with permission of the copyright owner. Further reproduction prohibited without permission.

monitor distributed impact wave on highway concrete slabs by the high-speed trucks or cars [Bao 2008]. The sensing scheme lies on the polarization change dependences on the Brillouin gain spectrum. It has demonstrated frequency detection as high as 200Hz over 300m of fiber. The test speed is limited by waveform averaging, which is used for eliminating signal fluctuation due to the weak Brillouin backscattering.

3.3 Optical time domain reflectometry (OTDR)

As mentioned in the previous section, OTDR and OFDR are two common schemes to achieve distributed sensing. In an OTDR system, a narrow laser pulse is launched into a fiber and a fraction of light is continuously backscattered and detected. The spectral linewidth of the laser is as wide as ~10nm to avoid the interference of backscattered light from different fiber portions. The spatial resolution of an OTDR system can be improved as the pulse is shortened and the measurement bandwidth is broadened. However, this leads to the increase of noise level and in turn the decrease of dynamic range (detailed discussions will be given in Section 3.3.3). In general, OTDR systems are applied to cover ~km range with several-meter spatial resolution. While in OFDR techniques, a highly coherent laser is linearly swept in a certain frequency range and the continuous wave (CW) light is coupled into a Michelson fiber interferometer. Then the interference patterns created from the interaction of the backscattered light from both sensing and reference arms are detected. The tunable laser is a crucial component in OFDR: the coherent length of the laser, the laser frequency sweep range as well as the sweep speed influence the achievable spatial resolution and measurement range. Since the currently available tunable lasers depart from perfect coherence and produce phase noises that

Reproduced with permission of the copyright owner. Further reproduction prohibited without permission.

prevents a wide frequency sweep range, OFDR is predominantly used for characterization of optical lines of medium length (tens to hundreds of meter) with sub-centimeter resolution [Oberson 2000].

Since perimeters and large structures are our target applications as stated in section 3.1, the OTDR type is chosen here to be the basic sensing configuration. This section introduces the theoretical background, operation fundamentals and key parameters of a conventional OTDR.

3.3.1 Rayleigh backscattering in the fiber

Scattering losses in fiber arise from local microscopic fluctuations in density occurring during fiber fabrication, which leads to refractive index variations on a scale smaller than the optical wavelength λ. This phenomenon is termed Rayleigh scattering [Born 1999]. The scattered intensity is proportional to $1/\lambda^4$, so that the longer wavelengths exhibit lower scattering losses than shorter wavelengths. The intrinsic loss of silica fibers from Rayleigh scattering is expressed as

$$\alpha_s = C/\lambda^4 \tag{3.1}$$

where the constant C is in the range of $0.7-0.9(dB/km)-\mu m^4$, depending on the constituents of the fiber core [Agrawal 2002]. Rayleigh scattering does not cause conversion of optical energy, in other words frequency of light remains unchanged during the process.

Rayleigh scattering and material absorption are two important causes of fiber losses. Hence, the total attenuation coefficient α (with units of km^{-1}) is composed of a scattering

Reproduced with permission of the copyright owner. Further reproduction prohibited without permission.

coefficient α_s and an absorption coefficient α_a

$$\alpha = \alpha_a + \alpha_s \tag{3.2}$$

At the telecommunication window, $\lambda = 1.55\mu m$, the scattering coefficient equals to 0.12-0.16dB/km, indicating that fiber loss is dominated by Rayleigh scattering near this wavelength [Agrawal 2002].

Owing to these fiber losses the optical power decreases exponentially as a function of the propagating distance z

$$P(z) = P_0 e^{-\alpha z} \tag{3.3}$$

where P_0 is the incident light power and $P(z)$ is the transmitted power at distant z. In practice, the attenuation coefficient α is usually expressed in units of dB/km. Then

$$P(z) = P_0 \cdot 10^{\frac{-\alpha_{dB} z}{10}} \tag{3.4}$$

with

$$\alpha_{dB} = \frac{10}{\ln 10} \cdot \alpha \approx 4.34\alpha \tag{3.5}$$

Now let's focus on the backscattered light along the fiber distance when a laser pulse with peak power P_0 and temporal duration T_0 is launched into the fiber. The backscattered power $dp_{bs}(z)$ from an infinitesimal small fiber section can be detected at the input end of the fiber [Neumann 1980].

$$dp_{bs}(z) = S \cdot \alpha_s \cdot P_0 \cdot e^{-2\alpha z} dz \tag{3.6}$$

Rayleigh scattering radiates in all directions and the backscattering capture coefficient S describes the part of light directed backwards. It can be obtained in the form of [Derickson 1998]

Reproduced with permission of the copyright owner. Further reproduction prohibited without permission.

$$S = \left(\frac{NA}{n_1}\right)^2 \cdot \frac{1}{m} \tag{3.7}$$

where $NA = \sqrt{n_1^2 - n_2^2}$ is the numerical aperture, n_1, n_2 are the refractive indexes of the core and cladding respectively. Coefficient m depends on the refractive index profile and has a typical value of 4.55 for single mode fibers [Hentschel 1989].

Light travels inside the optical fiber at the velocity $v_g = c/n_1$, where c is the light speed in vacuum. Using the relation $2z = v_g t$ and $dz = \frac{1}{2} v_g dt$, the equation (3.6) can be rewritten into the form

$$dp_{bs}(t) = \frac{S \cdot \alpha_s \cdot P_0 \cdot v_g}{2} \cdot e^{-\alpha v_g t} dt \tag{3.8}$$

Scattering processes at a certain position z only happen when the laser pulse is passing through. Taking the integration of (3.8) from $t - T_0$ (T_0 is the pulsewidth) to t yields the well-known formula for backscattered power $P_{bs}(z)$ [Jasenek]

$$P_{bs}(z) = \frac{S \cdot \alpha_s \cdot P_0 \cdot T_0 \cdot v_g}{2} \cdot e^{-2\alpha z} \tag{3.9}$$

The exponent of the last term in the above equation, $-2\alpha z$, is due to the fact that the light has travelled a round-trip inside the fiber.

If the fiber parameters (S, α_s, v_g, α) are constant, then the maximum detectable backscattered power can be enhanced by $P_0 \cdot T_0$, which defines the energy of the input pulse. For a certain laser source, the maximum launched power P_0 is fixed, so the backscattered power level only depends on pulsewidth T_0. Therefore, a backscatter factor

Reproduced with permission of the copyright owner. Further reproduction prohibited without permission.

σ in dB for a given pulsewidth has been introduced to indicate the maximum backscattered power that returns to the OTDR receiver.

$$\sigma = -10 \cdot \log(S \cdot \alpha_s \cdot T_0 \cdot v_g) \tag{3.10}$$

For standard SMF at $\lambda = 1.55\mu m$, the value of σ is about $52dB/1\mu s$ [Derickson 1998]. This means that for a $1\mu s$ rectangular pulse the near-end backscatter level $P_z(0)$ is 52dB below the pulse peak power P_0. If the pulsewidth decreases to $100ns$, then the backscatter level becomes 62dB lower accordingly.

3.3.2 Fundamentals of OTDR operation

The OTDR method was invented by Barnoski and Jensen in 1976 [Barnoski 1976], in a time when optical fiber manufacturing was at its early stages. The basic idea of the proposed method consisted of sending a short optical pulse into a testing fiber and detecting the continuous backscattered power at the input end. The measurement of backscattered power as a function of position provides a detailed picture about the local distribution of the attenuation effects such as: scattering loss, fusion splice, connector, bend and so on.

Fig. 3.5 illustrates the schematic block diagram of a conventional OTDR setup. A pulsed laser is commonly used to generate a short and intense pulse which is launched into the fiber under test (FUT) through a circulator or a 3dB coupler. As the pulse travels along the fiber, part of the light is lost by Rayleigh scattering and other attenuation events. The backscattered and back reflected light returning to the input end are guided to a photodetector through the circulator. The signal is then amplified, digitized and displayed for the operator to view.

Reproduced with permission of the copyright owner. Further reproduction prohibited without permission.

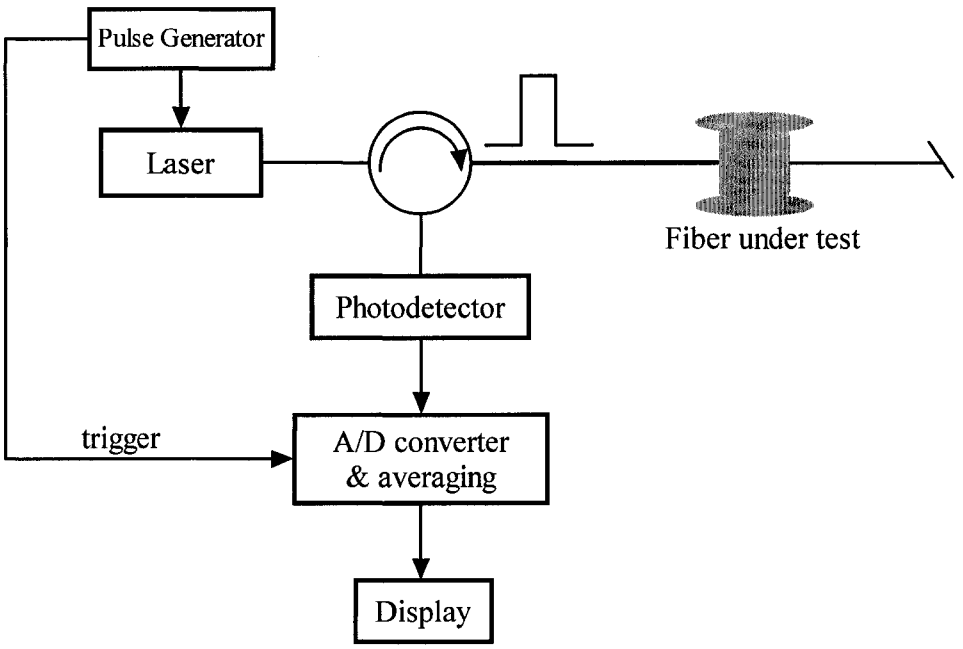

Figure 3.5 Schematic diagram of a conventional OTDR.

The photodetector typically used is an avalanche photodiode (APD). The design of APDs differs from that of p-i-n photodiodes mainly in one respect: an additional layer is added in which an accelerating electron can acquire sufficient energy to generate a new electron-hole pair. Due to this internal current gain, APDs have the ability to detect relatively weak optical power compared to p-i-n photodiodes. The photodetector's bandwidth should be carefully chosen as it may affect the SNR of the system and the spatial resolution. Due to two noise mechanisms, shot noise and thermal noise, the current fluctuates in all photodetectors even when the incident optical power is constant. And the total receiver noise is in direct proportion to the detector's bandwidth [Agrawal 2002]. On the other hand, small spatial resolution requires short input pulses and consequently a broader bandwidth to detect. Clearly wider bandwidth allows us to resolve two close events, but would lower the SNR.

Reproduced with permission of the copyright owner. Further reproduction prohibited without permission.

The testing results are represented by an OTDR trace as shown in Fig. 3.6. The horizontal axis is marked in distance units while the vertical scale corresponds to backscattered signal level on a logarithmic scale (dB). Actually, the photodetector measures the linear backscattered power $P_s(z)$ as function of time directly. Then considering the light travels a round-trip in the fiber, the power in dB units and fiber distance can be calculated using equation $5 \cdot \log(P_s(z)/1mW)$ and $v_g \cdot t/2$, respectively.

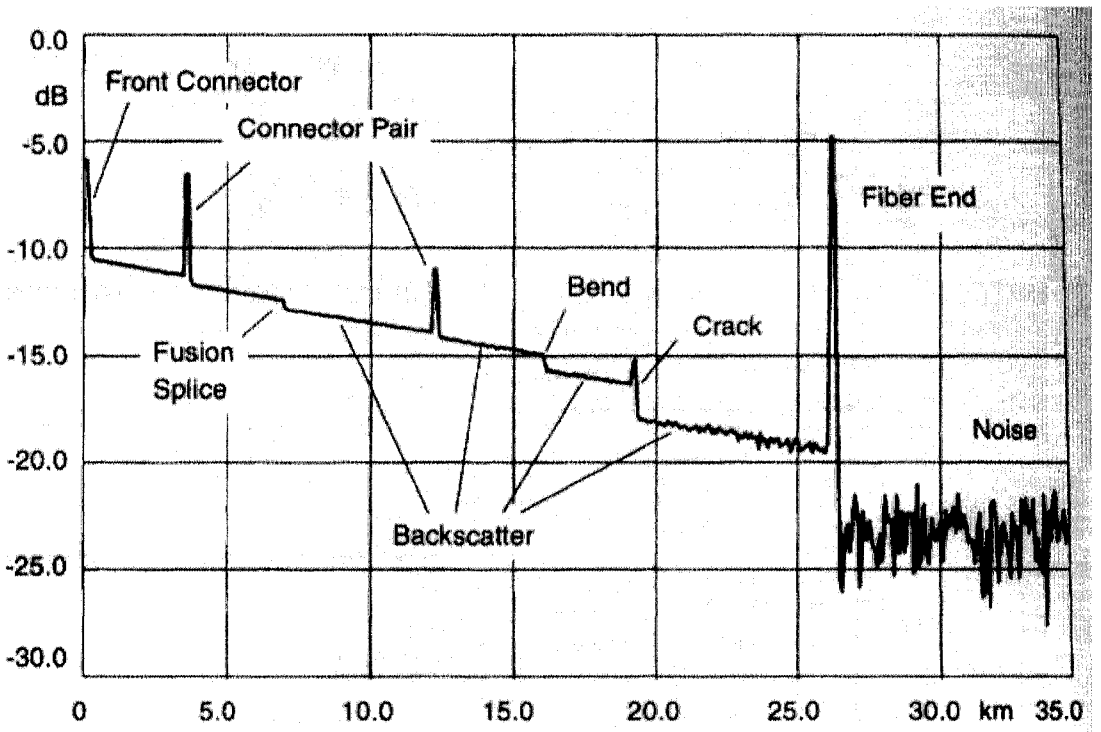

Figure 3.6 A typical OTDR trace [Derickson 1998].

The OTDR trace typically exhibits three types of features: 1) the straight decreasing line results from Rayleigh backscattering with the slope giving the attenuation coefficient of the fiber in dB/km; 2) sharp spikes caused by connectors or cracks with the height of the peak indicating the amount of reflection; 3) sudden drops caused by fusion splices or bends with the step size corresponding to the insertion loss. The large spike at the end of

Reproduced with permission of the copyright owner. Further reproduction prohibited without permission.

the trace results from the open non-terminated fiber end with a glass-to-air transition. Behind the fiber end, the received signal drops to the detector's noise which limits the OTDR system's ability.

3.3.3 Performance parameters

In order to further investigate the performance of the OTDR system, three key parameters are discussed in detail here. They are dynamic range, spatial resolution and dead zones.

Dynamic range is defined as the difference between the initial backscatter power level and the noise level of a measurement time, expressed in dB of one-way fiber loss [Derickson 1998]. Consequently, to increase the system's dynamic range one needs either to enhance the backscatter power or to decrease the noise level. From the discussion after equation (3.9), the backscatter level depends on the energy of the pulse $P_0 \cdot T_0$. However, the pulse peak power P_0 should be lower than a certain level to avoid the occurrence of non-linear effects in the fiber. For instance, the threshold of peak power for stimulated Brillouin scattering (SBS) and stimulated Raman scattering (SRS) is about tens of mW and hundreds of mW respectively [Agrawal 2002]. So for the purpose of increasing the pulse energy the only possibility left is to increase the pulsewidth T_0 to get higher backscattered level. As for the noise level (induced by shot noise and thermal noise), signal averaging is a common way of reducing the noise, but will sacrifice testing speed in the process. It has been shown that after the N times repeated measurements the SNR

Reproduced with permission of the copyright owner. Further reproduction prohibited without permission.

obtained by averaging signal is $\sqrt{N}$ times greater than that in one measurement [Sischka 1988].

Spatial resolution is regarded as an indicator of the system's ability to resolve two adjacent events. Provided the pulsewidth is T_0, the spatial resolution can not be better than $\Delta z = \pm T_0 v_g / 2$. Thus, the larger pulsewidth implies higher dynamic range but also a worse spatial resolution. This trade-off between the dynamic range and spatial resolution represents the fundamental limit of the conventional OTDR. During the system design there is always a need of some compromises among those performance parameters.

Dead zones are caused by strong reflection from reflective events along the fiber. During the time in which the whole input pulse passes through the reflective events and the recovery time from detector saturation, the attenuation information of a certain span of fiber close to the point of reflection is lost. Depending on the input pulsewidth and detector bandwidth, the value of dead zones is usually between several to hundreds of meters. An easy way for the elimination of the dead zones from the front connector is to add a blind subsidiary fiber before the tested fiber.

3.4 Polarization-OTDR

As we have seen in the previous section, the conventional OTDR only makes use of the intensity change of the backscattered or reflected light along the fiber link. Since the unpolarized light intensity is insensitive to environmental effects, the original OTDR technique was not able to work as a distributed sensor until Rogers proposed to a modified OTDR in which the state of polarization (SOP) of light is monitored rather than

Reproduced with permission of the copyright owner. Further reproduction prohibited without permission.

the intensity [Rogers 1981]. Later on this method was designated as the Polarization-OTDR. The principle is based on the fact that the Rayleigh backscattered light in fiber contains additional information about the spatially distributed polarization states. As the local birefringence in the fiber is very sensitive to environmental effects, the SOP of light varies accordingly.

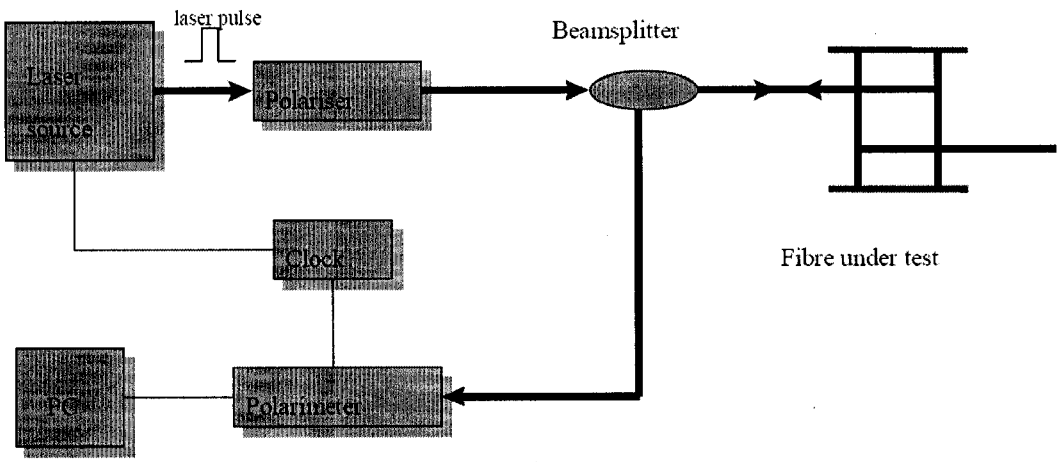

Figure 3.7 Basic arrangement for Polarization-OTDR system [Roger 2005].

The basic system arrangement is shown in Fig 3.7. A polarized optical pulse is launched into the fiber instead of using unpolarized light, and the continuous backscattered light is collected by a polarimeter via a beamsplitter. A polarimeter refers to the receiver end of a polarization analyzer as described in section 2.3.1 (Fig. 2.9 (a) and (b)): SOP of the backscattered light along the fiber can be determined through the detection of the four Stokes parameters. The linewidth of the laser source in Polarization-OTDR should be narrower than that in OTDR in order to prevent depolarization in wavelength [Chausse 1995]. Some possible measurements have been suggested by

Reproduced with permission of the copyright owner. Further reproduction prohibited without permission.

Rogers, including magnetic field, pressure, temperature and mechanical stress [Rogers 1981]. Distributed measurement of up to 50-bar pressure (normal air pressure = 1.013 bar) has been demonstrated by the Polarization-OTDR system in the lab environment [Rogers 2005]. However, the cross sensitivity of the polarization states change to various external disturbances makes it impossible to separate them through static measurement.

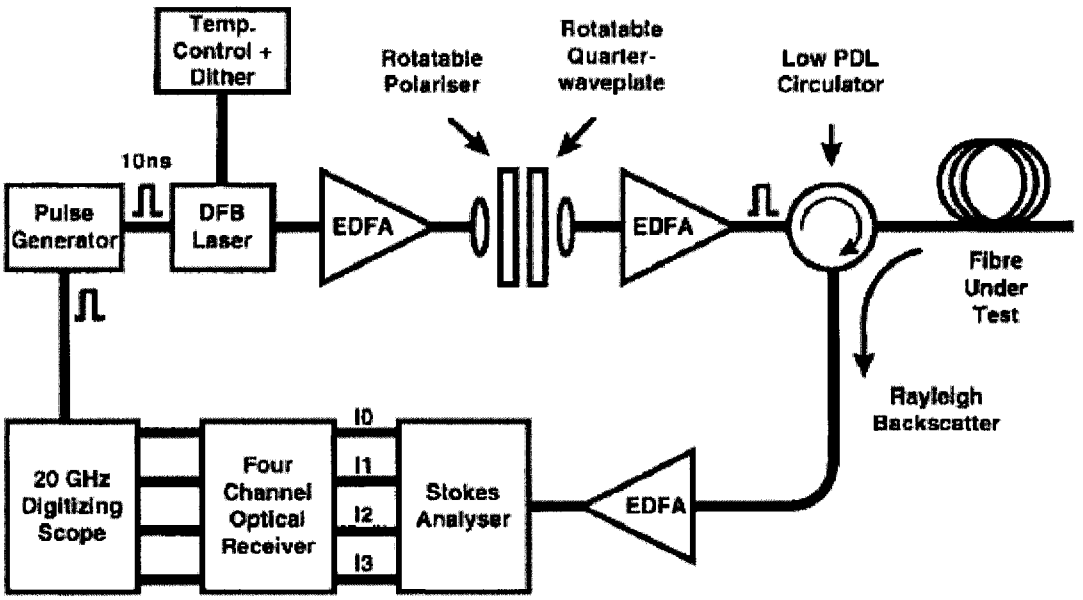

Figure 3.8 Another Polarization-OTDR arrangement [Ellison 1998].

With the rapid development of high bit-rate telecommunication systems, Polarization-OTDR re-gained attention around the late 90's for its ability of evaluating local birefringence properties of the fiber link and identifying the fiber sections with high PMD [Ellison 1998, Hunttner 1999, Galtarossa 2004]. The constructed model is to imagine the fiber as composed of a set of segments with individual Jones matrices. Having the knowledge of the input and backscattered polarization states from different segments

Reproduced with permission of the copyright owner. Further reproduction prohibited without permission.

makes it possible to derive those Jones matrices along the fiber and consequently obtain the local birefringence. As a result, different input polarization states need to be generated and launched into the fiber separately. As shown in Fig 3.8, the input polarization state is adjusted by a rotatable polarizer and a quarter-waveplate while the backscattered states at different locations are collected by a polarization (Stokes) analyzer. The Jones matrices along the fiber are then derived.

It is worth mentioning that this advanced Polarization-OTDR approach enables a static measurement for distributed birefringence in the fiber link. It involves four-channel detection, a complex algorithm and a large number of averages. As for the purpose of vibration measurement when the testing speed becomes the primary concern, a simplified system and faster data processing should be searched for. Details of our proposed Polarization-OTDR with corresponding analysis method can be found in Chapter 8.

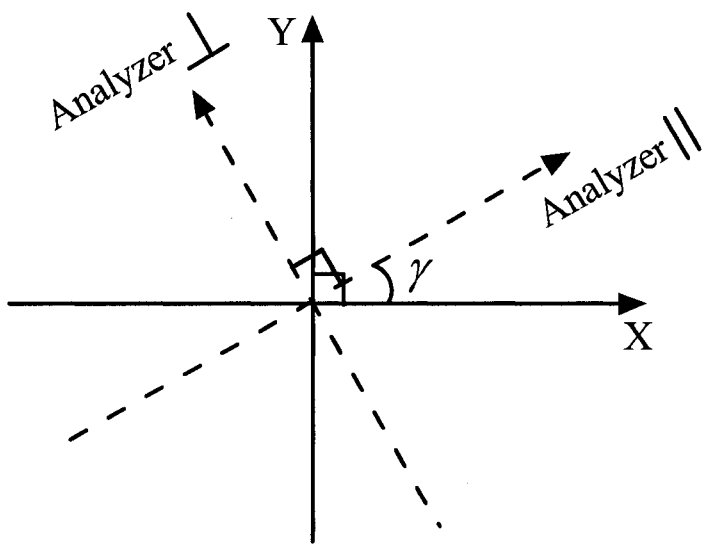

Figure 3.9 Schematic relation between the direction of the polarizer and the backscattered electric fields.

Reproduced with permission of the copyright owner. Further reproduction prohibited without permission.

Now let's focus on the measured Polarization-OTDR trace and how it differs from the conventional OTDR trace in Fig 3.6. Here we consider a simple case when the pulse is sent into a span of polarization maintaining fiber, so that the slow (x) and fast (y) axis remains unchanged.

If the analyzer element (i.e. polarizer) before the detector makes an angle γ with the x-axis of electrical field as illustrated in Fig 3.9, then the backscattered light power parallel or orthogonal to the analyzer has the form [Nakazawa 1981, Nakazawa 1983]:

$$P_{bs\parallel}(z) = [(P_{0x}\cos^2\gamma + P_{0y}\sin^2\gamma) + \sqrt{P_{0x}P_{0y}}\cdot\sin 2\gamma\left\{\frac{\sin(\Delta\beta v_g T_0/2)}{\Delta\beta v_g T_0/2}\right\}\cdot\cos 2\Delta\beta z]\cdot\frac{Sv_g T_0\alpha_s}{2}\cdot e^{-2\alpha z} \quad (3.11a)$$

$$P_{bs\perp}(z) = [(P_{0x}\sin^2\gamma + P_{0y}\cos^2\gamma) - \sqrt{P_{0x}P_{0y}}\cdot\sin 2\gamma\left\{\frac{\sin(\Delta\beta v_g T_0/2)}{\Delta\beta v_g T_0/2}\right\}\cdot\cos 2\Delta\beta z]\cdot\frac{Sv_g T_0\alpha_s}{2}\cdot e^{-2\alpha z} \quad (3.11b)$$

where P_{0x} and P_{0y} are the incident light power in x and y axis, respectively; $\Delta\beta = \beta_x - \beta_y$ is the difference between propagation constant along x and y axis; while T_0 is the pulse width. The first item $(P_{0x}\cos^2\gamma + P_{0y}\sin^2\gamma)\cdot\frac{Sv_g T_0\alpha_s}{2}\cdot e^{-2\alpha z}$ in equation (3.11) represents an exponential decay; while when combined to the second item with $\cos 2\Delta\beta z\cdot e^{-2\alpha z}$, it forms a damped fluctuation along the fiber length as illustrated in Fig. 3.10. It is evident that the beat length of the fiber ($L_b \propto \frac{1}{\Delta\beta}$) can be obtained by the Polarization-OTDR trace.

Reproduced with permission of the copyright owner. Further reproduction prohibited without permission.

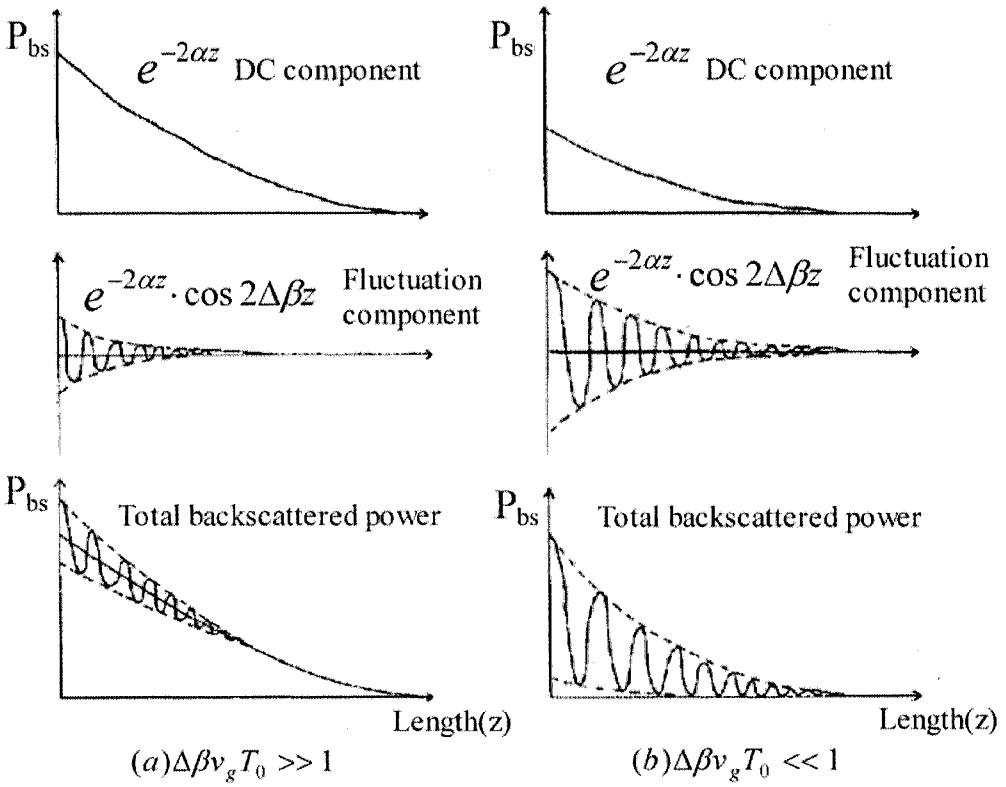

Figure 3.10 Polarization-OTDR trace: (a) for broad pulses; (b) for short pulses [Nakazawa 1983].

We further notice that the amplitude of the fluctuation is determined by the sinc function $\left\{\frac{\sin(\Delta\beta v_g T_0/2)}{\Delta\beta v_g T_0/2}\right\}$. For shorter pulses where $\Delta\beta v_g T_0 << 1$, $\left\{\frac{\sin(\Delta\beta v_g T_0/2)}{\Delta\beta v_g T_0/2}\right\}$ approaches its maximum value 1 which makes the fluctuation part being observed more clear, like as shown in Fig 3.10(b) [Nakazawa 1983]. Also, from equation (3.11), as the fluctuation parts of $P_{bs\parallel}(z)$ and $P_{bs\perp}(z)$ are with the same value but opposite signs, the fluctuation disappears by adding them. The total backscattered light power then becomes

$$P_{bs}(z) = P_{bs\parallel}(z) + P_{bs\perp}(z) = (P_{0x} + P_{0y}) \cdot \frac{S v_g T_0 \alpha_s}{2} \cdot e^{-2\alpha z} \qquad (3.12)$$

Reproduced with permission of the copyright owner. Further reproduction prohibited without permission.

This is exactly the same as equation (3.9), the one we derived for OTDR trace in the previous section.

Reproduced with permission of the copyright owner. Further reproduction prohibited without permission.

Chapter 4

Polarization dependent loss vector measurement in a system with polarization mode dispersion

[Liang Chen, **Ziyi Zhang** and Xiaoyi Bao, "Polarization dependent loss vector measurement in a system with polarization mode dispersion," *Optical Fiber Technology,* 12, 251-254 (2006)]

The first part of my thesis (Chapter 4 ~ Chapter 6) studies polarization effects in optical fiber communication system. This chapter proposes a fast PDL measurement method in a system with PMD.

As mentioned in Chapter 2, for a long fiber link with over km length the PSP and DGD fluctuate stochastically with frequency and time. This introduces complexity in the measurement or compensation of polarization effects. Thus it is impossible to predict the impairment of the system at any particular frequency and time; instead, one has to resort a statistical description as shown in Section 2.1.2. With the usage of >10Gbits/s high speed communication system polarization effects become a major impairment that may severely degrade the system performance. For the purpose of PMD mitigation, due to its stochastical nature, dynamic PMD and PDL need to be measured in real-time before

Reproduced with permission of the copyright owner. Further reproduction prohibited without permission.

making decision for any necessary compensation. As a result, a fast polarization measurement method has been always searched for.

A variety of PMD and PDL measurement techniques are available; in particular, two common techniques (the interferometric method and the JME method) have been discussed in details in Section 2.3. Since the JME method measures SOPs at different frequencies and then derives PMD vectors with respect to frequency, it has ability to obtain the statistical characteristics of polarization effects rather than a mean value. This is the reason why the JME is a widely used method for polarization measurement nowadays. The commercial polarization analyzer HP 8509B in our lab adopts the JME method and its block diagram and measurement setup have been presented in Fig. 2.9. The JME method needs complete knowledge of the input and the output SOP during polarization measurements.

Chen *et. al.* proposed a new PMD vector measurement method based on the equation of motion in Stokes space [Chen 2004], which only requires three output SOPs and their derivatives. My work in this chapter is to extend the above generalized Poincaré sphere method to derive a frequency dependent PDL vector in a system interacting with PMD.

With the output PDL vector equation of motion and one initial PDL vector at a specific frequency, the PDL vector at the neighboring frequencies can be computed using numerical integration. PDL obtained from our proposed method is in good agreement with the well-known JME method experimentally. Combined with the PMD vector method in [Chen 2004], we believe we are able to get spectrally resolved PMD and PDL vectors of a fiber link with the least measurement steps. Our new method should become

Reproduced with permission of the copyright owner. Further reproduction prohibited without permission.

superior over other available methods when the testing speed is critical to respond dynamic PMD and PDL, especially in field tests.

Reproduced with permission of the copyright owner. Further reproduction prohibited without permission.

Available online at www.sciencedirect.com
SCIENCE DIRECT®
Optical Fiber Technology 12 (2006) 251–254
Optical Fiber Technology
www.elsevier.com/locate/yofte

Polarization dependent loss vector measurement in a system with polarization mode dispersion

Liang Chen, Ziyi Zhang *, Xiaoyi Bao

Department of Physics, University of Ottawa, Ottawa, ON K1N 6N5, Canada

Received 14 March 2005; revised 23 June 2005
Available online 17 October 2005

Abstract

A polarization dependent loss (PDL) vector equation of motion in Stokes space was derived in a system interacting with polarization mode dispersion (PMD). A new PDL measurement method based on the PDL vector equation was proposed and validated by numerical simulation and experiment.
© 2005 Elsevier Inc. All rights reserved.

Keywords: Polarization mode dispersion; Polarization dependent loss

1. Introduction

Polarization mode dispersion (PMD) [1,2] and polarization dependent loss [3] have the potential to severely degrade the high bit-rate (>10 Gb/s) communication systems. Because of the dynamic disturbance of the environment to the field fiber it is very important to search method that can quickly and accurately monitor the PMD ad PDL properties of a fiber link. Our goal is to find a spectrally resolved PMD and PDL measurement method that requires the least measurement procedures. Gisin and Hunter first studied the combined effects [3] of PMD and PDL showing that the two principal states of polarization (PSP) are not orthogonal due to the interaction of PMD and PDL. Furthermore as a result of PMD and PDL interaction the PMD vector becomes complex. Analytical methods [4–6] have been reported to evaluate the pulse broadening using moment method. However all methods require the information of *input* wavelength dependent characterization of PMD and PDL vector of the fiber link. Although there is no principle difficulty in obtaining the *input* PMD and PDL vector, we find it is much easier to characterize a fiber link via its *output* PMD and PDL vectors. The complex PMD vector can be either measured by the Jones matrix eigenanalysis [7,8] or using the output state of polarization equation of motion on the Poincaré sphere [9]. PDL can be measured by deterministic methods [10,11] like Jones matrix eigenanalysis and Mueller matrix method, or nondeterministic method like polarization scanning [11]. However, both Jones matrix and Mueller matrix method requires the precise knowledge of both input and output state of polarization (SOP) during the measurement. In this paper we derived a new PDL equation of motion on Poincaré sphere, which allows wavelength dependent PDL vector measurement. This method requires the knowledge of PDL vector at only *one* specific wavelength and by using the wavelength dependent complex PMD vector the spectrally resolved PDL vector can be derived. Furthermore, because the PMD vector measurement method proposed by Chen et al. [9] does not need the precise knowledge of the *input* SOP we believe our proposed method is the one that requires the least measurement information to get both PMD and PDL vectors of a fiber link. To get the PMD information, one needs to scan three SOPs while PDL needs four SOPs. After determining the initial PDL vector, this new method is faster than other methods, which use both input and output SOPs for all PDL vectors at every wavelength. In the field test, unlike the static situation, the dynamic PMD and PDL have the critical requirements on the response speed to get real time information. This proposed PDL vector measurement method is validated by simulation and experiment.

* Corresponding author.
E-mail address: ziyi.zhang@science.uottawa.ca (Z. Zhang).

1068-5200/$ – see front matter © 2005 Elsevier Inc. All rights reserved.
doi:10.1016/j.yofte.2005.09.001

Reproduced with permission of the copyright owner. Further reproduction prohibited without permission.

2. Analytical derivation

Our method is based on the relations between Jones matrix, *output* PMD and PDL vectors, which have been first described by Gisin and Huttner [3]. The input electric field $|\vec{E}_{\text{in}}(\omega)\rangle$ and output electric field $|\vec{E}_{\text{out}}(\omega)\rangle$ are related by the Jones matrix $T(\omega)$ in the following:

$$\left|\vec{E}_{\text{out}}(\omega)\right\rangle = T(\omega)\left|\vec{E}_{\text{in}}(\omega)\right\rangle. \tag{1}$$

It is worth emphasizing that because of the interaction between PMD and PDL the Jones matrix is nonunitary in general. The complex output PMD vector $\vec{W}(\omega)$ is then written as [3]

$$\frac{dT(\omega)}{d\omega}\cdot T^{-1}(\omega) = -\frac{i}{2}\vec{W}(\omega)\cdot\vec{\sigma}, \tag{2}$$

where $\vec{\sigma}$ are Pauli matrices. In order to find the PDL information, we define the following relationship:

$$T(\omega)\cdot T^{+}(\omega) = t_0\cdot I + \vec{t}\cdot\vec{\sigma}, \tag{3}$$

where t_0 is a scalar, $\vec{t}$ is a real vector pointing in the direction of maximum transmission polarization in the Stokes space, and the superscript symbol + means Hermitian operation. Output electric field is $|\vec{E}_{\text{out}}(\omega)\rangle = g(\omega)|\vec{\varepsilon}_{\text{out}}(\omega)\rangle$, here $g(\omega)$ is output pulse shape, $|\vec{\varepsilon}_{\text{out}}(\omega)\rangle$ is a unit output Jones vector, then we can derive the following:

$$\begin{aligned}\left\langle\vec{E}_{\text{in}}(\omega)\middle|\vec{E}_{\text{in}}(\omega)\right\rangle &= \left\langle\vec{E}_{\text{out}}(\omega)\middle|[t_0+\vec{t}\cdot\vec{\sigma}]^{-1}\middle|\vec{E}_{\text{out}}(\omega)\right\rangle \\ &= \frac{|g(\omega)|^2}{t_0+\vec{t}\cdot\vec{m}},\end{aligned} \tag{4}$$

where $\vec{m} = \langle\vec{\varepsilon}_{\text{out}}(\omega)|\vec{\sigma}|\vec{\varepsilon}_{\text{out}}(\omega)\rangle$ is the *output* unitary Stokes vector. It is thus easy to find the maximum transmission coefficient to be t_0+t (t is the magnitude of the $\vec{t}$) and the minimum transmission coefficient to be $t_0 - t$. The PDL vector is defined as $\vec{\Gamma} = \vec{t}/t_0$. In this way the PDL in the unit of dB can be written as $\text{PDL}_{\text{dB}} = 10\log\frac{1+\Gamma}{1-\Gamma}$. We now derive an equation of motion for the PDL vector $\vec{\Gamma} = \vec{t}/t_0$. To do so we need the following two transformation equations:

$$T'(\omega)\cdot T^{+}(\omega) = -\frac{i}{2}\left(\vec{W}(\omega)\cdot\vec{\sigma}\right)(t_0\cdot I + \vec{t}\cdot\vec{\sigma}), \tag{5}$$

$$T(\omega)\cdot\left[T'(\omega)\right]^{+} = (t_0\cdot I + \vec{t}\cdot\vec{\sigma})\cdot\frac{i}{2}\left(\vec{W}^{*}(\omega)\cdot\vec{\sigma}\right). \tag{6}$$

One can find:

$$\begin{cases} t_0' = \operatorname{Im}\vec{W}\cdot\vec{t}, \\ \vec{t}' = t_0'\operatorname{Im}\vec{W} + (\operatorname{Re}\vec{W}\times\vec{t}). \end{cases} \tag{7}$$

Finally, we obtain the *output* PDL vector equation of motion:

$$\frac{d\vec{\Gamma}}{d\omega} = \operatorname{Im}\vec{W} + \operatorname{Re}\vec{W}\times\vec{\Gamma} - \vec{\Gamma}(\vec{\Gamma}\cdot\operatorname{Im}\vec{W}). \tag{8}$$

We emphasize that above equation is the main analytical result of this work and it is written in terms of the *output* PMD vector $\vec{W}(\omega)$. Similar equation has been derived in terms of the *input* PMD vector by Wang et al. [4]. From the equation above, it is easy to see that PDL becomes frequency dependent when PMD is added. Our result proposes a new method to measure PDL as a function of wavelength using output PMD vector $\vec{W}(\omega)$. It is now worthwhile to quote the equation of motion for the output SOP [9]

$$\vec{S}(\omega) = \frac{\langle\vec{E}_{\text{out}}(\omega)|\vec{\sigma}|\vec{E}_{\text{out}}(\omega)\rangle}{\langle\vec{E}_{\text{out}}(\omega)|\vec{E}_{\text{out}}(\omega)\rangle}$$

on the Poincaré sphere:

$$\frac{d\vec{S}}{d\omega} = \operatorname{Re}\vec{W}\times\vec{S} - (\operatorname{Im}\vec{W}\times\vec{S})\times\vec{S}. \tag{9}$$

Suppose the input SOP is independent of the wavelength. Chen et al. have successfully developed a PMD vector measurement method [9] based on the above equation of motion using three independent wavelength scans of the output SOP. In this work we report the PDL vector measurement method based on Eq. (8) and hybridized with Eq. (9). Our idea is based on the following observation, if one knows PDL vector $\vec{\Gamma}(\omega_0)$ at a specific frequency ω_0 and the PMD vector $\vec{W}(\omega)$ at all frequency are known, then one can calculate the PDL vector at any other frequency using numerical integration. Therefore three independent wavelength scans of output SOP plus a PDL vector at a specific frequency are enough to completely give wavelength dependent PMD vector $\vec{W}(\omega)$ and PDL vector $\vec{\Gamma}(\omega)$. Apparently, our method requires the least measurement information to get both PMD and PDL vectors of a fiber link.

3. Simulation and experimental results

To test our new method we have simulated a system made of four sections with PDL-PMD-PDL-PMD having values of 0.5 dB, 5 ps, 1 dB, and 2 ps, respectively. DGD of the whole system is about 6.83 ps. In the calculation we have used the recursion relations for PMD vector [12] and PDL vector [13] and we assigned a random orientation for each element. Figure 1 describes both the real and imaginary part of the output PMD vector $\vec{W}$, to be used for PDL vector calculation with Eq. (8). We have chosen different wavelength step size $\Delta\lambda$, i.e., different angular frequency step size $\Delta\omega$, so that the simple numerical integration of Eq. (8) is implemented:

$$\vec{\Gamma}(\omega+\Delta\omega) = \vec{\Gamma}'(\omega)\Delta\omega + \vec{\Gamma}(\omega). \tag{10}$$

Figure 2 plots PDL vector calculated using above scheme taking two different wavelength step sizes (20 and 1 pm) with initial PDL vector at 1550 nm and that of the exact result from the Jones matrix method. As expected the accuracy decreases as the angular frequency step size $\Delta\omega$ increases. Just like the Jones matrix eigenanalysis the larger the system PMD values the smaller the angular frequency step size $\Delta\omega$ should take in order to get the same measurement accuracy. From Fig. 2, we observed that for this specific simulation, a reasonable accuracy of this new PDL vector measurement method can be achieved within several nanometers around the specific frequency where one starts to use the integration to calculate PDL vector using Eq. (10).

We have also constructed an experiment to test this new PDL vector measurement algorithm. Figure 3 shows the schematics of the test setup. It consists of a tunable laser, two PMD elements (PM fibers), two PDL elements (blazed fiber Bragg gratings) and a polarization analyzer.

Reproduced with permission of the copyright owner. Further reproduction prohibited without permission.

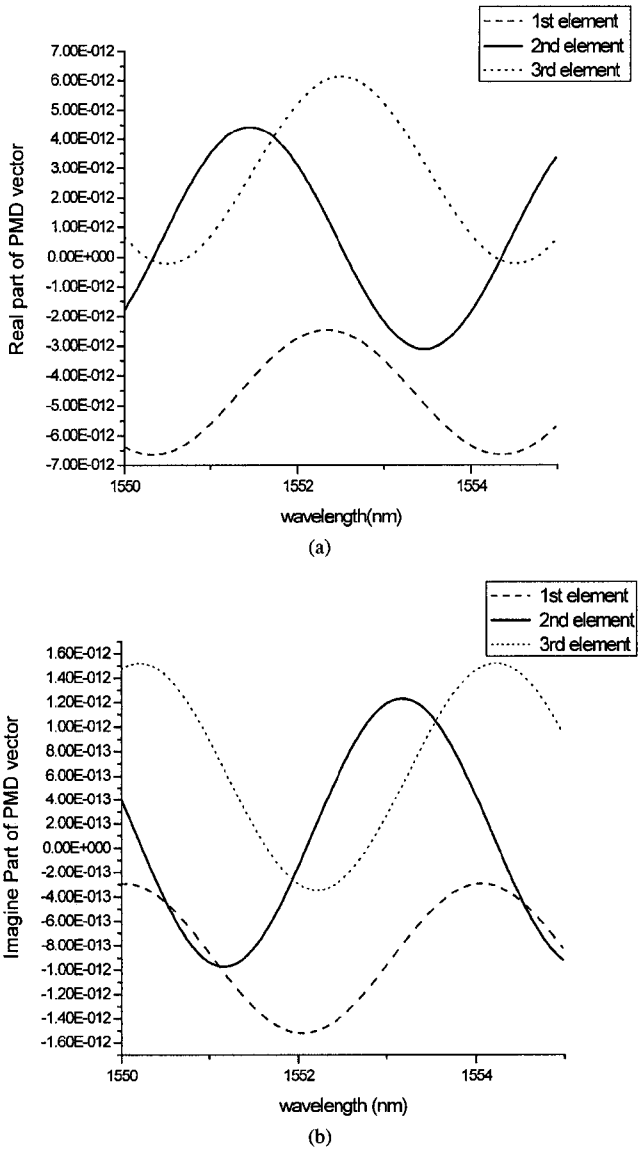

Fig. 1. Output PMD vector for one configuration of the wave plates PDL-PMD-PDL-PMD having values of 0.5 dB, 5 ps, 1 dB, and 2 ps, respectively.

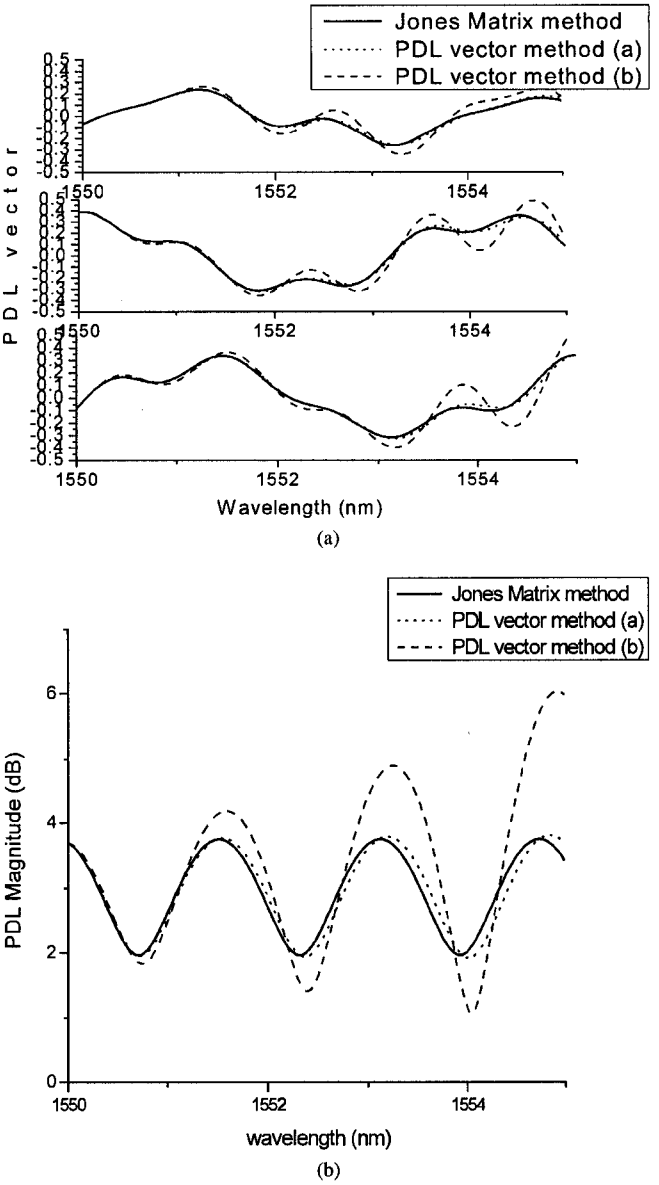

Fig. 2. PDL vector and PDL magnitude. (a) $\Delta\lambda = 1$ pm, (b) $\Delta\lambda = 20$ pm.

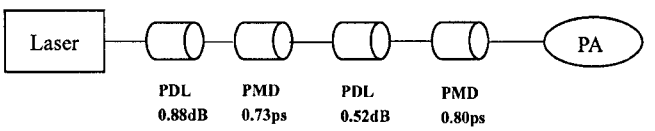

Fig. 3. Experimental setup for measuring PDL vector.

The step size of the wavelength for the tunable laser, which is dependent on the value of PMD in the system, is critical in this measurement accuracy. As usual the larger the PMD, the smaller the step size should be taken. The condition $\Delta\tau \cdot \Delta\omega \ll \pi$ should be satisfied all the time [8]. We have used the simulation above to determine a suitable step size for a given setup. Since the minimum wavelength interval of our tunable laser (HP 8164A) is 10 pm, according to the simulation result, we have to decrease the length of PM fibers in the elements to get less than 1 ps PMD emulators.

From the Jones matrix given by polarization analyzer (HP 8509B), we first calculated PMD vectors and then the PDL vectors with respect to optical frequency. In Fig. 4 we plotted the PDL value calculated via the simple numerical integration of Eq. (10) using the starting PDL vector at 1553.5, 1554, and 1554.5 nm, which are available from the polarization analyzer. While the PMD vectors are measured at a step size of $\Delta\lambda = 10$ pm. Due to the constrain of laser's resolution in the numerical integration method, the result obtained using our new algorithm agrees well with the Jones matrix eigenanalysis within about 0.5 nm and it starts to deviate noticeably beyond 0.7 nm. In order to track PDL more precisely during wider wavelength span for real-world fiber links, the following fashion was applied: measure the PDL vectors every 0.5 nm, then calculate PDL in this 0.5 nm. It would be of interest to compare this new technique with Jones matrix method here.

Reproduced with permission of the copyright owner. Further reproduction prohibited without permission.

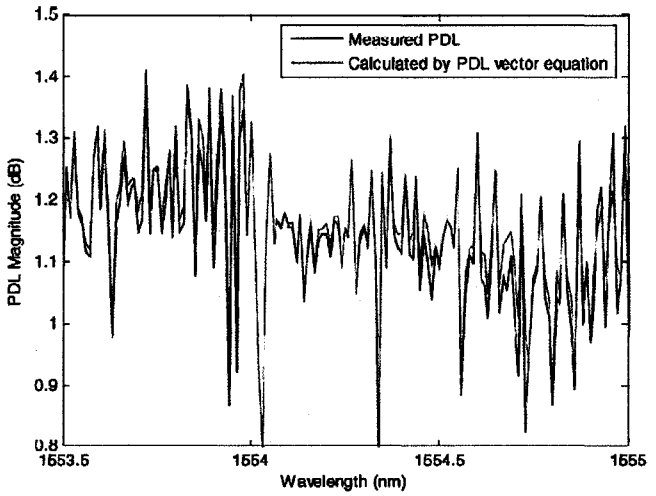

Fig. 4. A comparison of the calculated PDL magnitude (dotted line) with the measurement data (solid line).

From Fig. 4, there are 150 points in total. For the Jones matrix method, 600 output SOPs are needed to measure, while for our method, 453 output SOPs are needed. However it is important to point out that due the experimental fluctuations in the measured PMD vector and the initial PDL vector error the numerical integration procedure of Eq. (10) becomes unstable beyond wavelength range of ~1 nm in the current setup. We believe that if a smaller frequency step size is applied, one can get more accurate results at longer wavelength range for single integration using only one initial PDL vectors.

4. Conclusions

A new PDL vector measurement method has been proposed that uses three independent wavelength scans of the output state of polarization plus a PDL vector at a specific wavelength. Our method requires the least measurement information to give both spectrally resolved PMD and PDL characterization. The accuracy of the measurement is intrinsically limited by the wavelength resolution of the light source. Comparing to Jones matrix and Mueller matrix method, this new approach shows faster response speed, which is critical for field fiber testing. For a laser with given minimum wavelength resolution one perhaps can implement our new methods in the following fashion: (1) measure PDL vectors at some coarse wavelength steps, and (2) use the numerical integration to find the PDL vector in between these coarse steps. Finally, it is also interesting to note the possibility of measuring the transmission coefficient using Eq. (7) by the same numerical integration procedure.

Acknowledgments

We would like to acknowledge the discussion with Ping Lu. Also, we acknowledge the financial support from NSERC of Canada and from the Canadian Networks of Centers of Excellence: Canadian Institute for Photonic Innovations (CIPI) and Agile All-Optic Photonic Networks (AAPN).

References

[1] C.D. Poole, R.E. Wagner, Phenomenological approach to polarization dispersion in long single mode fibers, Electron. Lett. 22 (19) (1986) 1029–1030.
[2] J.P. Gordon, H. Kogelnik, PMD fundamentals: Polarization mode dispersion in optical fibers, Proc. Nat. Acad. Sci. 97 (9) (2000) 4541–4550.
[3] N. Gisin, B. Huttner, Combined effects of polarization mode dispersion and polarization dependent losses in optical fibers, Opt. Commun. 142 (1997) 119–125.
[4] M. Wang, T. Li, S. Jian, Analytical theory of pulse broadening due to polarization mode dispersion and polarization-dependent loss, Opt. Commun. 223 (2003) 75–80.
[5] L. Guo, Y. Zhou, Z. Fang, Pulse broadening in optical fiber with polarization mode dispersion and polarization dependent loss, Opt. Commun. 227 (2003) 83–87.
[6] M. Karlsson, M. Peterson, Quaternion approach to PMD and PDL phenomena in optical fiber systems, J. Lightwave Technol. 22 (4) (2004) 1137–1146.
[7] B.L. Heffner, Accurate, automated measurement of differential group delay dispersion and principal state variation using Jones matrix eigenanalysis, IEEE Photon. Technol. Lett. 5 (7) (1993) 814–817.
[8] B.L. Heffner, Automated measurement of polarization mode dispersion using Jones matrix eigenanalysis, IEEE Photon. Technol. Lett. 4 (1992) 1066–1069.
[9] L. Chen, O. Chen, S. Hadjifaradji, X. Bao, Polarization-mode dispersion measurement in a system with polarization-dependent loss or gain, IEEE Photon. Technol. Lett. 16 (1) (2004) 206–207.
[10] B.L. Heffner, Deterministic, analytically complete measurement of polarization-dependent transmission through optical devices, IEEE Photon. Technol. Lett. 4 (5) (1992) 451–454.
[11] Y. Zhu, E. Simova, P. Berini, C.P. Grover, A comparison of wavelength dependent polarization dependent loss measurements in fiber gratings, IEEE Trans. Instrum. Meas. 49 (6) (2000) 1231–1239.
[12] L. Chen, S. Hadjifaradji, D.S. Waddy, X. Bao, Effect of local PMD and PDL directional correlation on the principal state of polarization vector autocorrelation, Opt. Express 11 (2003) 3141–3146.
[13] L. Chen, S. Hadjifaradji, D.S. Waddy, X. Bao, Polarization dependent loss autocorrelation in the presence of combined polarization-mode dispersion and polarization dependent losses in optical fibers, Appl. Photon. Technol. 5260 (2003) 377–381.

Reproduced with permission of the copyright owner. Further reproduction prohibited without permission.

Chapter 5

Fast state of polarization and PMD drift in submarine fibers

[**Ziyi Zhang,** Xiaoyi Bao, Qinrong Yu and Liang Chen, "Fast state of polarization and PMD drift in submarine fibers," *Photonics Technology Letters, IEEE,* 18, 1034 –1036 (2006)]

Chapter 4 presents a new polarization measurement method and it has been verified in the lab environment. Another important aspect of polarization effects in communication systems lies in the characteristics of PMD and PDL in field fibers. These include mean DGD and PDL value, time evolution behavior of SOP and DGD, as well as probability density of DGD, and environmental effects on polarization effects.

In May 2005 we had an opportunity to conduct a field test on three pairs of submarine fibers under the Caribbean Sea, collaborated with Caribbean Crossing. One pair of fiber was measured ~26 hours with a fast PMD technique sampling at 15s intervals. To the best of our knowledge, this is the longest and the fastest polarization effects test on submarine fibers to date. This chapter studies SOP and DGD temporal drift properties while the next chapter gives statistics of the DGD data and correlates DGD with the fiber exposed environmental conditions. It is worth mentioning that since PDL in fiber communication system is primarily contributed by the components (such as amplifiers

Reproduced with permission of the copyright owner. Further reproduction prohibited without permission.

and filters) rather than the fiber itself, PDL does not fluctuate much with respect to environment effects as PMD [Lu 2001]. As a result, PMD information has usually been utilized to investigate the time evolution of polarization effects.

Caribbean Crossing planned to upgrade the submarine telecommunication system from 2.5Gbits/s to 10Gbits/s, so they must have the knowledge of the mean DGD and PDL as well as the worst-case maximum DGD to determine whether PMD compensation would be required or not. Since a fast polarization measurement was desired, the state-of-the-art polarization analyzer Adaptif A2000 was used. Comparing with HP 8509B, Adaptif A2000 implements a lithium niobate crystal to control the input polarization states by applied voltage, rather than using mechanically rotated waveplates. Comparison of some key performance parameters between these two analyzers can be found in Table 2.1 (section 2.3.1). Fig.5.1 shows the schematic configuration of a PMD and PDL test using the Adaptif A2000.

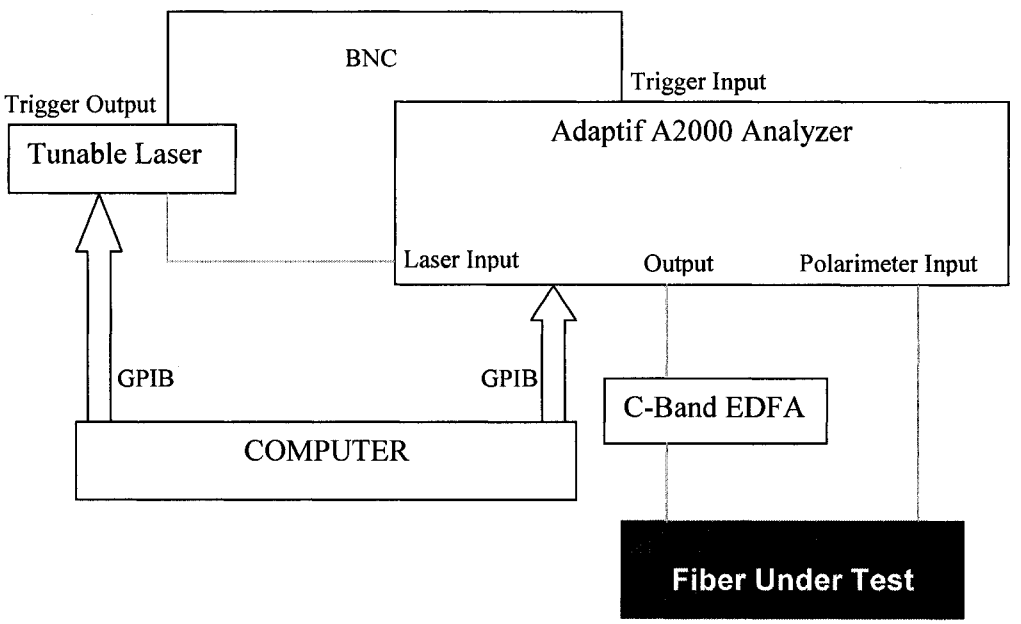

Figure 5.1 Schematic configuration of PMD and PDL test using Adaptif A2000.

Reproduced with permission of the copyright owner. Further reproduction prohibited without permission.

Three pairs of submarine fibers were measured: two pairs were in the same cable under the inner Caribbean Sea from Eleuthera to Nassau, and the third one was located from Eleuthera to Abaco on the boundary of Caribbean Sea and Atlantic Ocean. The deepest point of the first two pairs and the third fiber was 2.3km and 4.3km, respectively. As all the testing equipments were placed at Eleuthera Island, a jumper fiber at the other end was used to create a loop back fiber. Locations of three pair fibers are marked in red color in Fig. 5.2.

Figure 5.2 Map of Bahamas: two pairs of submarine fibers were between Eleuthera and Nassau while the third one was from Eleuthera to Abaco.

Reproduced with permission of the copyright owner. Further reproduction prohibited without permission.

Table 5.1 summarizes the polarization test results in terms of mean DGD, maximum DGD and mean PDL for three pairs of fibers. Even though Fiber A and Fiber B are in the same cable, they have different mean DGD values: 5.5ps for Fiber A, while 4.6ps for Fiber B. As for the Fiber C, which goes much deeper undersea than A and B, it has 7.42ps mean DGD. Based on those results, it is evident that DGD depends on location and routes. So each span of fiber should be tested separately. No significant differences were noticed for PDL values between Fiber A and Fiber B.

Table 5.1 PMD and PDL test results of three submarine fibers

Date	Testing hours	Location	Fiber	Mean DGD	Max. DGD	Mean PDL
May 13th	1.2 hours	Eleuthera-Nassau	Fiber A	5.52ps	19.9ps	0.105dB
May 14th	5.5 hours	Eleuthera-Nassau	Fiber B	4.54ps	15.6ps	0.115dB
May 15th	7 hours	Eleuthera-Nassau	Fiber B	4.65ps	14.4ps	0.115dB
May 16th May 17th	26 hours	Eleuthera-Nassau	Fiber A	5.45ps	16.1ps	0.105dB
May 18th	1 hour	Eleuthera-Abaco	Fiber C	7.42ps	19.1ps	0.145dB

Although different systems don't have the same ability to endure PMD, in general, taking no account of PDL, maximum DGD should be less than 10% bit period (for 10Gb/s system, it's 10ps) to avoid PMD-induced outage. Given PDL>0.1dB and ~19ps maximum DGD, PMD compensation should be designed for the system upgrading to 10Gbits/s.

Previous research [Takahashi 1993] with either short testing duration (7 hours) or slow sampling speed (15 minutes) has not been able to obtain the time evolution of

Reproduced with permission of the copyright owner. Further reproduction prohibited without permission.

polarization effects. For the first time, we reported the temporal drift time of both DGD and SOP is in the order of a few minutes. These test results provide valuable information for designing PMD mitigation in submarine fiber systems. Then the next question one might raise would be what causes such fast polarization fluctuations in submarine fiber. This becomes the topic of the next chapter.

Reproduced with permission of the copyright owner. Further reproduction prohibited without permission.

Fast State of Polarization and PMD Drift in Submarine Fibers

Ziyi Zhang, Xiaoyi Bao, *Senior Member, IEEE*, Qinrong Yu, and Liang Chen, *Member, IEEE*

***Abstract*—We report on the measurements of state of polarization (SOP) and differential group delay (DGD) in submarine fibers. The experimental autocorrelation function shows the fastest change in both SOP and DGD is faster than 15 s, which is limited by the measurement speed. The Fourier transform is utilized to study ocean-wave-induced vibrations on submarine fibers.**

***Index Terms*—Optical communication, polarization-mode dispersion (PMD), state of polarization (SOP), submarine fiber.**

I. Introduction

POLARIZATION-MODE dispersion (PMD) may severely degrade the system performance of optical communication systems with bit rates of 10 Gb/s and beyond. For communication systems, the biggest problem of PMD mitigation is the temporal drift of PMD due to the environmental disturbances, such as temperature, wind speed, sun altitude, etc. It is important to find the fastest changes in both state of polarization (SOP) and differential group delay (DGD) as they provide the speed requirement for PMD compensators. Previous experiments showed that the SOP drift is relatively slow in buried fibers [1], [2], on the order of hours or days, and relatively fast in aerial fibers [3], [4], on the order of microseconds in the winter.

Submarine cables are widely used in the global optical fiber system. Compared to buried and aerial fibers, very little work has been reported on the PMD characteristics of submarine fibers. In the late 1980s and early 1990s, submarine fibers were investigated [5]–[8] for the wavelength dependence of SOP and DGD [5] and the relationship between fiber length and the PMD value [6]. So far, the fastest PMD measurement was taken at 15-min intervals over 7 h [7]. Due to the limited data, its Fourier analysis result was not accurate. No detailed studies are available on SOP and PMD time drift in submarine fibers. In order to catch diurnal variation, PMD measurement should be at least 24 h. In this letter, we report both SOP and PMD drift properties in one pair of 240-km (although four fibers were measured with similar variation patterns) combined submarine/buried fibers with a fast PMD measurement technique sampling at 15-s intervals. Such information is important for PMD mitigation in undersea cable systems.

II. Experiment

The experiment was performed on one pair of combined submarine/buried fibers under the inner Caribbean Sea in the Bahamas. The testing office at Eleuthera Island was connected by a 10-km buried fiber to the beach. The 110-km submarine fiber between Eleuthera Island and Nassau was made by Corning, Submarine DA/SA/LW in 1994. The fiber was then looped back by a jumper fiber at Nassau to create a 240-km test fiber. The fiber was verified to not be exposed to the environment for the entire route. The submarine fiber went as deep as 2.3 km under the Caribbean Sea and most parts (around 75%) were submerged beyond 1 km.

An Adaptif Photonics Polarization Analyzer was used in this field test. PMD and polarization-dependent-loss (PDL) information was calculated by Jones Matrix Eigenanalysis. In order to match the dynamic range of this analyzer, one C-band erbium-doped fiber amplifier was added as a preamplifier at the testing office to give 12-dB amplification. As a result, the testing wavelength range was limited to 1520–1580 nm. The Agilent tunable laser scaned 40 nm/s and the analyzer sampled at 10 K samples per second. Thus, we collected data over the 60-nm wavelength range with 0.048-nm resolution within 15 s. The test fiber was measured over 26 h.

Compared to aerial fibers [3], [4], submarine fibers stay in a relatively static environment, but they still have the SOP temporal drift. For a fixed input SOP, the output SOP with changing wavelength is directly related to the DGD and principle state of polarization (PSP) [5]. Therefore, DGD data varies with time as well. Fig. 1(a) is the color map of DGD versus time and wavelength measured over 26 h. The PMD value (mean DGD) was calculated to be 5.45 ps and the maximum DGD was 16.1 ps. In order to increase the contrast of this color map, the maximum DGD was set to be 12 ps, i.e., all the larger DGDs were set to be 12 ps. Because the DGD data follows Maxwellian probability density function [2], only a small portion of DGD ($\sim$0.5%) was larger than 12 ps in our measurements. As expected, we observe that most fast DGD changes occur during the day time until $\sim$8:00 P.M., and then slow changes occur over night, until 9:00 A.M. the next morning. The mean SOP arc change and DGD change over 15 s were 33.1° and 0.25 ps, respectively. Fig. 1(b) shows the temperature and wind data versus time at Nassau, one end of the test fiber. No correlation between wind and polarization oscillation in the submarine fiber was observed.

III. Autocorrelation Function (ACF)

The ACF is a useful tool to analyze statistical properties of the SOP and PMD drift. Since the DGD is a function of both time and wavelength, the temporal ACF of DGD describes DGD correlation at two time instances, while the spectral ACF of DGD describes DGD correlation at two channels in the frequency do-

Manuscript received August 26, 2005.

The authors are with the Department of Physics, University of Ottawa, ON K1N 6N5, Canada (e-mail: zzhan089@uottawa.ca).

Digital Object Identifier 10.1109/LPT.2006.873513

Reproduced with permission of the copyright owner. Further reproduction prohibited without permission.

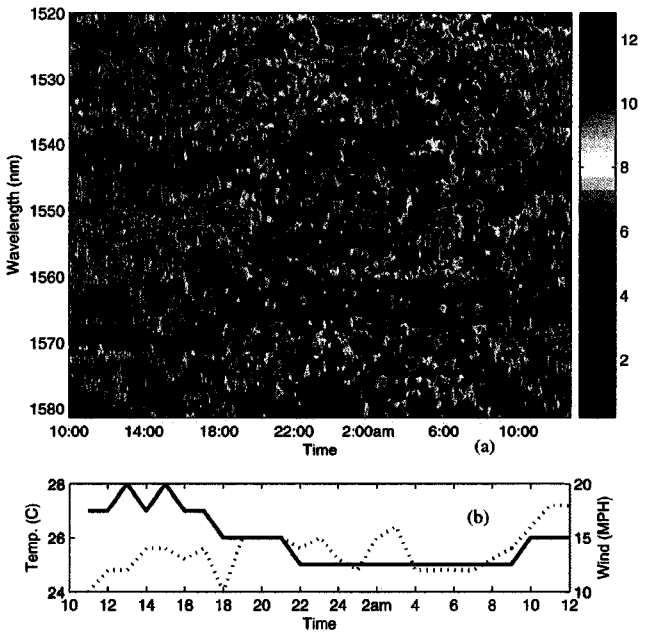

Fig. 1. (a) A 26-h color map of DGD wavelength spectrum for the 240-km submarine/buried combined fiber with (b) temperature (solid line) and wind speed (dotted line) during the testing period.

main. Here, we focus our effort on the temporal ACF in submarine fibers. The temporal ACF of SOP can be calculated by [3]

$$R(\Delta t) = \frac{1}{N}\sum_{t=0}^{N-1} \vec{S}(t) \bullet \vec{S}(t+\Delta t) \tag{1}$$

where $\vec{S}$ is the output normalized Stokes vector as a function of time, and N is the total number of scans over the measurement period. Similarly, the temporal ACF of DGD and PSP can be performed by replacing $\vec{S}$ in (1) with $\Delta\tau(t)$ (DGD value) and $\vec{\Omega}$ (PSP vector), respectively. Note that (1) assumes that N is large enough, so that $\vec{S}$ is distributed on the whole Poincaré sphere with zero average. Therefore, we used the normalized autocovariance, the mean-removed autocorrelation.

The results of the ACF of SOP and DGD at 1550 nm on the whole data set decorrelate quickly, within a few minutes, and then fluctuate around zero, although the amplitude of the ACF of DGD is relatively larger. Here, we ignore the effect of PDL on the fiber link (as PDL was 0.11 dB), so the cross-correlation function (CCF) is defined as:

$$R(\Delta t) = \frac{1}{N}\sum_{t=0}^{N-1} \vec{S}(t) \bullet \vec{\Omega}(t+\Delta t). \tag{2}$$

It has the similar fashion as the ACF of SOP and DGD. After several minutes, even SOP is not correlated any more, nor is the cross correlation.

What we are interested in is how fast the SOP and DGD decorrelate in submarine fibers, so we focus on the ACF in the first few minutes. Fig. 2(a) describes the normalized ACF of SOP, PSP, DGD, and CCF between SOP and PSP. There is some correlation between SOP and PSP within SOPs decorrelation

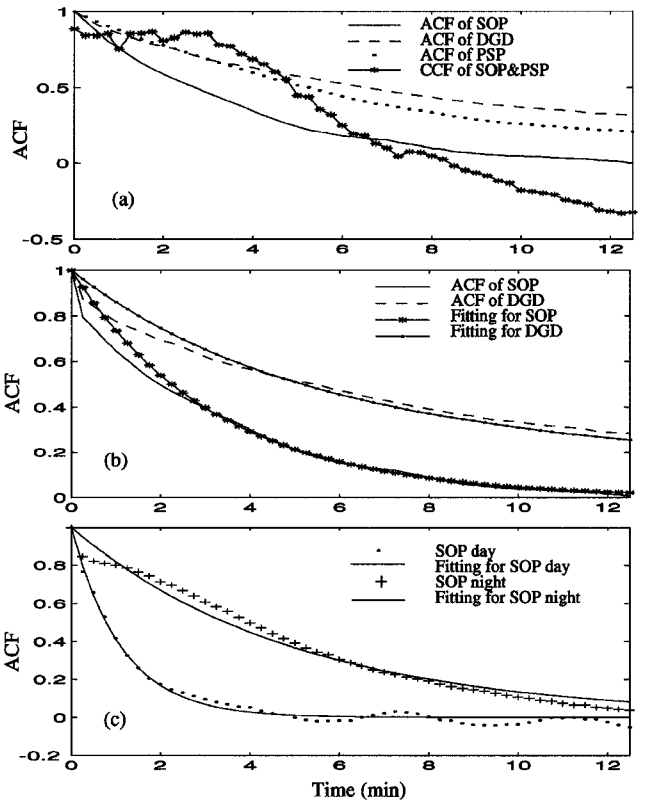

Fig. 2. (a) Small-scale view of experimental ACF of SOP; DGD; PSP and cross correlation between SOP and PSP. (b) Comparison of theoretical and experimental ACF of SOP and DGD. (c) Comparison of experimental ACF of SOP during the day (11:00 A.M. to 18:00) and the night (23:00 to 6:00 A.M. the next morning) with corresponding curve fittings.

time. Obviously, SOP decays faster than PSP and DGD, whose normalized form was described theoretically in [1]

$$\mathrm{ACF}_{\mathrm{SOP}}(\Delta t) = \exp\left(\frac{-|\Delta t|}{t_d}\right) \tag{3}$$

$$\mathrm{ACF}_{\mathrm{DGD}}(\Delta t) = \frac{1-\exp\left(\frac{-|\Delta t|}{t_d}\right)}{\frac{|\Delta t|}{t_d}} \tag{4}$$

where t is the time interval between two time instances, and t_d gives an average drift time for both SOP and DGD, which is unique for every fiber. However, [1] only includes the comparison between the measured ACF of DGD and its theoretical ACF. Here, we first report the experimental ACF of both SOP and DGD and compare them with their theoretical values. In Fig. 2(b), t_d was found to be 3 min for this combined submarine/buried fiber. The experimental ACF has a quick drop at the second point, which means the fastest change in this submarine fiber is less than 15 s. However, both fits are quite good for the choice of $t_d \sim 3$ min. Although [8] did not compute the exact drift time, one figure showed that the SOP rapidly changes from a linear polarization to an elliptical polarization state within 3 min, which agrees with our results. Fig. 2(c) compares the ACF of SOP during the day and night. The fitting parameter t_d is chosen to be 1.1 and 5 min, respectively. As we expected, ACF in the day has a faster decay, which means the cable is in a relative static environment during the night.

Reproduced with permission of the copyright owner. Further reproduction prohibited without permission.

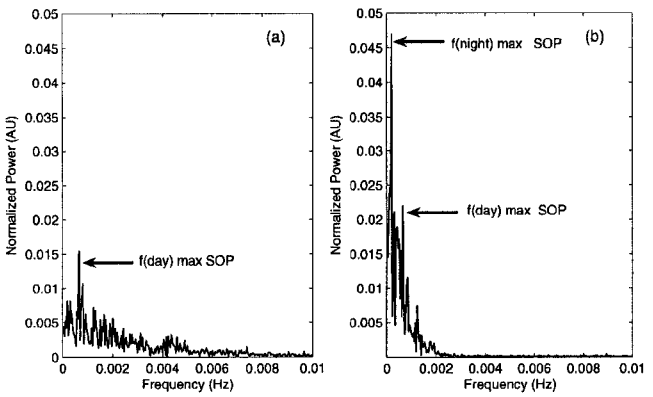

Fig. 3. FFT power spectrum of SOP at 1550 nm for 7-h data from 0 to 0.01 Hz in the (a) day from 11:00 A.M. to 18:00; and (b) night from 23:00 to 6:00 A.M. next morning.

Previous studies ([1], [2] and references therein) showed the drift time caused by temperature on buried fibers is on the order of hours or days. In addition, the ACF of SOP of a 220-km submarine fiber connecting Eleuthera and Abaco Island showed fast drift time comparable to the 240-km combined fiber. These led us to believe the fast fluctuation was mainly caused by the submarine portion. Similar to the wind effects on aerial fibers, the tension induced by ocean waves/currents may affect the signals in submarine fibers. Moreover, our fibers were not buried in the seabed. Some segments may not touch the seabed but suspend over the trough, which is a normal situation for submarine fibers. It is natural to think the sun is the main cause of the different current activities. The unevenness in ocean temperature, water density, and salinity are the direct causes for currents. In the daytime, the solar radiation can strengthen these perturbance and hence, produce stronger currents. This may explain the different SOP drift times between the day and the night.

IV. Fast Fourier Transfrom (FFT) Analysis of SOP

The power spectrum of SOP is of great interest as it could provide the characteristic frequency of fiber vibrations. Fig. 3(a) and (b) describes the normalized FFT power spectrum of fast SOP changing at 1550 nm during the daytime and slow SOP changing during the nighttime, respectively. SOP data during the night starts at a higher magnitude and drops faster than during the day, which means that during the day, the vibration frequencies of the cable shift to the higher frequencies. This supports our ACF analysis in Section III. From Fig. 3, the characteristic frequency is observed at 6.5×10^{-4} Hz in the day. As for the night, the first peak shows at 2×10^{-4} Hz and the second peak shows at 6.5×10^{-4} Hz the characteristic frequency for the day. In the time domain, these two frequencies correspond to 1.4 h and 26 min, respectively. These two characteristic frequencies of this fiber were verified by FFT analysis of SOP at 1525 and 1575 nm. The FFT results of two other fibers under a similar environment showed the same frequency distributions, i.e., most of the power spectrum was contributed by frequencies less than 0.02 Hz. Since the highest frequency was limited by the testing interval, we were only able to exam the vibration periods beyond 15 s.

In the aerial fiber, the fundamental frequency was found to be 0.5 Hz [4], which corresponds to the vibration frequency of the cable induced by the wind. However, the deep ocean is a complex system due to deep ocean wave mixing and it has not been understood entirely because of limited data collection [9]. The main classes of waves are wind waves, swells, tsunamis, long gravity waves, tides, etc. According to the ocean wave spectrum in [9], periods of the above waves are 0.5 s; 25 s; several minutes to 1 h; a few hours; 12.5 or 25 h, respectively. Furthermore, no correlation between wind waves and fiber vibration was noticed in this field test, as stated in Section II. Therefore, we may conclude that submarine fiber is affected by deep ocean waves, not by wind waves. Because of the ocean wave mixing, it is hard to measure the vibration frequency of the submarine cable induced by different waves separately.

V. Conclusion

We have performed a field test on one pair of 240-km submarine/buried fibers for SOP and DGD over 26 h. The average SOP fluctuation time in this fiber was about 3 min. The temporal ACF of SOP decayed much faster than that of DGD, supported by both the theory and the experimental data. The FFT analysis showed our fiber was associated with frequencies beyond half an hour and could be affected by deep ocean waves with longer periods.

Acknowledgment

The authors would like to thank J. Stears and many other individuals at Caribbean Crossings who helped with this field test. They also thank R. Stolte and D. S.Waddy for helpful discussions. The support from AAPN is appreciated.

References

[1] M. Karlsson, J. Brentel, and P. Andrekson, "Long-term measurement of PMD and polarization drift in installed fibers," *J. Lightw. Technol.*, vol. 18, no. 7, pp. 941–951, Jul. 2000.

[2] C. Allen, P. Kondamuri, D. Richards, and D. Hague, "Measured temporal and spectral PMD characteristics and their implications for network-level mitigation approaches," *J. Lightw. Technol.*, vol. 21, no. 1, pp. 79–86, Jan. 2003.

[3] D. Waddy, P. Lu, L. Chen, and X. Bao, "Fast state of polarization changes in aerial fiber under different climatic conditions," *IEEE Photon. Technol. Lett.*, vol. 13, no. 9, pp. 1035–1037, Sep. 2001.

[4] J. Wuttke, P. Krummrich, and J. Rosch, "Polarization oscillations in aerial fiber caused by wind and power-line current," *IEEE Photon. Technol. Lett.*, vol. 15, no. 6, pp. 882–884, Jun. 2003.

[5] C. Poole, N. Bergano, R. Wagner, and H. Schulte, "Polarization dispersion and principal states in a 147-km undersea light-wave cable," *J. Lightw. Technol.*, vol. 6, no. 7, pp. 1185–1190, Jul. 1988.

[6] Y. Namihira, Y. Horiuchi, K. Mochizuki, and H. Wakabayashi, "Polarization mode dispersion measurements in an installed optical fiber submarine cable," *IEEE Photon. Technol. Lett.*, vol. 1, no. 10, pp. 329–331, Oct. 1989.

[7] T. Takahashi, T. Imai, and M. Aiki, "Time evolution of polarization mode dispersion in 120 km installed optical submarine cable," *Electron. Lett.*, vol. 29, no. 18, pp. 1605–1606, Sep. 1993.

[8] Y. Namihira, T. Kawazawa, and H. Wakabayashi, "Field demonstration of endless polarization control in 195-km installed optical fiber submarine cable at a sea depth of 2900 m," *IEEE Photon. Technol. Lett.*, vol. 3, no. 4, pp. 384–386, Apr. 1991.

[9] S. Pond and G. Pickard, *Introductory Dynamical Oceanography*. New York: Pergamon Press, 1983.

Reproduced with permission of the copyright owner. Further reproduction prohibited without permission.

Chapter 6

Time evolution of PMD due to tides and sun radiation on submarine fibers

[**Ziyi Zhang,** Xiaoyi Bao, Qinrong Yu and Liang Chen, "Time evolution of PMD due to tides and sun radiation on submarine fibers," *Optical Fiber Technology,* 13, 62-66 (2007)]

Chapter 5 reveals that polarization states in submarine fibers fluctuate (~ several minutes) slower than aerial fibers (<1s) while faster than buried fibers (~ hours or days). As mentioned in Chapter 2, it is the environment conditions the fiber exposed to that results the changes of the local birefringence properties of the fiber link and consequently affects the polarization states travelling inside the fiber. Unlike buried and aerial fibers, submarine fibers often are quite difficult to access to due to their remote locations. As a result, very little research has been conducted for submarine fibers so far. This chapter continues the research done in the previous chapter to address the issue of environment conditions on time evolution of polarization effects.

Let's first find out geographical circumstances of the location where the submarine fibers were laid. The area around the Caribbean Sea is home to 22 island territories and borders 12 continental countries [Wikipedia Caribbean]. Many underwater ridges and mountain ranges make the sea floor very complex. Submarine fibers were laid by cable ships directly into the sea. Since there was no guarantee that every fiber portion had

Reproduced with permission of the copyright owner. Further reproduction prohibited without permission.

touched the sea floor, it was believed that some fiber portions had suspended over troughs. Thus, it is conceivable to speculate the effects of deep ocean currents on submarine fibers.

Fig. 6.1 plots ocean wave spectrum: shallow water waves include ripples and swells with periods of seconds; whereas deep water waves have periods of several minutes to hours, like tsunamis and tides. Tide information was available from a weather station; it enabled us to focus on the correlation between tides and our test data of polarization states.

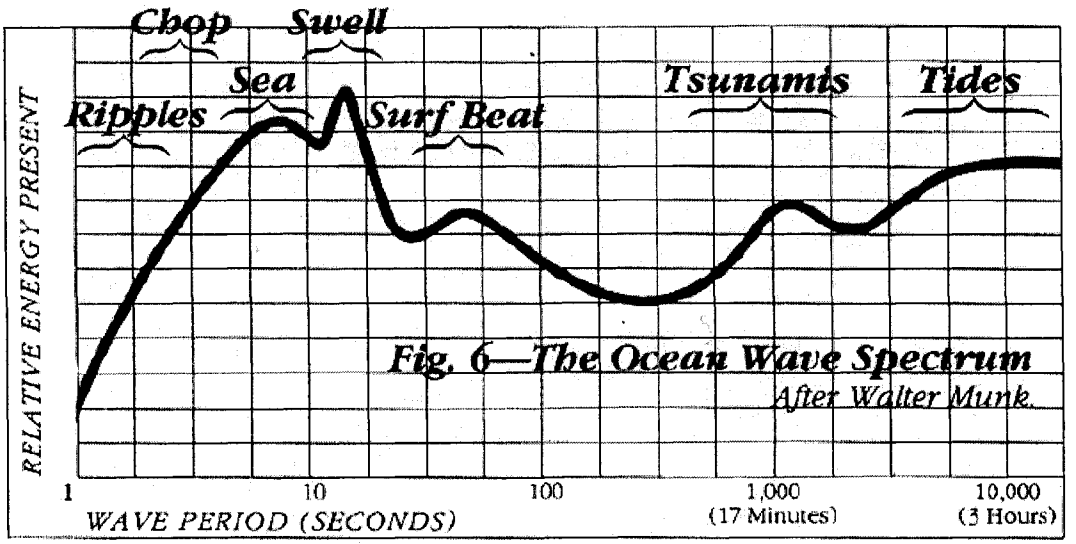

Figure 6.1 Ocean wave spectrum [Kampion 1997].

As it will be shown later in this chapter, mean DGD reaches its peak value twice a day, corresponding to the period of time when water current moves at maximum speed due to the semidiurnal tide around the testing place. Therefore, it leads us to believe the polarization effects in submarine fibers vary with the tension acted upon the fiber by tides.

Reproduced with permission of the copyright owner. Further reproduction prohibited without permission.

Available online at www.sciencedirect.com
ScienceDirect
Optical Fiber Technology 13 (2007) 62–66
Optical Fiber Technology
www.elsevier.com/locate/yofte

Time evolution of PMD due to tides and sun radiation on submarine fibers

Ziyi Zhang *, Xiaoyi Bao, Qinrong Yu, Liang Chen

Department of Physics, University of Ottawa, Ottawa, ON K1N 6N5, Canada

Received 21 December 2005; revised 12 May 2006

Available online 23 August 2006

Abstract

Using a fast polarization mode dispersion (PMD) set of 15-s interval and long measurement duration (>24 h), we found the correlation between polarization effects, tides and sun radiation on submarine fibers. We also found Maxwellian distribution for the differential group delay (DGD) even with strong biased output states of polarization (SOP) over 1 h measurement. PMD bandwidth and the fastest decorrelation time were calculated to be 165 GHz and less than 15 s.
© 2006 Elsevier Inc. All rights reserved.

Keywords: Polarization mode dispersion; Submarine fiber; Tide

1. Introduction

Polarization mode dispersion (PMD) is a limiting factor in the optical communication system with bit rates of 10 G/s and beyond. The environmental disturbances cause the PMD to fluctuate. In buried fibers, it is the temperature under the ground causing PMD to vary [1], while in aerial fibers, PMD fluctuation is caused by temperature, wind and power line current variations [2,3]. So far, the field tests [4–6] conducted on submarine fibers were for short time at slow speed. The data could not give accurate PMD distribution due to short duration nor correlation with the local weather condition due to slow speed, which have limited PMD impact study on submarine fibers. Here, we report the first long-term PMD measurement (over 24 h) at high speed (15 s) to investigate the various environmental disturbances on installed submarine fibers, specially the strong correlation between PMD value, tides and sun radiation. Even with those strong environmental effects, the PMD of submarine fibers tend to be Maxwellian distribution.

The experimental results on a simulator in lab [5] show loose correlation between temperature, pressure and SOP fluctuation but relative strong correlation between tension and SOP fluctuation. Takahashi et al. [6] studied the time evolution of PMD during 7-h testing period with 15 min measurement speed, which is insufficient to catch diurnal variation. Exposed to a different environment from buried or aerial fiber, submarine fiber might have some special PMD characteristics. In this paper, we studied the temporal and spectral fluctuation of PMD vector $\vec{\Omega}$ at time interval of 15 s. Principal state of polarization (PSP) gives direction of PMD vector while differential group delay (DGD) provides its magnitude. The statistical distribution and behavior of both PSP and DGD provide valuable information for system design and PMD mitigation in submarine cable system.

2. Test setup

As shown in Fig. 1, an Adaptif polarization analyzer was used with a tunable laser to measure the PMD and polarization dependent loss (PDL) information of fiber under test (FUT) by Jones Matrix Eigenanalysis method. $LiNO_3$ polarization controller in the analyzer sent six states of polarization into the fiber and the looped back signal was measured by a polarimeter. The tunable laser scanned from 1520 to 1580 nm in steps of 0.048 nm, which was limited by a C-band EDFA added as a pre-amplifier. Comparing to the fibers, PMD of this EDFA was negligible. Every 15 s, we can get polarization properties of 1248 steps to cover 1520–1580 nm over one scan. There were no exposed parts during the entire route.

Three pairs of looped back fibers located around Islands of Bahamas were measured during a few days. They were of the same type made by Corning, Submarine DA/SA/LW in 1994.

* Corresponding author.
E-mail address: zzhan089@uottawa.ca (Z. Zhang).

Reproduced with permission of the copyright owner. Further reproduction prohibited without permission.

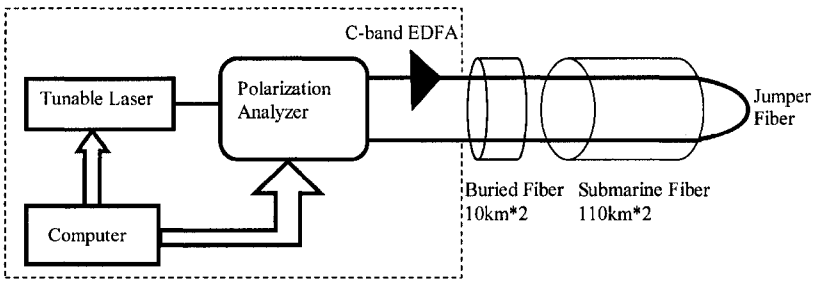

Fig. 1. The measurement setup for fibers A and B. The equipments in the dashed frame were located in an office at Eleuthera Island.

Table 1
Test fiber information

	Length (km)	Location	Depth	Testing hours	Manufacturer
Fiber A	220 km submarine + 20 km buried	Eleuthera–Nassau	0–2.3 km	26 h	Corning submarine DA/SA/LW
Fiber B	220 km submarine + 20 km buried	Eleuthera–Nassau	0–2.3 km	7 h during the day time	Corning submarine DA/SA/LW
Fiber C	220 km submarine	Eleuthera–Abaco	0–4.3 km	1 h during the day time	Corning submarine DA/SA/LW

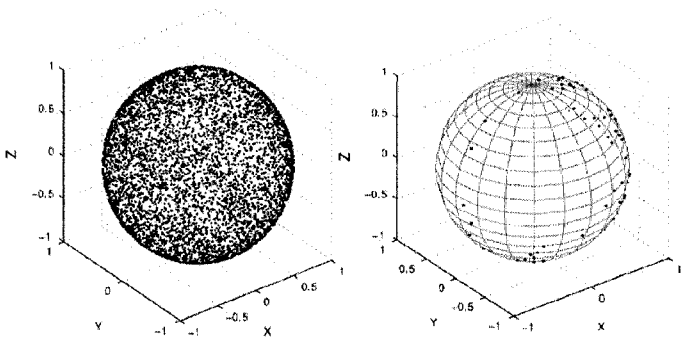

Fig. 2. Normalized output states of polarization (SOP) at 1550 nm of fiber A in 26 h (left) and fiber C in 1 h (right) on Poincaré sphere.

Fibers A and B were in the same cable under inner Caribbean Sea. Both fibers A and B were made up of 220 km submarine fiber and 20 km buried fiber. Thus, the total length of FUT was 240 km. Fiber C was a 220 km submarine fiber located near the boundary of Caribbean Sea and Atlantic Ocean. The depth of fibers A and B varied from 0 to 2.3 km (around 75% length was submerged beyond 1 km), while for fiber C, the deepest point was 4.3 km. All the test fibers' information were summarized in Table 1.

3. PMD statistics

We first check PMD distribution on Poincaré sphere for submarine fibers A and C. Normalized output states of polarization (SOP) distribution of fibers A and C at 1550 nm are shown in Figs. 2a and 2b, respectively. In fiber A, the SOP data takes "random walks" on the Poincaré sphere during 26 h. Thus, it results a uniform coverage. While for fiber C, only 1 h of SOP data are shown here covered partial sphere, from which we thought its DGD maybe far off from Maxwellian distribution.

DGD values, $\Delta\tau(\lambda, t)$, can be described by Maxwellian probability density function (PDF):

$$p(\Delta\tau) = \sqrt{\frac{2}{\pi}}\frac{\Delta\tau^2}{\sigma^3}e^{-\Delta\tau^2/2\sigma^2}, \tag{1}$$

where $\langle\Delta\tau\rangle = \sigma\sqrt{8/\pi}$ and mean DGD value is the only parameter that will affect the distribution. We first check the DGD data of fiber A and find Maxwellian PDF.

We plot the histogram of both fibers A and C together with corresponding Maxwellian PDFs using $\langle\Delta\tau\rangle_A = 5.45$ ps and $\langle\Delta\tau\rangle_C = 7.42$ ps for comparison. Experiments on fibers A and C were carried out for 26 and 1 h, respectively. From Fig. 3a, as expected, the histogram of fiber A fits well with Maxwellian distribution. In addition, the histograms of fiber A at a single wavelength all approximate to Maxwellian distributions, which means 26-h testing is sufficient for submarine fibers from statistical viewpoint. Although SOP distribution of fiber C on Poincaré sphere is biased, its histogram of DGD in Fig. 3b is very close to Maxwellian distribution.

The spectral characteristic of DGD is related to auto correlation function (ACF). The theoretical spectral ACF of DGD can be found in [7]

$$\mathrm{ACF}_{\mathrm{DGD}}(\Delta\omega) = 3\frac{1 - e^{-\langle\Delta\tau^2\rangle\Delta\omega^2/3}}{\Delta\omega^2}, \tag{2}$$

Reproduced with permission of the copyright owner. Further reproduction prohibited without permission.

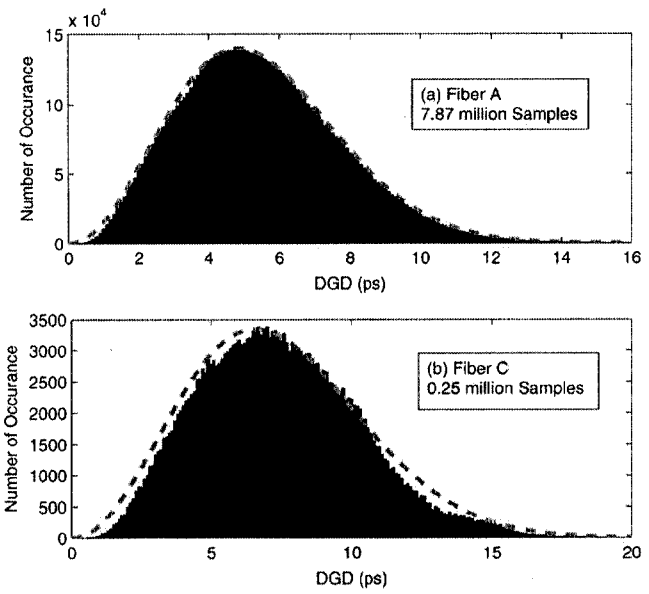

Fig. 3. Histogram of DGD data of (a) fiber A over 26 h and (b) fiber C over 1 h, respectively; dashed lines show the theoretical Maxwellian PDFs for comparison.

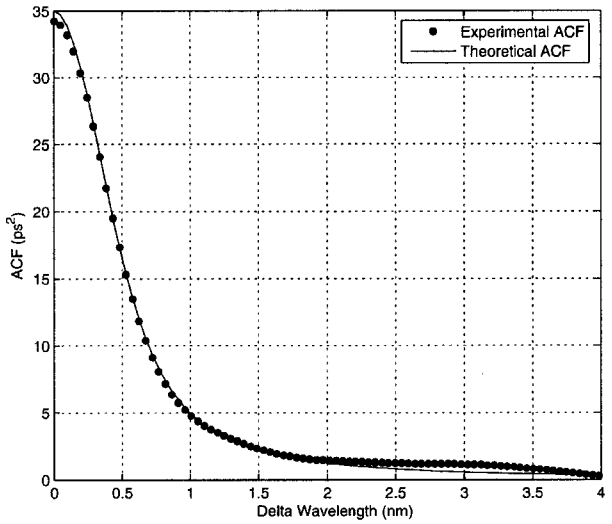

Fig. 4. Spectral auto correlation function (ACF) of DGD data of fiber A and theoretical spectral ACF for comparison.

where $\Delta\omega$ is the radian frequency and since DGD is a Maxwellian random variable, $\langle\Delta\tau^2\rangle = 3\pi\langle\Delta\tau\rangle^2/8$. Furthermore, [7] defines the DGD bandwidth as $\omega_C = 4\sqrt{2}/\langle\Delta\tau\rangle$, so the bandwidth increases as mean DGD decreases. Figure 4 describes the ACF of DGD averaged by 300 scans in fiber A and its theoretical ACF; theory and experiment are in good agreement. Using the same definition for DGD bandwidth as in [7], PMD bandwidth is calculated to be 165 GHz or 1.3 nm, of which range the DGD values are correlated.

4. Experimental results

Fiber A was tested over 26 h, and a total of 6428 scans were performed. The time evolution of DGD averaged over wavelength and each 10-min interval is shown in Fig. 5a. The PMD (mean DGD) over 26 h was calculated to be 5.45 ps. It was found in [8] that with mean PMD $\langle\Delta\tau\rangle$ over wavelength range $\Delta\omega$, the uncertainty is $\langle\Delta\tau\rangle * 0.9/\sqrt{\langle\Delta\tau\rangle\Delta\omega}$. Using this equation, the uncertainty of our measurement was 0.27 ps. In order to investigate the PMD fluctuation within every 10 min, Fig. 5b plots the difference between maximum and minimum PMD value (mean DGD). The fluctuation is relatively large during the day and relatively small during the night, then it increases again in the following morning. We may conclude sun radiation is correlated to PMD fluctuation in submarine fibers. Figure 5d shows the water level of the sea during the measurement period at one end of FUT. Two PMD peaks are observed in Fig. 5a at 18:20 in the first day and 6:00 am next morning. They have some correlation to the large downward changes on tide level.

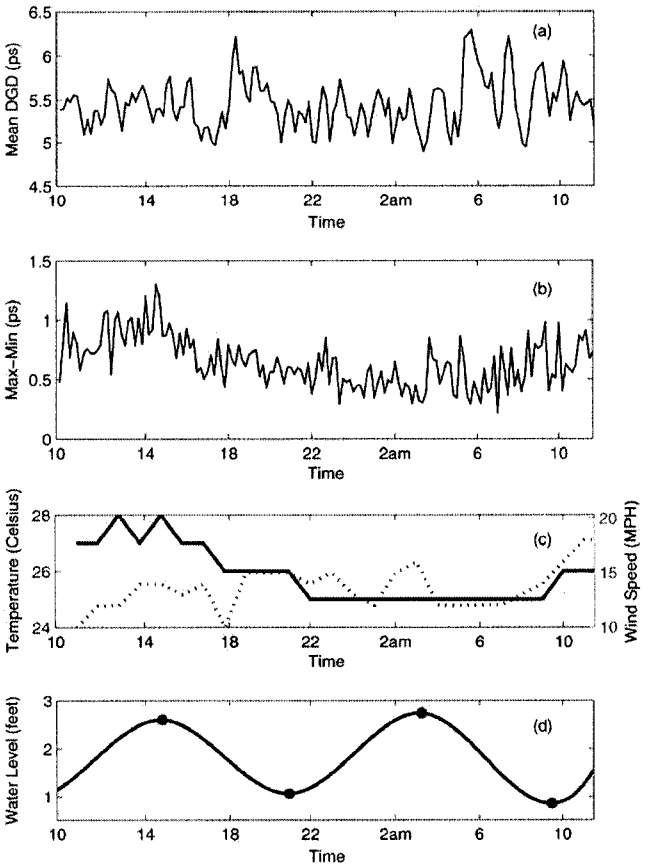

Fig. 5. (a) Time evolution of DGD averaged over both wavelength and 10-min time, (b) wavelength-averaged DGD fluctuation in every 10 min of fiber A, (c) temperature (solid line) and wind (dotted line) data during measurement period, (d) tide (vertical water level) information.

Before explore the causes of PMD fluctuation, it is necessary to know how fast the submarine fibers fluctuate and the measurement accuracy. With 5.45 ps mean DGD of fiber A, the accuracy of this polarization analyzer is $0.03 + 2\%\langle\Delta\tau\rangle = 0.14$ ps assuming 100 nm testing wavelength range. Considering that our range was 60 nm, limited by C-band EDFA, we use 0.25 ps as the criteria of the DGD fluctuation. Thus, for a certain wavelength, DGD values of time t and $t + 15$ s were compared. If the difference is larger than 0.25 ps, we conclude during this

Reproduced with permission of the copyright owner. Further reproduction prohibited without permission.

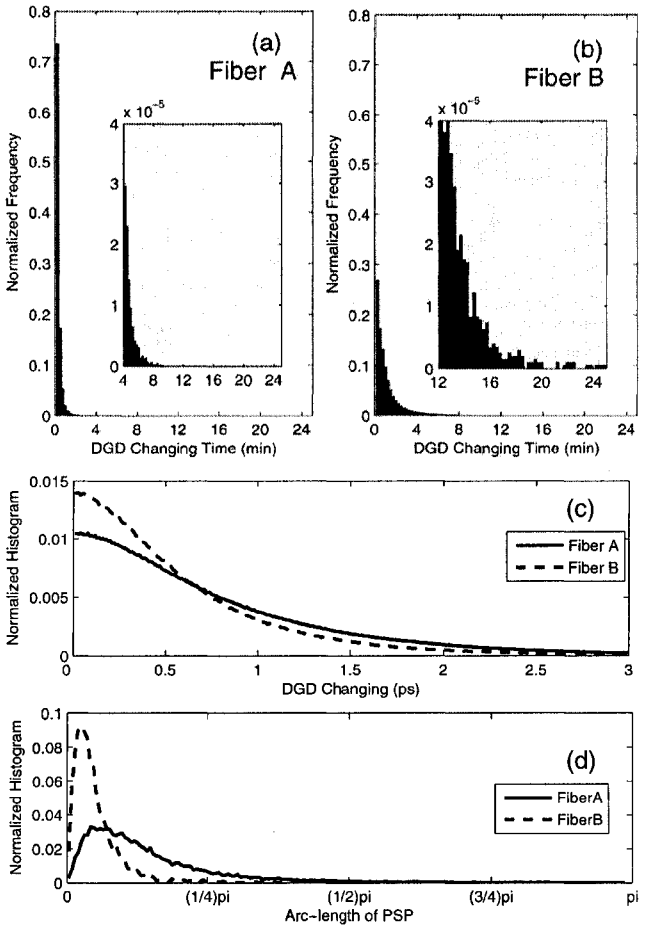

Fig. 6. Normalized histogram of DGD changing time in (a) fiber A and (b) fiber B, respectively; inserts show the tail parts of two profiles. (c) Normalized histogram of DGD change amplitude during every 15 s. (d) Normalized histogram of PSP changing during every 15 s on both fibers A and B.

15-s period DGD had changed; otherwise, we searched for the next DGD changes. We define "decorrelation time" as the time when the change of DGD reaches 0.25 ps. The analysis was performed across the whole testing wavelength range. Figures 6a and 6b describe the normalized histogram of DGD changing time in fiber A over 26 h and fiber B over 7 h (during the daytime), respectively. It shows more than 70% DGD data in fiber A while 25% DGD data in fiber B changed within 15 s. And the slowest decorrelation time in fibers A and B was 10 and 25 min, respectively. One figure in [9] showed SOP rapidly changes from a linear polarization to an elliptical polarization state within 3 min, which has the same order as our results. Figures 6c and 6d show the DGD change amplitude and the arc-length of PSP during every 15 s interval on both fibers A and B, respectively. Since these two fibers sit in the same cable but were tested in two different days, it is reasonable to believe the cable was affected by environmental disturbances.

Here we consider both temperature and tension on submarine fibers. According to [10,11] and references therein, temperature changing may affect fibers in hours or days, not less than a few minutes. In addition, as shown in Fig. 7, the temporal ACF of SOP of fiber C (220 km submarine fiber only, connecting

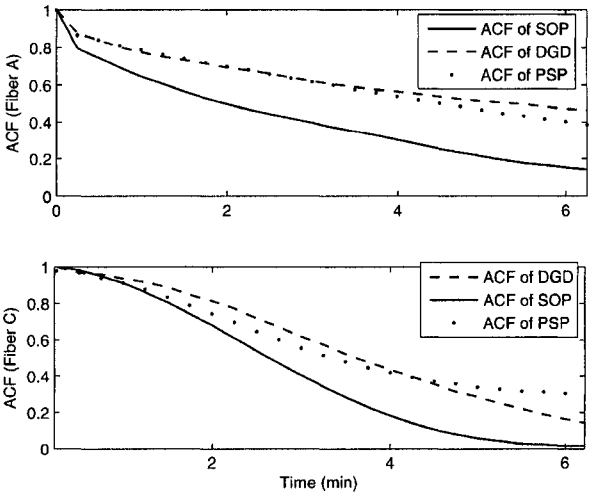

Fig. 7. Temporal ACF of SOP, DGD, and PSP of both fibers A and C for comparison.

Eleuthera and Abaco Island) showed fast drift time comparable to the 240 km combined fiber. These led us to believe the fast fluctuation was mainly contributed by the submarine portion. Similar to the wind effects on aerial fibers, which was reported to be 10 ms [2], the tension induced by ocean waves/currents may affect the signals in submarine fibers. Moreover, our fibers were not buried undersea. Some segments may not touch the seabed but suspend over the trough, which is a normal situation for submarine fibers.

Although [9] mentioned a little about correlation between SOP fluctuation and tides, it left out analysis. Here, we focus on the time evolution of PMD, which is of greater interest to system designers. Tide is the periodic rise and fall of a body of water resulting from gravitational interactions between the Sun, Moon, and Earth. It is the observed recurrence of high and low water along the seashore—usually, but not always, twice daily. Current associated with tide, is the horizontal flow of water. It floods in which makes the tide rise and ebbs out which makes the tide falls. As described in Fig. 5d, the type around testing place is semidiurnal tide, which means there are two high tides and two low tides in one day. The current may flow quickly when a high tide recedes. One high tide appeared at 15:00 and the subsequent low tide arrived at 21:00, so the current with maximum speed was around 18:00. Similarly the current flows quickly at about 6:15 am next morning. Since the tidal/current effect has particular direction, at the moment of maximum current, submarine fiber should have the maximum induced tension or displacement if any, which corresponds to the large absolute PMD value. Therefore, around those two time moments, PMD reached two peak values as shown in Fig. 5a. Since the distance between two ends of fiber is about 80 km, it is conceivable that tide times at two ends are different. And the fluctuation of PMD magnitude is a combined tidal effect on the cable over the whole length. Therefore, there are some smaller peaks following main peaks in Fig. 5a. We also measured fiber C during the maximum drop of tide level according to tide broadcast. The PMD value (mean DGD) was calculated to be 7.42 ps in 1 h, and it corresponds to the period of maximum DGD for fiber C.

Reproduced with permission of the copyright owner. Further reproduction prohibited without permission.

The different PMD fluctuation speed between the daytime and nighttime might be related to the Sun and associated currents activities. The unevenness in ocean temperature, water density and salinity are the direct causes for currents. In the daytime, the solar radiation can strengthen these perturbance and hence produce stronger currents.

5. Conclusion

We performed fast PMD measurements on three installed submarine fibers under Caribbean Sea, and observed Maxwellian distribution of DGD. The PMD fluctuation was mainly contributed by the tension induced by currents on submarine fibers, which led two PMD peaks during about 24 h. The fastest changing of DGD in two fibers was found to be less than 15 s, limited by testing speed.

Acknowledgment

The authors thank J. Stears and many other individuals at Caribbean Crossings who helped this field test. We also thank R. Stolte and D.S. Waddy for helpful discussions.

References

[1] J. Cameron, L. Chen, X. Bao, J. Stears, Time evolution of polarization mode dispersion in optical fibers, IEEE Photon. Technol. Lett. 10 (9) (1998) 1265–1267.

[2] D. Waddy, P. Lu, L. Chen, X. Bao, Fast state of polarization changes in aerial fiber under different climatic conditions, IEEE Photon. Technol. Lett. 13 (9) (2001) 1035–1037.

[3] J. Wuttke, P. Krummrich, J. Rosch, Polarization oscillations in aerial fiber caused by wind and power-line current, IEEE Photon. Technol. Lett. 15 (6) (2003) 882–884.

[4] C. Poole, N. Bergano, R. Wagner, H. Schulte, Polarization dispersion and principal states in a 147-km undersea lightwave cable, J. Lightwave Technol. 6 (7) (1988) 1185–1190.

[5] Y. Namihira, Y. Horiuchi, S. Ryu, K. Mochizuki, H. Wakabayashi, Dynamic polarization fluctuation characteristics of optical fiber submarine cables under various environmental conditions, J. Lightwave Technol. 6 (5) (1988) 728–738.

[6] T. Takahashi, T. Imai, M.A. Takahashi, T. Imai, M. Aiki, Time evolution of polarization mode dispersion in 120 km installed optical submarine cable, Electron. Lett. 29 (18) (1993) 1605–1606.

[7] M. Karlsson, J. Brentel, Autocorrelation function of the polarization mode dispersion vector, Opt. Lett. 24 (14) (1999) 939–941.

[8] N. Gisin, B. Gisin, J.P.V. der Weid, R. Passy, How accurately can one measure a statistical quantity like polarization-mode dispersion?, IEEE Photon. Technol. Lett. 8 (12) (1996) 1671–1673.

[9] Y. Namihira, T. Kawazawa, H. Wakabayashi, Field demonstration of endless polarization control in 195-km installed optical fiber submarine cable at a sea depth of 2900 m, IEEE Photon. Technol. Lett. 3 (4) (1991) 384–386.

[10] M. Karlsson, J. Brentel, P. Andrekson, Long-term measurement of pmd and polarization drift in installed fibers, J. Lightwave Technol. 18 (7) (2000) 941–951.

[11] C. Allen, P. Kondamuri, D. Richards, D. Hague, Measured temporal and spectral pmd characteristics and their implications for network-level mitigation approaches, J. Lightwave Technol. 21 (1) (2003) 79–86.

Reproduced with permission of the copyright owner. Further reproduction prohibited without permission.

Chapter 7

Continuous and damped vibration detection based on fiber polarization diversity detection sensor by Rayleigh backscattering

[**Ziyi Zhang** and Xiaoyi Bao, "Continuous and Damped Vibration Detection Based on Fiber Diversity Detection Sensor by Rayleigh Backscattering," *Journal of Lightwave Technology, IEEE,* 26, 852-838 (2008)]

So far, we have studied polarization effects in optical fiber communication system. From the communication's perspective, fluctuation of polarization states increases the complexity of system design and PMD mitigation. However, from the standpoint of sensing, it is the sensitivity of polarization states to environmental effects that can be utilized to monitor external conditions. Good sensitivity and quick response of polarization effects with respect to disturbances are two key characteristics in order to develop a vibration sensor. The following chapters (Chapter 7 ~ Chapter 9) form the second part of this thesis: using polarization effects to build an optical fiber vibration sensing system.

Among various optical fiber sensors as mentioned in Section 3.2, OTDR has been chosen as the basic configuration due to its distributed sensing ability for large infrastructures. According to the calculation shown in Section 3.3.1, for a $100ns$ pulse

Reproduced with permission of the copyright owner. Further reproduction prohibited without permission.

input the Rayleigh backscattering level is 62dB lower than the pulse peak power. Thus, in order to get enough backscattered power, continuous wave (CW) light has been used instead of pulsed light in this chapter to verify whether the Rayleigh backscattering of polarized light is sensitive to external disturbances or not. So this chapter serves as the first research phase; the aim is to build a vibration sensor without resolving the location information along the fiber link.

A laser source and a detector are two critical components for a vibration sensor. Several types of laser source with various coherence lengths have been investigated, including a tunable laser, a DFB laser (distributed feedback laser) and a fiber laser. As for the detection requirement, the weak backscattered signal suggests a sensitive and low noise detector is needed. As discussed in Section 3.3.2, two noise mechanisms exist in a photodetector: shot noise and thermal noise, both of which increase with the detector bandwidth. Moreover, since location information is not required in phase one, the detector bandwidth can be as low as the target vibration frequency (~kHz) in order to reduce the noise level. Most of the commercial photodetectors are specialized for high speed detection with wide bandwidth (hundreds of MHz to tens of GHz), which would introduce more noises. As a result, a narrow bandwidth detector has been developed in our lab to fulfill the detecting requirement for the vibration sensor. More details about the sensor setup will be given in this chapter.

After successfully developing the polarization-based vibration sensor, we then conducted a series of experiments in the lab: continuous vibration induced by a piezo fiber stretcher and damped vibration associated with a cantilever beam. All the test results have been confirmed either by a piezoelectric accelerometer or a polarization analyzer.

Reproduced with permission of the copyright owner. Further reproduction prohibited without permission.

Continuous and Damped Vibration Detection Based on Fiber Diversity Detection Sensor by Rayleigh Backscattering

Ziyi Zhang and Xiaoyi Bao, *Senior Member, IEEE*

***Abstract*—An optical fiber vibration sensor based on a polarization diversity scheme has been developed to study structural vibration properties under external disturbance. The polarization diversity scheme has improved signal-to-noise ratio (SNR) by over 13 dB with capability of detection frequency of sub-hertz to tens of kilohertz. The minimum dynamic strain we have detected is 3 nε, and the SNR of the sensor is >37 dB without any averaging. For the first time, Rayleigh backscattering has been utilized to detect continuous and damped vibration generated by a piezo fiber stretcher and vibrating cantilever with a frequency range of sub-hertz to 16 kHz. We also use this sensor and polarization analyzer to characterize the polarization state change and phase shift of the piezo fiber stretcher in transmission and Rayleigh backscattering up to kilohertz frequency, both results agrees quantitatively.**

***Index Terms*—Polarization, Rayleigh backscattering, vibration detection sensor.**

I. Introduction

TO MONITOR and detect damage at the earliest possible stages is crucial for civil infrastructures, mechanical processes, and aerospace transportation. A promising technique of measuring structural response under impact wave has been proposed to identify, locate, and characterize damage as a global damage detection method [1]. The time domain signal under impact wave or the vibration frequency spectrum is taken as an indicator of mechanical condition with changes being recognized as structure degradation. These kinds of responses are mainly in the range of low frequencies as our applications mostly focus on large structures such as bridges, highway pavements, pipeline leakage, offshore platforms, and seismic activity.

The accelerometer is the most conventional vibration sensor for monitoring dynamic properties of structures in the presence of external disturbance. A piezoelectric accelerometer is an electromechanical device that produces an output voltage proportional to an applied vibratory acceleration [2]. Although it is accurate and sensitive, the nature of covering a relative small area and the difficulty of electrical isolation make it unsuitable for health monitoring on large civil structures and certain applications surrounded by electrical and magnetic field, such as power transformers.

Recently, optical fiber vibration sensors have received more and more attention for such purpose with superiority of electromagnetic interference immunity, corrosion resistance, chemically inert, and lightweight. These sensors include Fabry–Perot interferometers [2], intensity-based optical fiber cantilever with two cleaved fiber ends in a capillary tube [3], fiber bragg grating (FBG) array [4] and Mach–Zehnder interferometer for measuring mechanical vibrations at magnetic cores of power transformers [5]; all of which either work as point sensor or are able to cover the short sensing length with relatively large strains and lower vibration, or cut off from sub-hertz frequency components.

This paper presents an optical fiber vibration sensor based on a polarization diversity scheme, which is sensitive to the structural vibration induced by small external forces with 3 n ε minimum detectable dynamic strain. Benefited from its high signal-to-noise ratio (SNR) (>37 dB) without signal averaging, this sensor is capable of detecting continuous and damped vibration with frequency range of sub-hertz to 16 kHz. Also, a configuration based on Rayleigh backscattering has been proposed for the first time to detect a structure's response under impact efficiently in real time. Both transmission and backscattering setups have been investigated experimentally by a few meters long piezo fiber stretcher and vibrating cantilever. Compared to the commercial polarization analyzers, our sensor could provide real-time monitoring and phase shift information of continuous vibration, which is useful to study structural vibration properties. Finally, with a pulsed laser in the backscattering configuration, we demonstrate that our sensor is able to detect external disturbances along the fiber length in a fully distributed manner.

II. Principle and Background

Our optical fiber vibration sensor is based on birefringence properties of single mode fibers (SMF). It is known that in single mode fiber, some random imperfections breaks the circular symmetry of the fiber core, causing two orthogonally polarized components of light to travel with different velocities. The birefringence in fiber varies with many physical parameters such as: strain, temperature, pressure wave, ultrasonic fields, etc., leading to changes in the phase shift between two polarization eigenmodes. Thus, the output state of polarization (SOP) changes at the fiber end. By monitoring the power change of the polarized light in time and frequency domain, one can detect the

Manuscript received August 23, 2007; revised December 18, 2007. This work was supported by the Canadian Networks of Centers of Excellence: CIPI, GEOIDE and the Natural Sciences and Engineering Research Council (NSERC) of Canada.

The authors are with the Physics Department, University of Ottawa, Ottawa, ON K1N 6N5, Canada (e-mail: xbao@uottawa.ca).

Color versions of one or more of the figures in this paper are available online at http://ieeexplore.ieee.org.

Digital Object Identifier 10.1109/JLT.2008.919446

Reproduced with permission of the copyright owner. Further reproduction prohibited without permission.

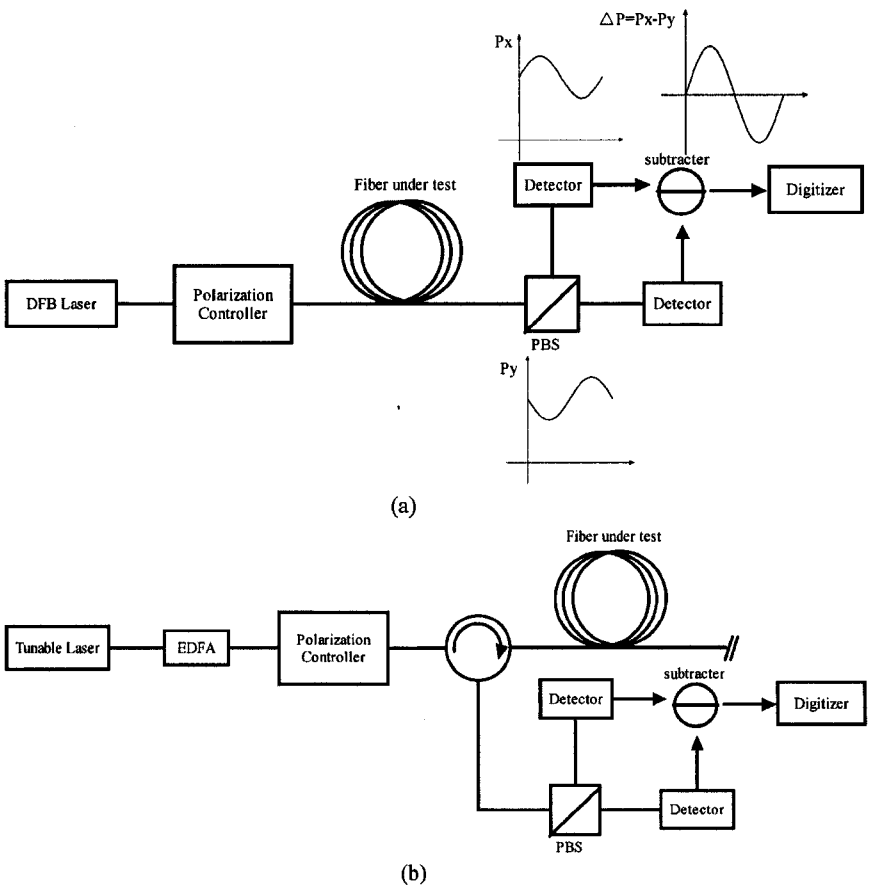

Fig. 1. Experimental setup to detect continuous and damped vibration by (a) transmitted light and (b) Rayleigh backscattering.

impact wave as well as the vibration frequency in real time. The temperature change is a slow process, which can be neglected.

For detection in large structures, not only the dynamic response or vibration frequency, but also the impact location is of great interest. In order to achieve a distributed vibration sensor, a configuration based on Rayleigh backscattering is proposed to measure impact wave information as well as vibration frequencies. The time resolved polarization state of backscattered light provides polarization properties along the fiber link. Similar setup was developed as a first fully distributed optical fiber measurement for physical parameters in earlier 1980s [6] and then adopted as a diagnostic tool in optical communication system to identify high polarization mode dispersion (PMD) fiber sections [7]. Both cases are for static measurements as SOP or degree of polarization (DOP) of backscattered light should be obtained through a polarization analyzer, which extracts four Stokes components, s_0, s_1, s_2, and s_3. However, for purpose of dynamic measurement, the sensor should respond fast enough in order to catch the structure's response to the impact wave. It will be shown in Section III that one Stokes component s_1 is sufficient to provide frequency and damping properties of structural vibrations without knowledge of full SOP information, which is very important for dynamic monitoring. First, continuous wave (CW) light is used to detect continuous and damped vibration using Rayleigh backscattering in real time and then a pulsed laser is applied to prove the concept of fully distributed vibration sensing.

III. Experimental Setup

Fig. 1 depicts the optical fiber vibration sensor in two different forms: one is using transmitted light and the other is using Rayleigh backscattering.

For the transmitted light as in Fig. 1(a), a linearly polarized light from a DFB laser source passing through a polarization controller launches into a few meters long sensing fiber. At the other end of the sensing fiber, a polarization beam splitter (PBS) is positioned to separate the input light into two orthogonally polarized beams, which are detected by two photodetectors with 16-kHz bandwidth low noise amplifiers to minimize the noises and to enhance the sensitivity.

The two output beams from PBS will encounter relative π phase shift when two beams are balanced, as illustrated in Fig. 1 both outputs consist of a small ac component plus a large dc portion. Thus by subtracting the two signals, we are able to enhance the ac signal by 3 dB and remove the dc portion as only ac signals include vibration information under external perturbations. The signal is amplified before digitized and displayed on the computer. In order to show the benefit of such a polarization diversity scheme, we recorded the signal from one beam (Px) and the subtracted signal ($\Delta \mathrm{P} = \mathrm{Px} - \mathrm{Py}$) with condition of stable sensing fiber simultaneously as plotted in Fig. 2(a). The peak to peak value of Px and P are about 22 and 2 mV, respectively, which illustrates the polarization diversity scheme not only provides ac signal but also reduces the noises caused by power fluctuation. Furthermore, the power

Reproduced with permission of the copyright owner. Further reproduction prohibited without permission.

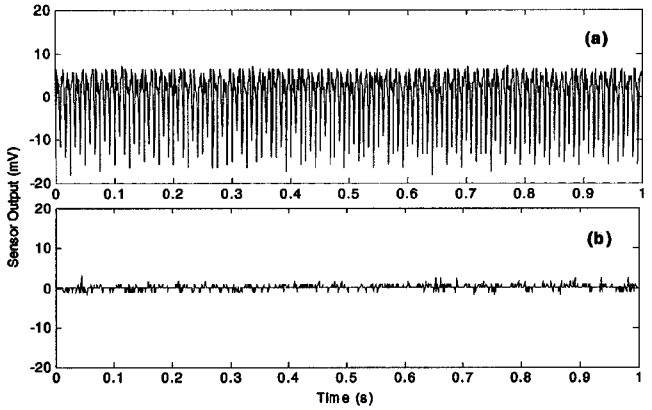

Fig. 2. SNR improvement by polarization diversity scheme; signal from (a) Px and (b) $\Delta P = Px - Py$.

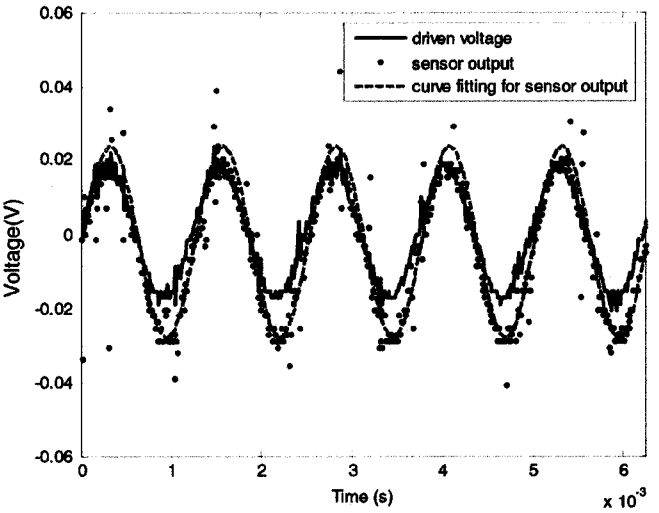

Fig. 3. Minimum detectable signal with 20-mV driven signal (solid line) on piezo plate: sensor output data (dots) and the curve fitting (dashed) line.

spectrum by fast Fourier transform (FFT) of Fig. 2(a) shows a 60-Hz peak, which comes from ac supply, while that of Fig. 2(b) does not. In our case, considering combination of (x) and (y) signal with 11 times less noises, the SNR is improved by 13.4 dB compared to merely detecting one beam of PBS or using a polarizer instead of a PBS. Another advantage of this scheme is the capability to measure sub-hertz vibration. P is usually read out by a dc coupled digitizer, while for Px alone, usually it is ac coupled with cutoff frequency around 10 Hz; here dc offset has been removed, so we can detect sub-hertz signal at very low signal level.

Various light sources have also been investigated in this setup. They are a fiber laser (NP Photonics), a DFB laser (JDSU CQF938/500), and a tunable laser (Agilent 8164A) with coherent control off or on, which have 3 kHz, 1 MHz, 100 kHz, and 50 MHz linewidths, respectively. Since the polarization diversity scheme is capable of eliminating source noises, no obvious differences have been noticed and they all experimentally work well for a few to a hundred meters sensing fiber.

While measuring polarization change of Rayleigh backscattering as shown in Fig. 1(b), the choice of light source is critical. Conventional optical time domain reflectometry (OTDR) uses a relatively broad linewidth laser to avoid ripples in the Rayleigh backscattering curve caused by coherent effects. While for our purpose, the laser linewidth should be narrow enough to prevent depolarization in wavelength, induced by different polarization transformations of various frequency components in light source [7]. Here, the fiber under test is a few meters sensing fiber (either 4.4 m SMF wounded on piezo fiber stretcher or 0.8 m SMF tapped on the vibrating cantilever) connected with 100 m SMF on spool. We found the tunable laser (Agilent 8164A, wavelength fixed at 1550 nm) with 50 MHz linewidth provides a better overall result. If the linewidth is further reduced to a few megahertz, the interference effect arises seriously so that the sensor output fluctuates even for stable sensing fibers, which makes it not appropriate for such application. As described in Fig. 1(b), light after boosted by EDFA is about 17 dBm, and the backscattered intensity is -40 dBm at the photodetectors. The detection end configuration is the same as the one in the transmission setup. Several tiny loops were made at the end of fiber under test to avoid the end-reflection by bending loss.

IV. Results and Discussion

Two experiments were performed to evaluate the sensor: one is the continuous vibration induced by a piezo fiber stretcher, while the other is the damped vibration caused by a cantilever beam.

A. Continuous Vibration Detection

On the piezo fiber stretcher (model 915, Canadian Instrumentation and Research Ltd.), 4.4-m-long SMF is wounded on the piezo plate to produce continuous vibration by an applied periodic signal. The upper limit of its frequency response is 20 kHz and it provides fairly small stretch. The minimum detectable signal is for 20 mV periodic voltage on the piezo plate giving 3 $n\varepsilon$ dynamic strain on the fiber, which is not detectable for any static strain gauges. Fig. 3 shows the sensor's performance with an 800 Hz, 20 mV sinusoidal driven signal, the spikes are due to the high voltage dc power supply on the piezo plate.

Fig. 4 provides the response of our vibration sensor following the fiber stretcher under a sinusoidal driven signal (black dotted line) at 10 Hz, 100 Hz, 1 kHz, and 5 kHz. The blue and red solid lines represent the results from transmitted and backscattered light, respectively. All the results here are without averaging or filtering at signal processing, so the sensor response time is microseconds. However, in order to improve SNR of weak backscattered light, sinusoid curve fitting has been utilized in Fig. 4 (red lines).

In Fig. 4, both the amplitude and the phase delay of sensor output relative to driving signal vary with different vibration frequencies. Fig. 5(a) describes the frequency response by transmitted light with maximum at ~800 Hz corresponding to the resonant frequency of the piezo plate. This nonuniform response can be demonstrated by the output SOP change on Poincaré sphere, measured by an Agilent 8095-B polarization

Reproduced with permission of the copyright owner. Further reproduction prohibited without permission.

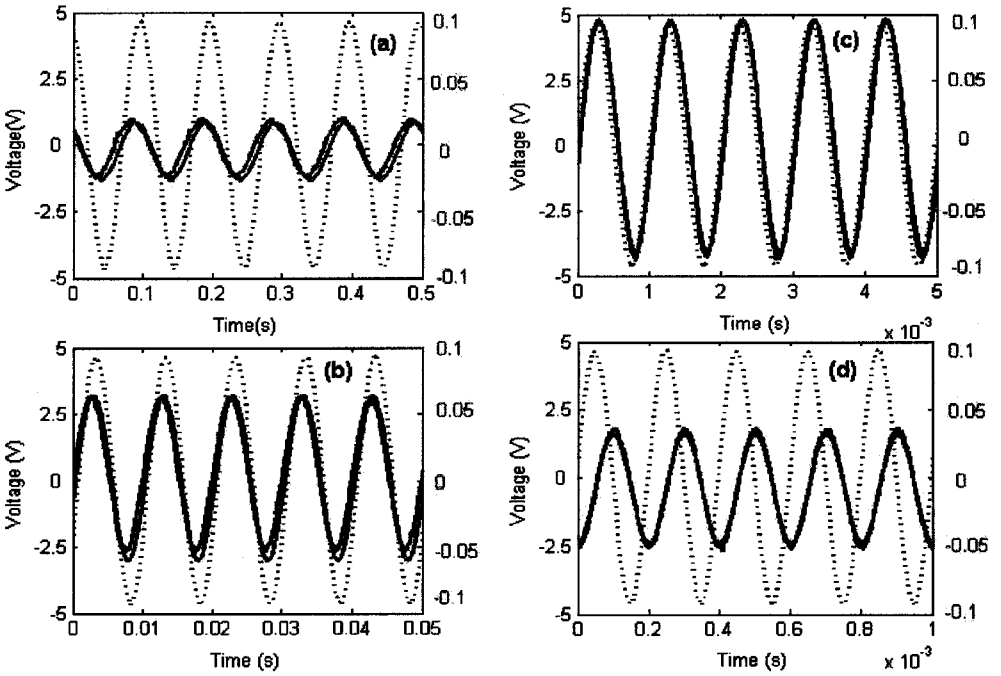

Fig. 4. Sensor output detected of transmitted light (blue line, left label) and backscattered light (red line, right label) along with 5-V driven signal (dotted line) of piezo fiber stretcher at (a) 10 Hz, (b) 100 Hz, (c) 1 kHz, and (d) 5 kHz.

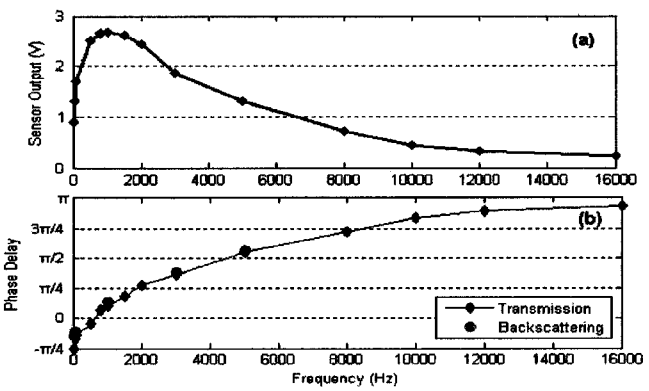

Fig. 5. (a) Frequency response of piezo fiber stretcher by transmitted light. (b) Phase delay of piezo fiber stretcher by transmitted (diamond) and backscattered light (circle).

analyzer, as described in Fig. 6 (blue). Among 10 Hz, 100 Hz, and 1 kHz driven frequencies, the output SOP at 1 kHz is the largest, while 10 Hz is the smallest, which agrees the trend of frequency response curve from our vibration sensor. As for the phase delay, Fig. 5(b) shows it is negative at low frequencies and turns to positive at ~800 Hz and then keeps increasing at higher frequencies. This phenomenon is related to material dispersion of the piezo plate: at the turning point, its response synchronizes with the driving signal. In other words, the turning point (~800 Hz) is the piezo plate's resonant frequency, which explains why the sensor output reaches maximum at this frequency. Therefore, we have demonstrated that the sensor can be utilized to study structural vibration properties and material processing. It is worthy to point out that with our sensor, both amplitude and phase shift could be extracted while the polarization analyzer does not give the phase information.

To investigate the efficiency of backscattered and transmitted light, with the setup in Fig. 1(b), we first measure the output SOP change of backscattering on the Poincaré sphere by the polarization analyzer and then release those tiny loops at fiber end to measure the SOP of transmitted light again, which would guarantee the input SOP keeps unchanged during short testing period. Since the DOP of backscattering is less than 1.0, three stokes components have been normalized before plotting on the sphere. Fig. 6 compares output SOP at three driven frequencies on the piezo fiber stretcher: 10 Hz, 100 Hz, and 1 kHz, which shows backscattering has comparable efficiency to transmitted light although it yields weak output signals, almost reaching our photodetector limit.

B. Damped Vibration Detection

Impact wave is difficult to detect as the process is not repeatable, hence, waveform averaging would lose information. While due to the high SNR of the polarization diversity detection, this sensor does not need averaging, making it suitable to detect the structure's responses to the impact wave. In order to prove this concept, a simple cantilever beam has been constructed as illustrated in Fig. 7. An elastic steel meter ruler is used as a beam here with dimension 400 × 20 × 1 mm($L \times W \times H$), and one end is clamped on the optical table. An SMF is taped on top of it from one end to the other and then returned back giving 0.8 m sensing length and lead fibers are all taped on the table to avoid extra noise. Hence, sensing fiber is able to follow damped

Reproduced with permission of the copyright owner. Further reproduction prohibited without permission.

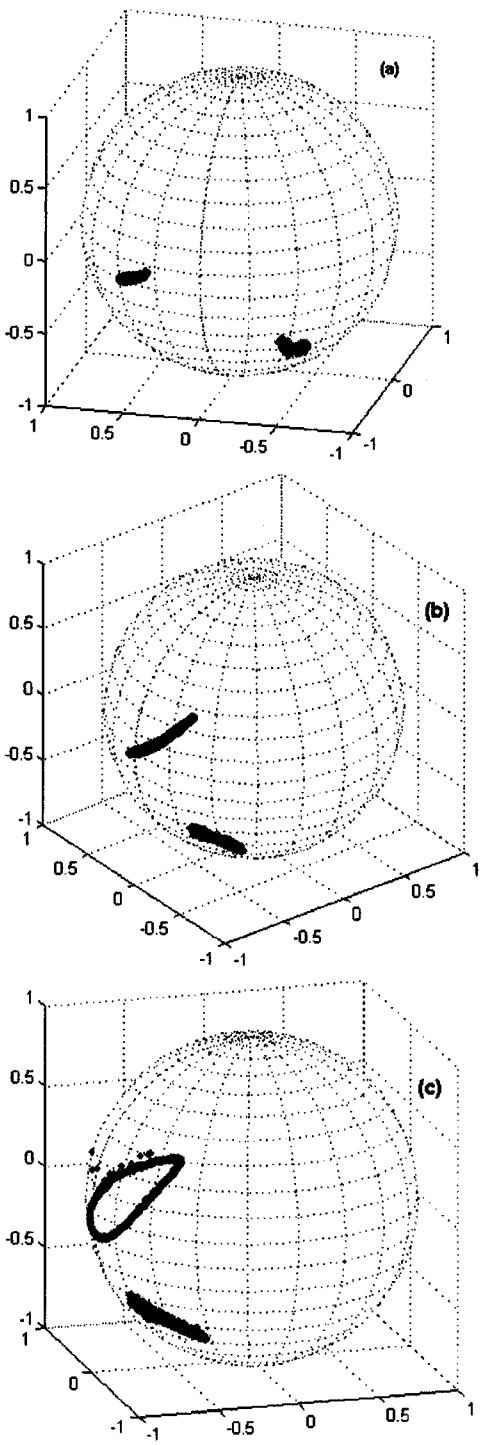

Fig. 6. SOP change of transmitted light (blue) and backscattered light (red) on Poincaré sphere at (a) 10 Hz, (b) 100 Hz, (c) 1 kHz.

vibration of the ruler after an external force applied on it, for example, by impact hammer or by hand.

Fig. 8(a) and (c) depicts time trace curve of the sensor response for the first 10 s after flipping the ruler by hand using transmission and backscattering, respectively. They both clearly show a damped vibration with fundamental frequency 8.3 Hz and harmonics at 16.6 Hz computed by power spectrum after FFT analysis as in Fig. 8(b) and (d). We have noticed that the time trace is asymmetric with larger amplitude at the upper half and smaller at the lower half. This is because the bottom of the steel ruler has limited space, leading to a slightly asymmetric cantilever beam. It is also noticed that the amplitude of sensor output depends on the input SOP, but one still can obtain correct vibration frequency and damping trend from the traces in time domain. Nevertheless, this simple test setup has successfully demonstrated our vibration sensor can measure the dynamic property of the structures under impact wave.

As we know, the longer beam corresponds to lower vibrating frequency, based on cantilever beam theory, the first resonant frequency f_1 is given by

$$f_1 = \frac{C_1}{2\pi}\sqrt{\frac{EI}{\rho L^4}} \tag{1}$$

where C_1 is a coefficient for the first mode; E is Young's modulus of the material, I is the moment of inertia; ρ is the mass per unit length; and L is the beam length. The experiment has been carried out with different lengths from 20 to 50 cm in 5-cm intervals, and the linearity between the resonant frequency f_1 and $1/L^2$ is clearly observed in Fig. 9.

C. Feasibility Study of Fully Distributed Vibration Sensing

To prove our sensor's ability for distributed vibration sensing, a simple fiber under test has been constructed by making several small fiber loops with 8-cm diameter sandwiched between two spools of SMF with 500 and 300 m long, respectively. The setup is similar to the one in Fig. 1(b) except a pulse laser to replace CW laser and APD detector is used due to the weak backscattering signals. Here, we use 100-ns pulse with 10-kHz repetition rate, corresponding to 10-m spatial resolution. Fig. 10(a) depicts the backscattering curve after 100 times averaging along the fiber length when all of the fiber under test remains stable. Once the fiber loops is dynamically disturbed, the time domain waveform varies from the disturbing point. Considering the 10-m resolution in this case, signal variations at 495 and 505 m within 1.5-s detecting time have been compared in Fig. 10(b). The signal at 495 m is stable, while the signal at 505 m contains variations due to four disturbances, hence, the external disturbance up to 100 Hz can be monitored with 10-m spatial resolution. This frequency range is adequate for most civil structural monitoring, such as bridges, building, and pipelines.

V. Conclusion

We have successfully demonstrated a polarization-based optical fiber vibration sensor to measure very small vibration (3-n strains) of structure in real time over a large frequency range (sub-hertz to 16 KHz), which shows its promising applications for impact and early damage detection in civil infrastructures. This sensor system does not give the value of dynamic strain, but rather provides the response of the structure under external disturbances by extracting the frequency information and decay (damping) processing. Furthermore, an experimental setup based on Rayleigh backscattering has been developed to monitor continuous and damped vibration efficiently without

Reproduced with permission of the copyright owner. Further reproduction prohibited without permission.

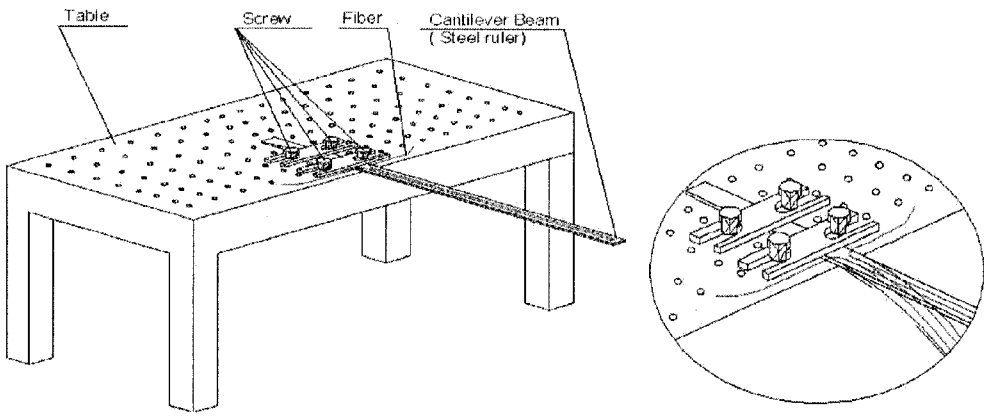

Fig. 7. Simple cantilever beam for impact detection. Red line represents SMF tapped on the beam.

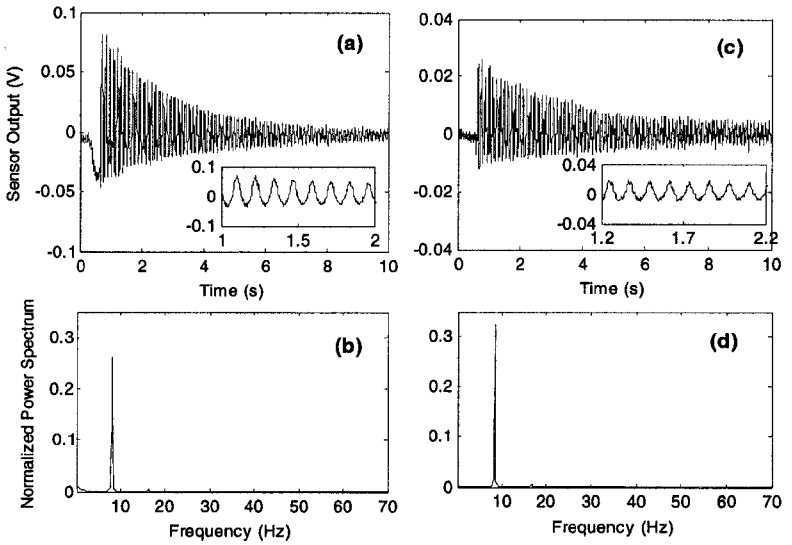

Fig. 8. Impact detection of a vibrating cantilever: (a) time trace by transmitted light, inset shows the beginning part of the profile; (b) normalized power spectrum of (a) with peak at 8.3 Hz; (c) time trace by Rayleigh backscattering, inset shows the beginning part of the profile; (d) normalized power spectrum of (c) with peak at 8.3 Hz.

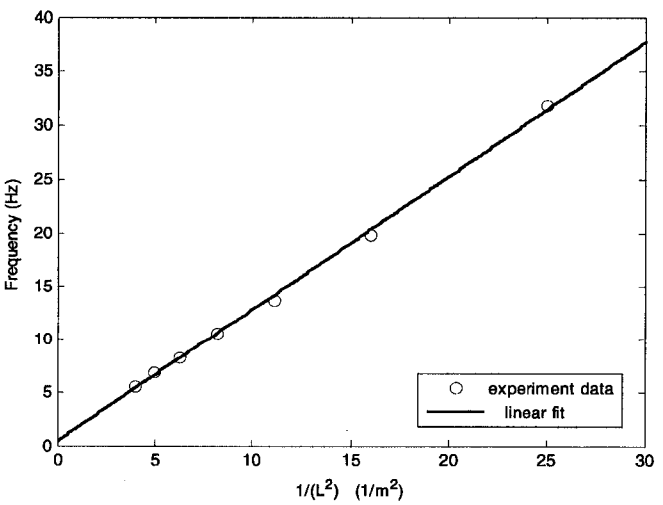

Fig. 9. Relationship between vibration frequency and beam length.

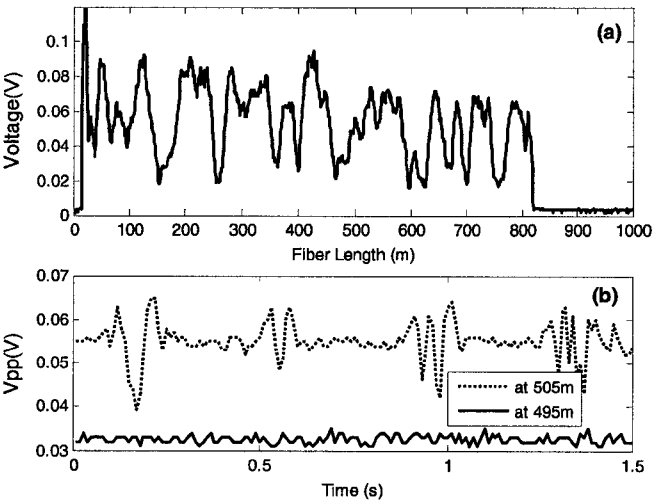

Fig. 10. Distributed vibration sensing: (a) a typical backscattering curve with stable fiber under test and (b) time varied signal at 495 and 505 m when the fiber loops at 500 m has been disturbed dynamically.

full knowledge of SOP in the fiber link. The feasibility study of fully distributed vibration sensor suggests numerous potential applications on structure health monitoring and homeland security.

Reproduced with permission of the copyright owner. Further reproduction prohibited without permission.

ACKNOWLEDGMENT

The authors would like to thank Dr. P. Zhu and R. Bolen for their helpful discussions.

REFERENCES

[1] S. W. Doebling, C. R. Farrar, M. B. Prime, and D. W. Shevitz, "Damage identification and health monitoring of structural and mechanical systems from changes in their vibration characteristics: A literature review," Los Alamos National Laboratory, Tech. Rep. LA-13070-MS, 1996.

[2] T. K. Gangopadhyay and P. J. Henderson, "Vibration: History and measurement with an extrinsic Fabry-Perot sensor with solid-state laser interferometry," *Appl. Opt.*, vol. 38, no. 12, pp. 2471–2477, Apr. 1999.

[3] Y. C. Yang and K. S. Han, "Damage monitoring and impact detection using optical fiber vibration sensors," *Smart Mater. Struct.*, vol. 11, pp. 337–345, 2002.

[4] M. A. Davis, A. D. Kersey, J. Sirkis, and E. J. Friebele, "Shape and vibration mode sensing using fiber optic Bragg grating array," *Smart Mater. Struct.*, vol. 5, pp. 759–765, 1996.

[5] H. L. Rivera, J. A. García-Souto, and J. Sanz, "Measurements of mechanical vibrations at magnetic cores of power transformers with fiber-optic interferometric intrinsic sensor," *IEEE J. Sel. Topics Quantum Electron.*, vol. 6, no. 5, pp. 788–797, Sep./Oct. 2000.

[6] A. J. Rogers, "Polarization-optical time domain reflectometry: A technique for the measurement of field distributions," *Appl. Opt.*, vol. 20, pp. 1060–1074, 1981.

[7] B. Hunttner, B. Gisin, and N. Gisin, "Distributed PMD measurement with a Polarization-OTDR in optical fibers," *J. Lightw. Technol.*, vol. 17, no. 10, pp. 1843–1848, 1999.

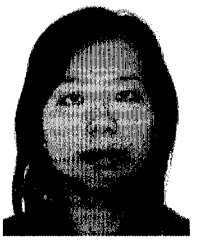

Ziyi Zhang received the B.Eng. degree from Huazhong University of Science and Technology, Wuhan, China, in 2003. She is currently pursuing the Ph.D. degree with the Fiber Optics Group, University of Ottawa, Ottawa, ON, Canada.

Her research interests include distributed optical fiber sensors for dynamic measurement and polarization effects on high-speed communication systems.

Xiaoyi Bao (SM'04) is a Professor with the Physics Department, University of Ottawa, Ottawa, ON, Canada. She is also the Canada Research Chair in Fiber Optics and Photonics. Her research interests include development and applications of the distributed fiber optics sensors for temperature, strain, and vibration measurement, polarization mode dispersion and polarization-dependent loss and chromatic dispersion effects on high-speed communication systems, laser development, and nonlinear effects in fibers. She has published over 200 technical papers in journals and refereed conference proceedings in the previous fields.

Reproduced with permission of the copyright owner. Further reproduction prohibited without permission.

Chapter 8

Distributed optical fiber vibration sensor based on spectrum analysis of Polarization-OTDR

[**Ziyi Zhang** and Xiaoyi Bao, "Distributed optical fiber vibration sensor based on spectrum analysis of Polarization-OTDR system," *Optics Express* 16, 10240-10247 (2008)]

In the previous chapter, a polarization-based optical fiber sensor has been developed and applied to measure continuous and damp vibration. The obtained results have confirmed the feasibility of building a vibration sensor by Rayleigh backscattering. However, owing to the CW input light, we are not able to pinpoint the location of vibration events. Instead only the vibration frequency and damping trend in time domain can be provided. This chapter, as the second research phase, addresses this problem by launching narrow laser pulses to add distribution function to the sensing system.

Narrow pulses bring some special requirements on both laser source and detector. In OTDR or Polarization-OTDR systems the extinction ratio (ER) of pulses should be as high as possible. This increases the system's SNR by eliminating unwanted backscattered light from the pulse base. The ER of a pulse is defined by the ratio of the peak power to

Reproduced with permission of the copyright owner. Further reproduction prohibited without permission.

the base power and is often expressed in decibel, $ER(dB) = 10 \cdot \log\left(P_{peak} / P_{base} \right)$. To generate narrow pulses, two methods are often employed: one is to modulate CW light with an electro-optical modulator (EOM) or an acousto-optical modulator (AOM); the other is to build a pulsed laser which is directly modulated by electric current. In order to detect the backscattered light from narrow pulses (tens to hundreds of ns pulsewidth), the detector should be not only sensitive to weak signals but also with a suitable bandwidth which corresponds to the pulse width. Section 3.3.2 discusses the relationship between pulse width, detector bandwidth, and achievable system's spatial resolution of the sensor.

After careful consideration of all above requirements we decided to custom design a transceiver module. The optical transmitter and receiver were then assembled into one case. The pulsed laser is based on a DFB laser diode that produces optical pulses from an external electrical pulse generator. The pulse ER reaches 45dB, which is higher than that modulated by the EOM (normally ~20dB). The receiver consists of an APD and an amplifying circuit. The receiver bandwidth is designed to be 20MHz, so it should be able to resolve vibrating events with a few meters spatial resolution. Some parameters of the transceiver are summarized as follows and a picture of the transceiver module is shown in Fig. 8.1.

Optical transmitter

- Wavelength – 1550 nm;
- Linewidth – 0.2 nm by -3 dB level;
- Pulse peak power – 30 mW;
- Launch signal – electrical pulse, +3.3V level;
- Pulsewidth – $10ns$ to $10\mu s$
- Relative pulse duration - no more 1%.

Reproduced with permission of the copyright owner. Further reproduction prohibited without permission.

Optical receiver

- Electrical bandwidth – DC ~ 20 MHz.
- NEP (noise equivalent power, when SNR=1) – 2nW;
- Output impedance – 50 Ohm.

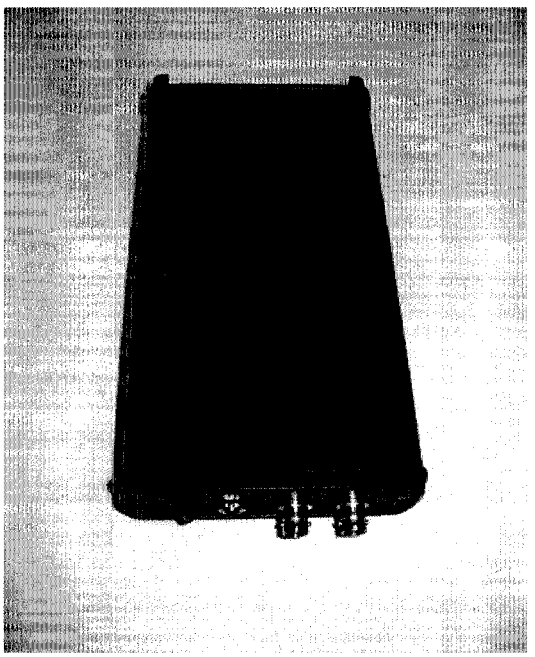

Figure 8.1 A picture of the transceiver module.

With the transceiver module, we have successfully developed a fully distributed vibration sensor based on intensity changes of polarized light in Rayleigh backscattering. Experimental setup and data processing will be given in details in this chapter. Moreover, a spectral analysis has been utilized to detect multiple events even with the same vibrating frequency. This is a desirable function for field applications on structural health monitoring or intrusion sensing, where it is common to have multiple events happening simultaneously.

Reproduced with permission of the copyright owner. Further reproduction prohibited without permission.

Distributed optical fiber vibration sensor based on spectrum analysis of Polarization-OTDR system

Ziyi Zhang and Xiaoyi Bao*

Physics Department, University of Ottawa, 150 Louis Pasteur, Ottawa, ON, K1N 6N5, Canada
**Corresponding author: xbao@uottawa.ca*

Abstract: A fully distributed optical fiber vibration sensor is demonstrated based on spectrum analysis of Polarization-OTDR system. Without performing any data averaging, vibration disturbances up to 5 kHz is successfully demonstrated in a 1km fiber link with 10m spatial resolution. The FFT is performed at each spatial resolution; the relation of the disturbance at each frequency component versus location allows detection of multiple events simultaneously with different and the same frequency components.

©2008 Optical Society of America

OCIS codes: (060.2370) Fiber optics sensors; (120.7280) Vibration analysis; (260.5430) Polarization; (280.1350) Backscattering.

References and links

1. A. J. Rogers, "Polarization-optical time domain reflectometry: A technique for the measurement of field distributions," Appl. Opt. **20,** 1060-1074 (1981).
2. B. Soller, D. Gifford, M. Wolfe, and M. Froggatt, "High resolution optical frequency domain reflectometry for characterization of components and assemblies," Opt. Express **13,** 666-674 (2005).
3. L. Zou, G. A. Ferrier, S. Afshar, Q. Yu, L. Chen, X. Bao, "Distributed Brillouin scattering sensor for discrimination of wall thinning defects in steel pipe under internal pressure," Appl. Opt. **43,** 1583-1588 (2004).
4. C. Zhang, X. Bao, W. Li, A. Deif, B. Cousin and B. Martín-Pérez, "Crack detection of a reinforced concrete beam with distributed Brillouin fiber sensor," Appl. Opt. (to be published)
5. K. Hotate and S. S. L. Ong, "Distributed fiber Brillouin strain sensing by correlation-based continuous-wave technique: cm-order spatial resolution and dynamic strain measurement," Proc. SPIE **4920,** 299-310 (2002).
6. X. Bao, W. Li, C. Zhang, M. Eisa, S. El-Gamal, and B. Benmokrane, "Monitoring the distributed impact wave on concrete slab due to the traffics based on polarization dependence on the stimulated Brillouin scattering," Smart Mater. Struct. **17,** 015003-015008 (2008).
7. B. Hunttner, B. Gisin, and N. Gisin, "Distributed PMD measurement with a Polarization-OTDR in optical fibers," J. Lightwave Technol. **17,** 1843-1848 (1999).
8. A. J. Rogers, Y. R. Zhou, and V. A. Handerek, "Computational polarization—Optical time domain reflectometry for measurement of the spatial distribution of PMD in optical fibers," in 4th Optical Fiber Measurement Conf., *OFMC '97,* (Teddington, U.K.1997), pp.126–129.
9. J. C. Juarez and H. F. Taylor, "Polarization discrimination in a phase-sensitive optical time-domain reflectometer intrusion-sensor system," Opt. Lett. **30,** 3284-3286 (2005).

1. Introduction

Distributed optical fiber sensing has been extensively investigated in past decades due to its superiority over other conventional sensors. The most widely used approaches are based on either the optical time domain reflectometer (OTDR) [1] or the optical frequency domain reflectometer (OFDR) [2], both of which locate external disturbances by optical characteristics of various backscattered light including Rayleigh, Brillouin, and Raman. Distributed Brillouin sensors offer truly distributed sensing capability for deformation and crack detection of steel and concrete structures for static measurement [3, 4]. They can be used to monitor pipelines and bridges, where large size structures have very low vibration frequency, usually of a few Hz. For crack and vibration detection on small structures, such as

#96288 - $15.00 USD Received 16 May 2008; revised 24 Jun 2008; accepted 24 Jun 2008; published 26 Jun 2008
(C) 2008 OSA

Reproduced with permission of the copyright owner. Further reproduction prohibited without permission.

engines and airplane parts of aerospace structures, power cables, trolley cables and impact damage detection, hundreds to kHz frequency detection is required in addition to location information.

Up to now, distributed optical fiber sensors have been mainly studied for static measurements, i.e. no time-varying or slowly time-varying signals, such as, static strain or temperature. Dynamic measurements using the above techniques is difficult to achieve because of the large number of waveforms required to average out the polarization effect induced signal fluctuation or because of the large range of frequency scans that are needed in order to obtain a reasonable signal to noise ratio (SNR) and spatial resolution over a kilometer fiber length.

Hotate et al. recently presented a frequency modulation of the distributed Brillouin sensor by correlation-based continuous wave to implement vibration measurement without suffering weak backscattered signals [5]. However, each time only one sensing point is chosen by the correlation peak of pump and probe light, it is particularly suitable for material processing over a short fiber distance while it is not essentially a fully distributed sensor which should provide information for every point along the fiber under test simultaneously. Time domain analysis based on Brillouin gain dependence of the polarization change is proposed for the dynamic monitoring of highway concrete slab [6]. However, waveform averaging is required to reduce signal fluctuation, limiting the frequency response to 200Hz over 300m sensing fiber.

In this paper, for the first time, a spectrum density of Polarization-OTDR system is proposed to realize fully distributed dynamic measurement along a 1km fiber link with 10m spatial resolution. By carefully designing the transceiver module, high SNR is available to detect up to 5 kHz vibration signals without averaging. Polarization-OTDR was developed as the first fully distributed optical fiber measurement for static physical parameters in the earlier 80's [1] and then adopted as a diagnostic tool in optical communication systems to identify high polarization mode dispersion (PMD) fiber sections [7]. Polarization-OTDR systems described in [1, 7] utilize a polarization analyzer containing three polarizers at the receiver end to extract full knowledge of the state of polarization (SOP) which consumes the testing time severely; based on the analysis of the rotation of polarization state one can get the distributed polarization state change [8]. Here we will show in section 3 that one polarizer is sufficient to identify dynamic events, through which the birefringence change along the fiber could be detected. Moreover, with a novel fast Fourier transform (FFT) spectrum analysis, multiple simultaneous events with different vibration frequencies or even with the same frequencies are able to be accurately located. The spectral density function of location change is equivalent to many variable narrowband filters with bandwidth of <1Hz to improve the SNR of multiple events detection, which allows the disturbance to be detected simultaneously at any location along the sensing fiber. This new technology could in a cost-effective manner provide intrusion sensing for perimeter security at various places or structure health monitoring for large structures, such as bridges, highway pavements, pipeline leakage, etc. with low fault rate due to the multiple frequency components discrimination at <1Hz narrow band.

2. Experimental configuration

2.1 Setup

The choice of the light source is critical for the Polarization-OTDR system. The laser linewidth should be narrow enough to prevent the depolarization in wavelength that is induced by different polarization transformations of various frequency components in the light source [7]; while the interference of backscattered components from different parts of the fiber due to the coherent light source should be avoided. Therefore, the laser linewidth of Polarization-OTDR usually falls between that of conventional OTDR and Coherent-OTDR which requires kHz bandwidth [9]. Here, a pulsed laser with 0.2nm spectral linewidth has been chosen as the light source.

#96288 - $15.00 USD Received 16 May 2008; revised 24 Jun 2008; accepted 24 Jun 2008; published 26 Jun 2008
(C) 2008 OSA

Reproduced with permission of the copyright owner. Further reproduction prohibited without permission.

The experimental setup constructed is shown in Fig. 1. A 100ns pulse of polarized light with 10kHz repetition rate is used. The input polarization direction is chosen to ensure zeros of the Rayleigh scattering to be minimized in the fibers, and the signal strength is maximized along the fiber length. As the pulse propagates along the fiber under test, the Rayleigh backscattering is continuously collected at the input end via a circulator. An avalanche photodiode (APD) detector and amplifiers of 20MHz bandwidth is designed to detect weak backscattered signals and to eliminate extra noises. As we know the SOP evolves in periodical oscillation due to the beat length of the single mode fiber.

The measurement range can be improved by increasing pump power or pulse width; while the spatial resolution is determined by the pulse width. The long sensing length means pulse takes longer time to travel in the fiber, which leads to the decrease of the maximum detectable frequency. Therefore, there is always a trade off between the sensing length, spatial resolution and vibration frequency range. Thus, all the parameters should be carefully chosen according to a specific application.

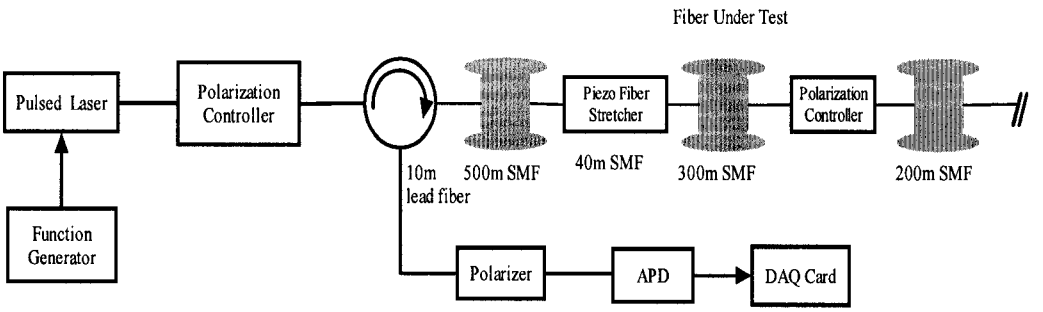

Fig. 1. Experimental setup of Polarization-OTDR system

2.2 Data processing

In order to achieve a fully distributed vibration sensor, the signals collected by DAQ card (NI-PCI 5122) have been processed in the following way as illustrated in Fig. 2. First, one Polarization-OTDR curve is stored onto the on-board memory of the DAQ card every 0.1ms, corresponding to a 10kHz repetition rate. Once the memory is filled up, all of thousands of curves will be transferred to computer to be further analyzed. Then, the signals at a certain position will be extracted out and plotted verse time as in step ii. So if the fiber at z_1 is dynamically disturbed, the time trace at z_1 will vary from constant, indicating one disturbing point.

However, there was a problem remaining in the Polarization-OTDR system preventing its application in multiple events detection: the backscattered signals beyond the disturbing point z_1 would be affected as well. Rogers implemented a complicated algorithm [8] to correct the subsequent effects in static measurement; however, such method is not suitable for the purpose of dynamic measurement due to time requirements. Here, a novel FFT spectrum method is proposed for the first time to identify multiple events along a fiber link for the distributed vibration sensor. As shown in step iii, the FFT spectrum is computed for every point beyond the disturbing point z_1. Multiple events with different frequency components are able to be distinguished by the peak readings of the spectrums. As for multiple events with exactly the same frequency f_1, we will demonstrate that by plotting the intensity of f_1 along the fiber as in step iv, these events could be located successfully. Results and further discussions can be found in section 3.2 and 3.3.

#96288 - $15.00 USD Received 16 May 2008; revised 24 Jun 2008; accepted 24 Jun 2008; published 26 Jun 2008
(C) 2008 OSA

Reproduced with permission of the copyright owner. Further reproduction prohibited without permission.

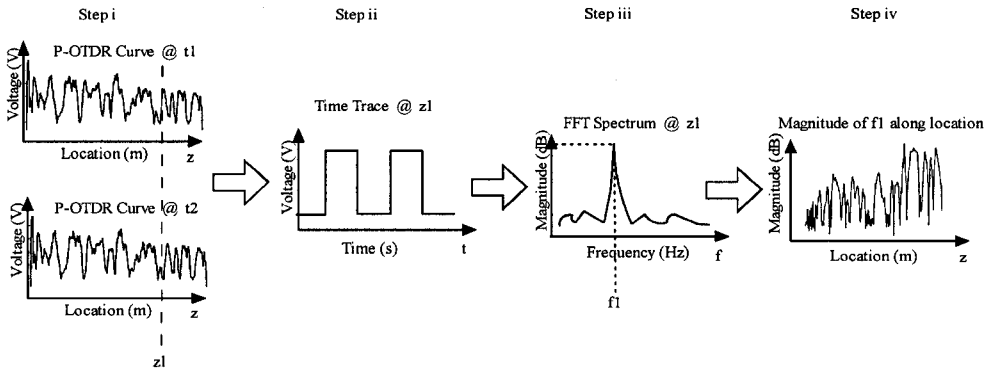

Fig. 2. Schematic diagram for data processing

3. Results and discussion

3.1 Single event detection

The fiber under test consists of a piezo fiber stretcher (OptiPhase PZ2) sandwiched between two spools of SMF with 500m and 300m long, respectively. And several small loops are made at the end of the fiber to avoid the end-reflection by bending loss. The piezo fiber stretcher is constructed by a 40m long single mode fiber (SMF) wounded on a piezo plate to produce continuous vibration by an applied periodic signal and with 1~5 milli-radians/V birefringence modulation. Although the piezo is able to stand 800V peak to peak input, only a 5Vpp driven signal is used here, which causes ~0.5 micro-strain equivalent stretch. The amount of birefringence modulation detected by spectral analyzed POTDR is not strain, rather the birefringence induced intensity change by the piezo fiber stretcher. A low drive voltage is used as we want to check the minimal detectable birefringence change caused by a disturbance. And the birefringence change is detectable for the driven signal reduces to 2Vpp, corresponding to 2~10 milli-radians change and it is equivalent to 0.2 micro-strain change for PZT stretcher.

Post-signal processing as shown in Fig. 2, step i to iii, is employed here by taking an average every 100 Polarization-OTDR curves in step ii. Considering a 10kHz repetition rate of the pulsed light, the effective sampling rate becomes 100Hz, which has set the limitation for impact wave detection. Figure 3(a) plots the FFT spectrum of 1.5 seconds time domain data at 550m with a peak at 22Hz when the piezo is driven by 5Vpp, 22Hz square wave. It is worthy to mention that the on-board memory of the DAQ card would be full with 1.5 seconds of raw data, and after transferring and analyzing the data, it is able to collect data again. Benefited to its high sensitivity, this Polarization-OTDR system makes it possible to measure higher frequency disturbance without any averaging in step ii. Hence, the maximum detectable frequency is 5kHz using a 10kHz sampling rate. As plotted in Fig. 3(b), we demonstrate that when driven frequency of the piezo is set to 4234Hz, this peak frequency is clearly shown in the FFT spectrum at 550m.

Furthermore, in real field applications, a vibrating event usually contains a frequency spectrum rather than one distinct frequency. In order to stimulate events with multi-frequencies, a sweep function is used as the driven signal for the piezo fiber stretcher. Figure 3(c) plots a FFT spectrum of the P-OTDR time trace at 550m (black solid line) compared to a spectrum of the driven signal (red dotted line), which sweeps from 15Hz to 30Hz in 1.5 seconds. This result is obtained by averaging 100 P-OTDR waveforms. If no average is taken, higher frequency components are detectable. Figure 3(d) shows the spectrum of a signal at 550m at a higher vibrating frequency range of 4600 to 4680Hz, the measured vibration spectrum agrees well with its corresponding driven signal over 1.5 seconds. For the same driving power the wider the spectrum is equivalent to lower the energy of each frequency component, hence the detected spectrum range is limited by signal to noise ratio.

#96288 - $15.00 USD Received 16 May 2008; revised 24 Jun 2008; accepted 24 Jun 2008; published 26 Jun 2008
(C) 2008 OSA

Reproduced with permission of the copyright owner. Further reproduction prohibited without permission.

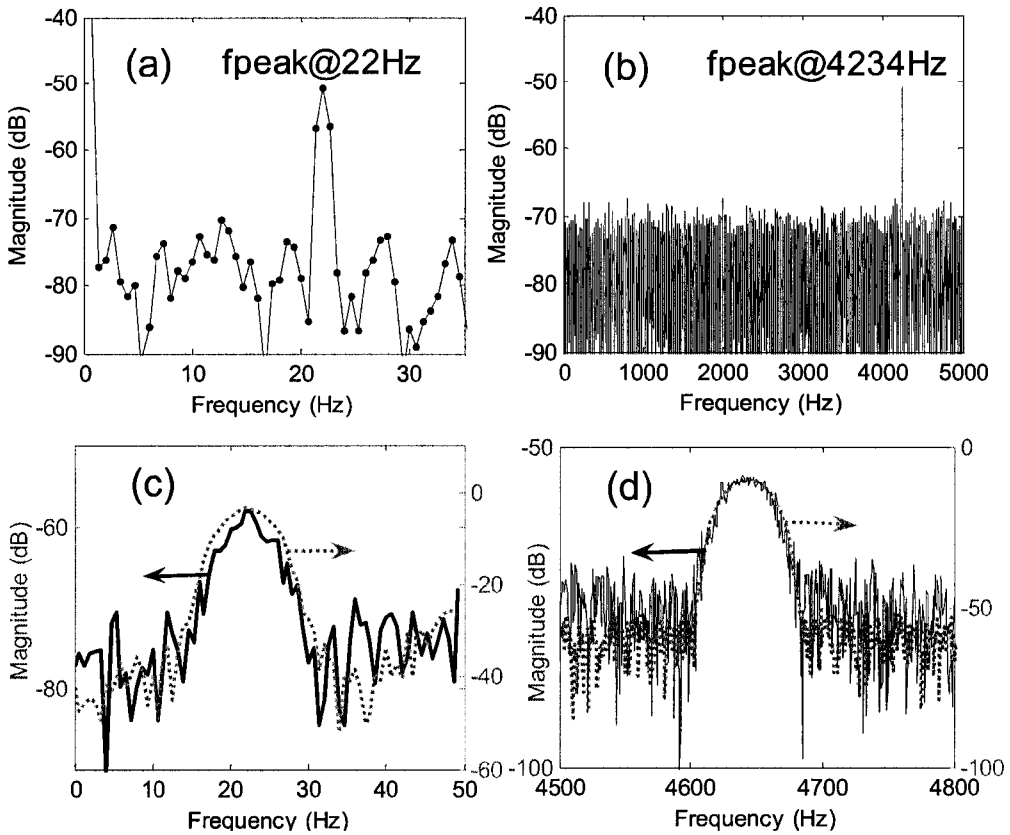

Fig. 3. Piezo fiber stretcher driven by 5Vpp square wave, FFT spectrum of time trace signal at 550m of (a) 22Hz driven signal; (b) 4234Hz driven signal; (c) FFT spectrum of P-OTDR signal (black solid line) comparing to the spectrum of sweep driven signal (red dotted line), from 15Hz to 30Hz; (d) FFT spectrum of P-OTDR signal (black solid line) comparing to the spectrum of sweep driven signal (red dotted line), from 4600 to 4680Hz.

3.2 Double simultaneous events with different vibration frequencies

In order to identify two simultaneous events with different vibration frequencies (f_1 and f_2), an electrically driven polarization controller (EO Space) and another 200m spool of fiber are added into the fiber link. Since the polarization controller is made of $LiNO_3$, it has 3dB loss one way, leading to 6dB total loss for backscattered light. As shown in Fig. 4(a), before the polarization controller (at 850m), the amplitude (peak to peak voltage) of the oscillating curve is about 80mV, compared to the 20mV afterwards. Although the backscattered light at the detection end has been significantly attenuated, the second disturbing point still could be located. Due to the speed limitation of our analog output driven card to polarization controller, the SOP of light is tuned at 25Hz (f_2=25Hz). While the driven frequency of the piezo fiber stretcher is set to 37Hz (f_1=37Hz). By processing data from step i to step iii as in Fig. 2 with 100 curves averaging, we obtain the following results from the FFT spectrums: any point before the first disturbing point, its FFT spectrum doesn't have any obvious peak; any point between the first and the second disturbing points, it has a peak at 37Hz; and any point beyond the second disturbing points, its spectrum has two peaks, one at 37Hz and the other at 25Hz. The typical FFT spectrums of the above three cases are plotted in Figs. 4(b), 4(c), 4(d), respectively.

#96288 - $15.00 USD Received 16 May 2008; revised 24 Jun 2008; accepted 24 Jun 2008; published 26 Jun 2008
(C) 2008 OSA

Reproduced with permission of the copyright owner. Further reproduction prohibited without permission.

This multiple simultaneous events detection is valuable and crucial for distributed vibration sensor. Taking fence intrusion sensor for example, different intruder would cause different disturbing frequencies due to all facts of the intruder, like size, weight, way of climbing, etc. Hence, from the FFT spectrum analysis, multiple intruders could be easily distinguished and located.

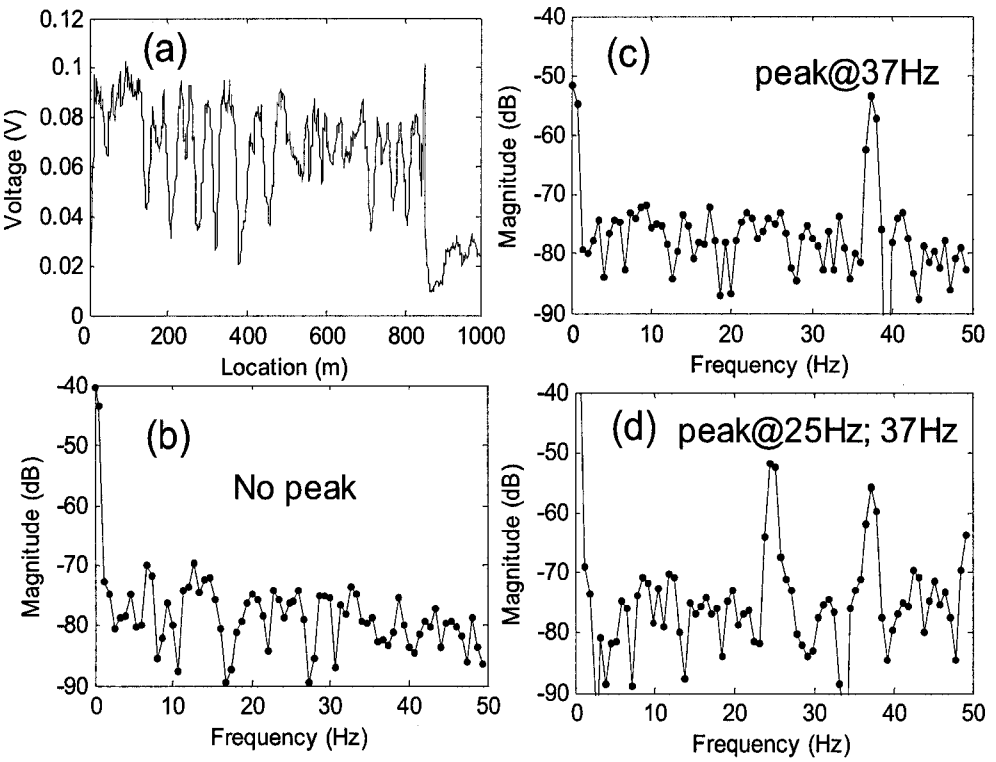

Fig. 4. (a). a typical Polarization-OTDR curve for 10m lead fiber + 500m SMF + 40m piezo fiber stretcher + 300m SMF + polarization controller + 200m SMF; (b). FFT spectrum for any point before the piezo fiber stretcher: no obvious peaks; (c). FFT spectrum for any point between the piezo fiber stretcher and polarization controller: one peak at 37Hz; (d). FFT spectrum for any point beyond the polarization controller: one peak at 37Hz and the other at 25Hz

3.3 Double simultaneous events with the same vibration frequency

In section 3.2, we demonstrate two simultaneous events with different vibration frequencies, which should be sufficient for most applications. However, in some rare situations, it might happen that two simultaneous events have exactly the same vibration frequency. In order to capture every disturbing event, as shown in step iv in Fig. 2, we propose to utilize the magnitude of the peak frequency along the fiber to identify the second event. In other words, a narrow filter with bandwidth <1Hz has been put in the vicinity of the peak frequency, so that the SNR would be tremendously improved.

First, when the piezo fiber stretcher vibrates at 25Hz (f_1=25Hz) while the polarization controller remains stable, the magnitude of 25Hz in the FFT spectrum has been plotted as in Fig. 5(a). As it has been mentioned in section 2 that the SOP evolves through the fiber and only one polarizer is placed at the detection end, the magnitude of 25Hz oscillates along the fiber link. Due to the large insertion loss (6dB) of the polarization controller for the same

#96288 - $15.00 USD Received 16 May 2008; revised 24 Jun 2008; accepted 24 Jun 2008; published 26 Jun 2008
(C) 2008 OSA

Reproduced with permission of the copyright owner. Further reproduction prohibited without permission.

birefringence change amount, the signal variation from the second half (beyond 850m) is much smaller than that from the first half (before 850m). If the second polarization controller has negligible insertion loss, and then the noise floor will be the same for the first and second half with the same environmental and electrical noises. Nevertheless, this phenomenon won't affect our results of two events detection and could be avoided by using a zero insertion loss vibrating component, like an optical fiber based polarization controller. In Fig. 5(a), at certain locations, since the SOP change is perpendicular to the direction of the polarizer, no intensity change appears at the detector, leading to the magnitude of 25Hz reaches the noise floor (-70dB for the first half and -75dB for the second half). This effect would have an influence upon accuracy of the event's location decision. However, since the uncertainty is in the order of a few meters, which is less than the 10m spatial resolution equivalent to 100ns pulse width. The oscillation amplitude would be reduced when two or more polarizers and detectors are used, but yet it would sacrifice the maximum detectable frequency.

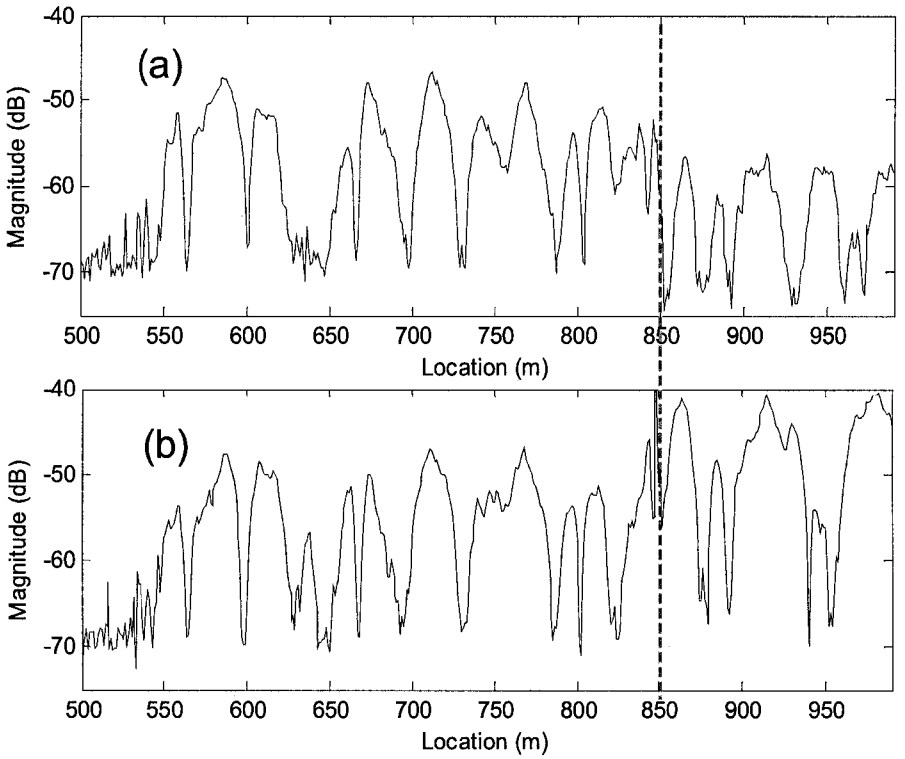

Fig. 5. Magnitude of 25Hz along the fiber link for (a) only the piezo fiber stretcher vibrating at 25Hz; (b) both the piezo fiber stretcher and the polarization controller vibrating at 25Hz.

If the piezo fiber stretcher is the only disturbing event, the maximum magnitude of the second half will be remain around -57dB. However, once the polarization controller starts to vibrate at the same frequency (f_1=f_2=25Hz), the maximum of the second half increases 16dB to about -41dB even though the time domain backscattered signal beyond the controller is very weak. As in Fig. 5(b), this sudden "jump" indicates the second event with the same frequency as the first one. Since at some locations, the SOP change of two events adds up together for a certain polarizer alignment, the maximum of the second half would always be larger than that of the first half regardless of the SOP at the second event. Without 1Hz frequency filter this "jump" would not be observable.

#96288 - $15.00 USD Received 16 May 2008; revised 24 Jun 2008; accepted 24 Jun 2008; published 26 Jun 2008
(C) 2008 OSA

Reproduced with permission of the copyright owner. Further reproduction prohibited without permission.

Using micro-processor can reduce the signal processing time significantly without going through computer for digitization and programming time, making current system response in the ms time frame, as the FFT signal processing and averaging are conducted by electronic circuits directly.

4. Conclusion

We have presented a spectral Polarization-OTDR system that provides fully distributed vibration information. Benefited to its high sensitivity, our current configuration has been demonstrated to detect up to 5kHz vibrating events without any data averaging in a 1km fiber link with 10m spatial resolution. Also, by plotting the magnitude of a certain frequency component from a FFT spectrum along the fiber position, two simultaneous disturbances with the same frequency can be successfully identified. The obtained results imply that the proposed distributed vibration sensor would find numerous applications on intrusion sensing and structure health monitoring.

Acknowledgments

Support from the Canadian Networks of Centers of Excellence: CIPI, GEOIDE and the Natural Sciences and Engineering Research Council (NSERC) of Canada are greatly appreciated.

#96288 - $15.00 USD Received 16 May 2008; revised 24 Jun 2008; accepted 24 Jun 2008; published 26 Jun 2008
(C) 2008 OSA

Reproduced with permission of the copyright owner. Further reproduction prohibited without permission.

Chapter 9

Application of polarization based optical fiber sensor

This chapter is a collection of studies on applying the polarization based optical fiber sensor to several distinct practical situations. Here, all the test results are obtained from the transmission setup as described in Fig. 1(a) in Chapter 7, i.e. the sensor works like a point or area sensor with ability to provide the impact time trace and the vibration frequency caused by various disturbing events. In order to be carried to perform field tests, the detection end of the sensor has been assembled and packed to an enclosure. Fig. 9.1 shows a picture of all the equipments involved in the tests.

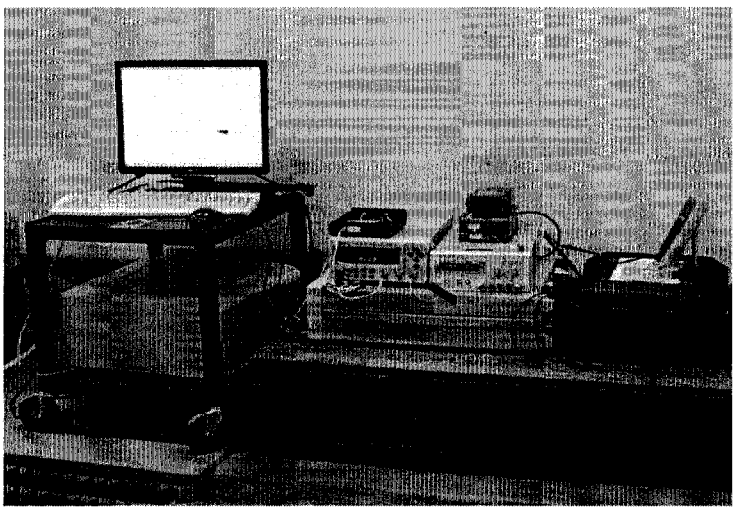

Figure 9.1 A picture of all the equipments using the transmission sensor setup.

Reproduced with permission of the copyright owner. Further reproduction prohibited without permission.

The main purpose of the field tests is to verify whether our sensor has sufficient sensitivity to detect a certain type of vibration event. Therefore, our work here is an important step towards field applications of the distributed vibration sensor (as developed in Chapter 8). With the knowledge of signals from the transmission setup, the distributed vibration sensor can be improved or specially designed for one specific circumstance, in terms of system's sensitivity, detector bandwidth, spatial resolution as well as the data processing approach.

This chapter includes three tests conducted by our vibration sensor with transmission setup. They are: detection of water wave frequency for both regular and irregular wave in a long water channel, vibration of highway pavement slabs induced by cars passing, and study of bending and torsion mode frequencies of a lightweight cantilever beam. From our results, it is clear that our sensor is capable of measuring vibration events in various field situations. It is then feasible to apply the distributed vibration sensor in the field of structural health monitoring and intrusion sensing, which will become our major work in the near future.

Reproduced with permission of the copyright owner. Further reproduction prohibited without permission.

9.1 Water wave frequency test

[**Ziyi Zhang**, Xiaoyi Bao, Colin D. Rennie, Ioan Nistor, Andrew Cornett, "Water Wave Frequency Detection by Optical Fiber Sensor," *Optics Communications,* 281, 6011-6015 (2008)]

9.2 Highway pavement vibration test

[**Ziyi Zhang,** Samuel LeBlanc and Xiaoyi Bao, "Concrete pavement vibration monitoring due to the car passing using optical fiber sensor," 19th International Conference on Optical Fiber Sensors, *Proc. SPIE* 7004, 70041U (2008)]

9.3 Lab tests on cantilever beam mode frequencies

[**Ziyi Zhang,** Pingyu Zhu and Xiaoyi Bao, "Measurement of the cantilever bending and torsion mode frequency by optical fiber sensor and accelerometer," submitted to *Optical Engineering*]

Reproduced with permission of the copyright owner. Further reproduction prohibited without permission.

Optics Communications 281 (2008) 6011–6015

Contents lists available at ScienceDirect

Optics Communications

journal homepage: www.elsevier.com/locate/optcom

Water wave frequency detection by optical fiber sensor

Ziyi Zhang [a,*], Xiaoyi Bao [a], Colin D. Rennie [b], Ioan Nistor [b], Andrew Cornett [c]

[a] Physics Department, University of Ottawa, Ottawa, ON, Canada K1N 6N5
[b] Civil Engineering Department, University of Ottawa, Ottawa, ON, Canada K1N 6N5
[c] NRC Canadian Hydraulics Centre, Ottawa, ON, Canada K1A 0R6

ARTICLE INFO

Article history:
Received 24 July 2008
Received in revised form 11 September 2008
Accepted 11 September 2008

ABSTRACT

An optical fiber sensor has been developed and applied to measure frequency of water waves based on wave induced polarization change of the light. The fiber sensor can accurately detect water wave frequency for regular and irregular waves. The optimum sag of sensing fiber to the sensor output's linearity has been studied. The agreement of the fiber sensor and wave gauge in frequency and time domain suggests that the fiber sensor has great potential for passive acoustic sensing and wave monitoring.

© 2008 Elsevier B.V. All rights reserved.

1. Introduction

There are many applications for marine passive acoustic sensing in environments such as seaports, rivers and waterways. Port security requires monitoring and tracking of commercial ships, submarines, pleasure boats and divers. Marine biologists use sound to identify marine mammals. Geophysicists record deep-sea seismic events from resulting pressure waves. The measured acoustic frequency varies for each application, with seismicity monitored around 5 Hz, marine mammals around 50 Hz, and ship passage around 100 Hz [1]. Ambient noise in the ocean at these frequencies is generated from the same sources, as well as from surface wind-generated waves. Acoustic monitoring has traditionally been conducted using piezoelectric transducer hydrophones. However, a large array of hydrophones is required to survey an area and to pinpoint locations of sound sources.

Underwater acoustic sensing is an area in which fiber optic sensors have great advantages due to the possibility of multiplexing and distributed techniques existing in the fiber communication and fiber sensor systems. Acoustic detection using fiber optic hydrophones has been developed for military sonar and in seismic surveying for the oil–gas industry [2]. In order to cover large areas, hundreds to thousands of the sensor arrays are required to be included in seabed or towed arrays, such as streamers in the seismic industry. The installation of the sensor arrays may take months to years. However, if fiber optics-based sensors are used, electronics components need not be submerged. Further, optical fibers are much lighter and less corrodible than copper wires. In an acoustic sensor array, a large number of fiber hydrophones or geophones (hundreds to thousands) as point sensors are distributed every meter or few meters along a pair of fiber buses. The current state of technology includes using the point sensor, such as interferometer and fiber Bragg grating (FBG) sensors, and then using time domain multiplexing (TDM) and wavelength division multiplexing (WDM) techniques to get multiple points [2,3]. The difficulty with the Michelson-based sensor array includes: (1) the sensitivity varies with the propagation and polarization direction of the acoustic waves relative to the orientation of the fiber sensor and the polarization orientation of the optical beam in the fiber; (2) the fringe visibility varies with random fluctuations in the state of polarization of the two interfering beams; (3) an interferometer measures phase change, which requires stabilized laser and narrow band which is extremely sensitive to the environmental conditions and noise. Although a FBG acoustic sensor can simply detect and locate reflections, each FBG covers only a small area and a feedback circuit should be used for each one. Moreover, to test a large number of points, one needs to lay one optical fiber for each testing point, which is not convenient for field test of a large area.

In this paper, the authors demonstrate usage of the state of polarization (SOP) in optical fiber to measure the power spectrum of the oscillatory water currents under water waves. SOP of light may be changed by external disturbances on the fiber; for submarine fiber cables, the main factor is water wave movements [4,5]. In this case, the fiber has been laid across the section of a wave flume, which is essentially a long water channel equipped with wave generator at one end and a wave absorbing device at the other end; hence the fiber serves as a point sensor acting as a wave gauge. The fiber sensor is capable of detecting water wave frequencies accurately for all types of wave generated by the flume. With the optimum sag of fiber, the output response of optical fiber sensor is linear within 0.7 m ± 0.2 m wave level.

Furthermore, we believe this sensor has potential to realize distributed water wave monitoring using backscattered light as devel-

* Corresponding author.
E-mail addresses: ziyi.zhang81@gmail.com (Z. Zhang), xbao@uottawa.ca (X. Bao).

0030-4018/$ - see front matter © 2008 Elsevier B.V. All rights reserved.
doi:10.1016/j.optcom.2008.09.038

Reproduced with permission of the copyright owner. Further reproduction prohibited without permission.

oped in [6]. A distributed water wave sensor may be tested by laying the fiber along the flume rather than at cross section.

2. Experimental configuration

Experiments were conducted in a 63 m long by 1.22 m wide steel wave flume located at the Canadian Hydraulics Centre (CHC) of the National Research Council (NRC) in Ottawa, Canada (see Fig. 1). For these experiments, the flume was filled with freshwater to a depth of 0.7 m. A variety of regular and irregular water waves were generated at the north end of the flume using a computer-controlled hydraulic wave machine operating in piston mode. The wave time-histories were synthesized using CHC's GEDAP software, and the wave machine was controlled through NDAC software, also developed at CHC. The waves were absorbed by a highly efficient beach located at the south end of the flume.

Regular wave trains with wave periods of 1.0, 1.5, 2.0 and 3.0 s, and wave heights of 0.1, 0.15 and 0.2 m were generated in these experiments. Irregular (pseudo-random) wave trains were generated which had peak wave periods of 2.55 s and 1.94 s, and a significant wave height of 0.15 m. The irregular waves were sampled for 5 min, while the regular waves were recorded for 1 min.

2.1. Wave gauge

The water waves generated in the flume were measured using capacitance wave gauges developed at CHC. These gauges consist of an insulated copper wire passing vertically through the free surface, connected to an electronic circuit. The gauges sense the change in capacitance (proportional to the immersed wire length) resulting from the vertical movement of the free water surface. The wave gauges were calibrated by moving them vertically, through precise distances, in still water. The gauge response was stable and linear, with calibration errors less than 0.5% of the measurement range.

The time-history of the water surface elevation was measured using one capacitance wave gage located approximately 25 m away from the wave machine and immediately downstream from the optical fiber. Prior to that, two wave gauges were calibrated and tested to ensure the proper functioning of the one wave gauge used to measure the same data as the optical fiber.

2.2. Optical fiber sensor

The optical fiber vibration sensor is based on birefringence properties of single mode fibers (SMF), which can be affected by many external disturbances, such as strain, temperature, pressure etc. By sending polarized light into the fiber and monitoring its intensity change through a polarizer at the detection end, the polarization change due to environmental perturbations can be obtained. The water wave alters the stress on the fiber, thus by measuring the induced polarization state change, the intensity change of polarized light inside the fiber, and then the frequency distribution of the water wave could be measured. A continuous polarized light is launched into the sensing fiber through a polarization controller, then the output light is separated by a polarization beam splitter (PBS) into two photodetectors, which can greatly improve the system signal-to-noise ratio comparing with a single photodetector. Detailed description of the sensor setup and laboratory experiment results on vibration characterization of PZT materials can be found in [7].

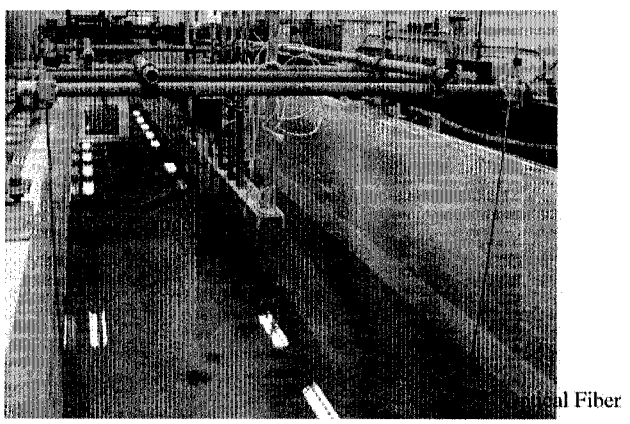

Fig. 1. Mount of optical fiber and wave gauge.

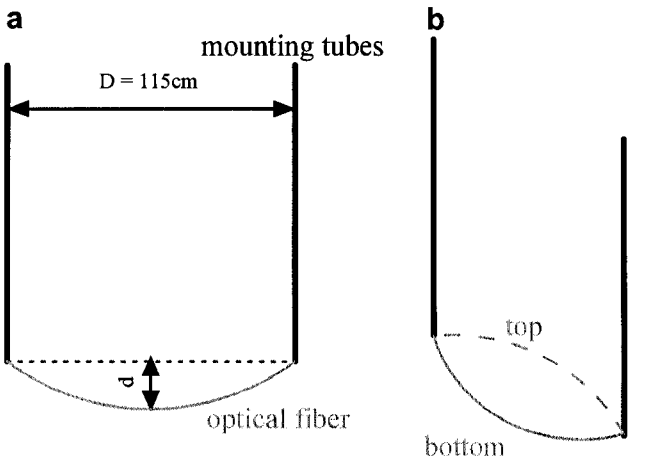

Fig. 2. Schematic diagram of the fiber mount (a) front view; and (b) oblique side view.

The sensing fiber is fully submerged in the water and is laid in the cross section of the flume. The lead-in fiber portion is protected by tubes or taped down by transparent tapes to guarantee the portion under water is the only sensing part. It is shown in Fig. 1 that the mount of the optical fiber is placed close to that of the wave gauge, in order to compare their test results. Fig. 2 illustrates the schematic diagram of the fiber mount.

3. Results and discussion

Outputs from the wave gauge and optical fiber sensor are collected by one DAQ card simultaneously, and the time traces are plotted in black and red color, respectively. It is worth mentioning that the DC (direct current) part of the signal from the optical fiber sensor depends on the chosen input polarization state, which has been usually set to zero to increase signal to noise ratio due to the polarization diversity scheme designed in the detector [7]. The wave gauge was calibrated before the testing, but its output has been kept as the voltage reading without converting to the actual wave height. Therefore, in order to compare the results from wave gauge and optical fiber sensor, the raw testing data have been processed: the DC value of both sensors has been set to zero and then the data have been normalized to $[-0.5, 0.5]$. Also, the power spectrum of the testing data is computed through FFT (fast Fourier transform) to get the frequency distribution of the water wave.

3.1. Best length of the sensing fiber

The first set of experiments determined the optimal fiber tension for wave frequency detection. The actual length of the sensing

Reproduced with permission of the copyright owner. Further reproduction prohibited without permission.

Table 1
Regular wave profile for Section 3.1

No.	Water level (m)	Wave height (m)	Wave period (s)	Test time (min)
a	0.7	0.15	2.0	1

Table 2
Regular wave characteristics for Section 3.2

Number	Water level (m)	Wave height (m)	Wave period (s)	Test time (min)
a	0.7	0.15	2.0	1
b	0.7	0.15	1.5	1
c	0.7	0.10	1.0	1
d	0.7	0.15	3.0	1

fiber should be carefully chosen: if the fiber is too taut then the polarization change of light caused by the water wave would be hardly detectable; while if the fiber is too loose, since the fiber has its own restoring force, it would not follow the wave profile (a sinusoidal wave in this case) all the time. The wave profile (sinusoidal wave) used for these tests is listed in Table 1. As shown in Fig. 2a, the distance between the two mounting tubes is $D = 115$ cm. Here, the authors defined the percentage sag as: sag(%) = d/D, which serves as an indicator of fiber tension.

First, the sensing fiber was set relatively loose with 8% sag, and the test results are shown in Fig. 3, including the raw data, normalized data and power spectrum for both wave gauge and optical fiber sensor. In the frequency domain, the peak frequency reading of optical fiber sensor matches that of the wave gauge: 0.5 Hz corresponds to the 2.0 s wave period setting. In the time domain, the waveform measured by optical fiber sensor is slightly distorted from a perfect sine wave. This is due to the fact that the sensing fiber affected by the water wave orbital velocity swings like a "skipping rope", from bottom to top as depicted in Fig. 2b. For the loose fiber, when it swings at the vertex, it stays at maximum height for a short period of the time due to its own resistance before being pushed forward.

The sensing fiber was then stretched a little bit tighter to be 6% sag. As plotted in Fig. 4, the time trace of optical fiber sensor in this case follows the sine wave well since there is much less resistance comparing to the previous case with 8% sag. When the sensing length was further tightened to be 4% sag, the amplitude of output signal decreased, leading to lower signal to noise ratio (SNR).

For the three cases above, the frequency peak reading of 0.5 Hz was always accurately measured by the optical fiber sensor, and was thus independent of the actual length of the sensing fiber. As there is a tradeoff between the testing wave profile and the SNR, it was determined that 6% sag was the optimal fiber tightness, and 6% sag was employed for all subsequent experiments.

The sag(%) depends on various factors: the water wave force acting on the fiber; the distance between the fiber supporting tubes, the type of fiber, etc. Therefore, the optimum sag should be carefully studied before conducting the tests.

In order to estimate the frequency measurement precision for the case of optimal fiber length, the frequency value obtained from each cycle has been calculated individually for 10 cycles in Fig. 4b. The mean value and standard deviation are 0.50002 Hz and 0.0049 Hz, respectively. This result is in a good agreement with the frequency reading from wave gauge within the same time range, 0.5000 ± 0.0026 Hz.

3.2. Regular wave (sine wave) with different wave periods

Four regular wave trains were generated and their wave characteristics are listed in Table 2.

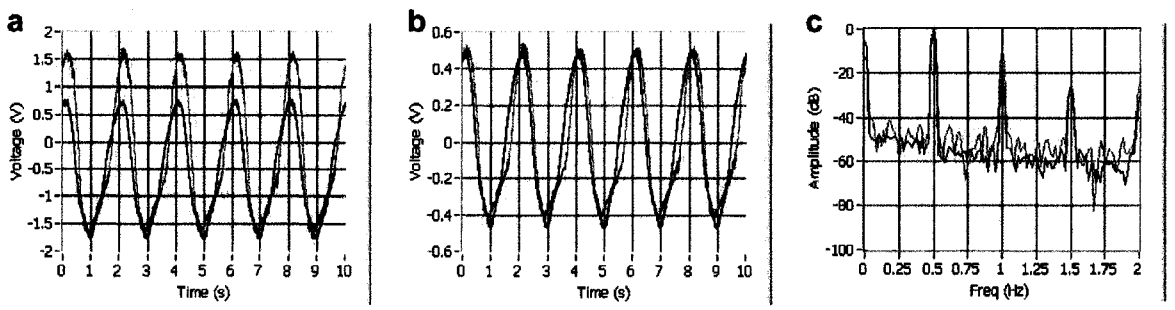

Fig. 3. Test results of wave gauge (black curve) and optical fiber (red curve) with 8% sag: (a) raw data, (b) normalized data, and (c) power spectrum. (For interpretation to color in Fig. 3, the reader is referred to the web version of this article.)

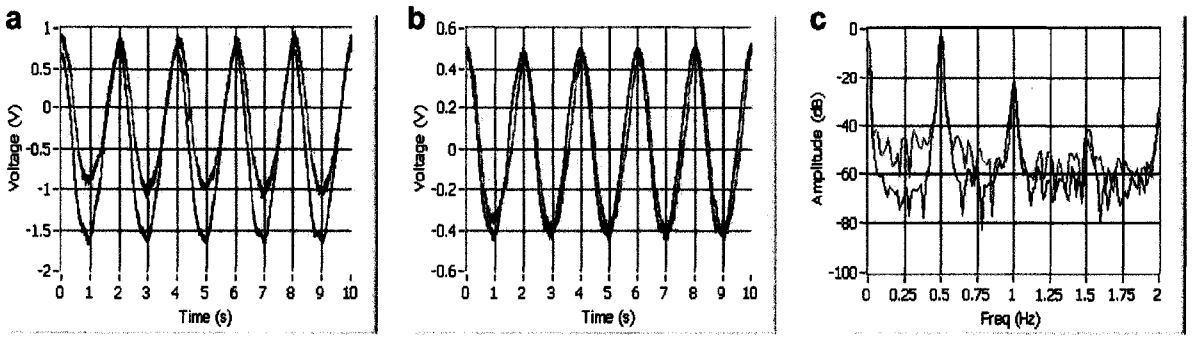

Fig. 4. Test results of wave gauge (black curve) and optical fiber (red curve) with 6% sag: (a) raw data, (b) normalized data, and (c) power spectrum. (For interpretation to color in Fig. 4, the reader is referred to the web version of this article.)

Reproduced with permission of the copyright owner. Further reproduction prohibited without permission.

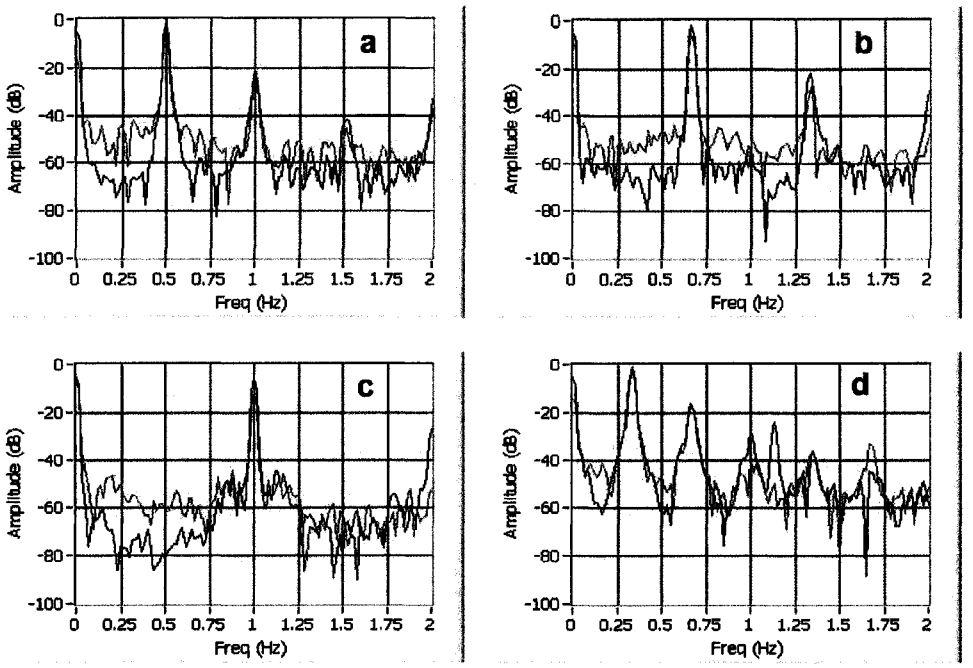

Fig. 5. Power spectrum of time trace obtained by wave gauge (black curve) and optical fiber (red curve) with different wave period: (a) 2.0 s, (b) 1.5 s, (c) 1.0 s, and (d) 3.0 s. (For interpretation to color in Fig. 5, the reader is referred to the web version of this article.)

Table 3
Irregular wave characteristics for Section 3.3

Number	Water level (m)	Wave height (m)	Wave period (s)	Test time (min)
e	0.7	0.15	Peak = 2.55; Avg. = 1.96	5
f	0.7	0.14	Peak = 1.94; Avg. = 1.67	5

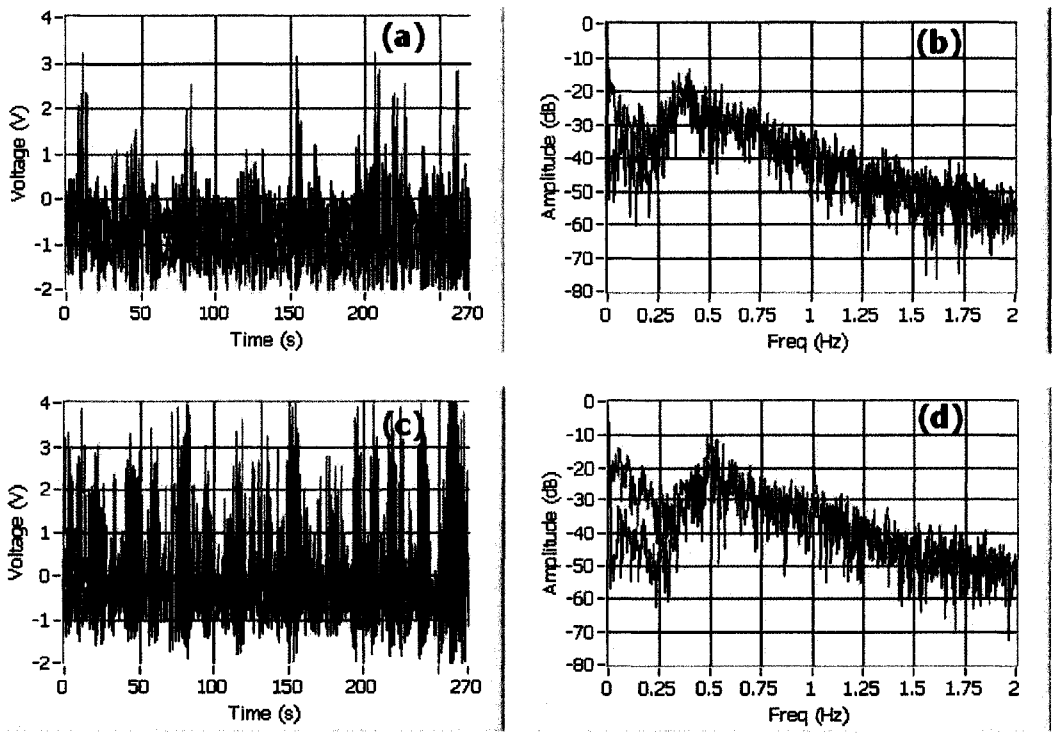

Fig. 6. Irregular wave test results by wave gauge (black curve) and optical fiber (red curve): test #e: (a) time trace, (b) power spectrum; test #f: (c) time trace, and (d) power spectrum. (For interpretation to color in Fig. 6, the reader is referred to the web version of this article.)

Reproduced with permission of the copyright owner. Further reproduction prohibited without permission.

Table 4
Wave characteristics used for the linearity analysis

Number	Water level (m)	Wave height (m)	Wave period (s)	Test time (min)
a1	0.7	0.10	2.0	1
a2	0.7	0.05	2.0	1
a3	0.7	0.20	2.0	1
a4	0.7	0.15	2.0	1

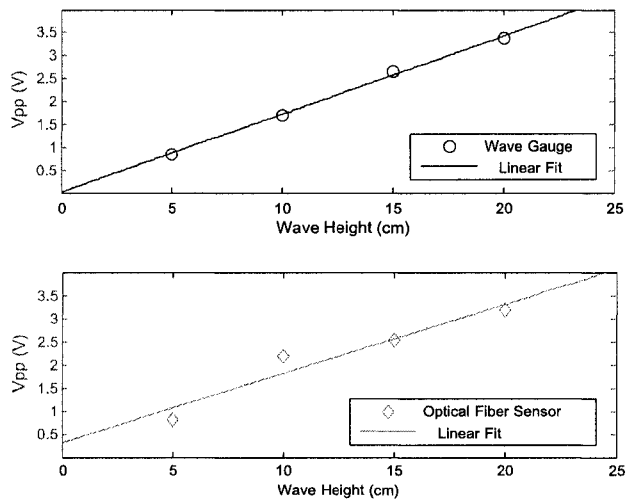

Fig. 7. Linearity of the (a) wave gauge and (b) optical fiber sensor.

Fig. 5 shows the power spectra computed from time domain results for both the wave gauge and the optical fiber sensor. The peak readings are all accurate, at 0.5 Hz, 0.67 Hz, 1 Hz and 0.33 Hz, corresponding to the pre-set wave period 2.0 s, 1.5 s, 1.0 s and 3.0 s, respectively.

3.3. Irregular wave

An irregular wave train contains more frequency components than a regular wave one, so it is considered to be more difficult to monitor. Nevertheless, the authors show that the optical fiber sensor is capable of giving the correct frequency distributions for irregular waves.

The type of generated irregular wave in the flume is of JONSWAP distribution. And, as described in Table 3, the authors tested two different irregular wave trains with duration of 5 min each.

Fig. 6a–d shows the raw data in time domain and its power spectrum for both irregular wave trains: #e and #f. The time trace demonstrates that the optical fiber follows the wave profile quite well. Since the raw time data from the optical fiber have a DC (direct current) portion, in the power spectrum, the beginning part (0–0.2 Hz) of the optical fiber is distinct from that of the wave gauge. Nevertheless, the rest of the frequency distributions from the optical fiber sensor match well with that of the wave gauge.

3.4. Linearity of the optical fiber sensor output

In order to check the linearity of the optical fiber sensor, waves with different heights, from 0.05 m to 0.20 m, were generated, as shown in Table 4, with 0.05 m interval.

As plotted in Fig. 7, wave gauge output is linear with wave height; and optical fiber output at wave height 0.05 m; 0.15 m; 0.20 m is quite linear, while the output at 0.10 m shows a small deviation from linear fit. According to the results from [7], the signal variation (*Vpp*) is related to the input polarization state and the disturbance direction, so a possible reason for the 0.10 m result is that the input polarization state changed after the first test (Test a1). The authors believe that with the same input polarization state, the optical fiber sensor should respond in a linear manner, for conditions of small wave height and optimum sag of the fiber.

4. Conclusions

An optical fiber vibration sensor has been successfully developed to measure water wave frequency. The sensor monitors the polarization state change induced intensity variation of the light when the sensing fiber is affected by the presence of the water wave. As a result, the sensing fiber should be fully submerged in the water and be able to be moved physically by the water wave. The sensor is capable of providing accurate frequency distributions for both regular waves and irregular waves, confirmed by a conventional wave gauge. Moreover, the sag of fiber is found to be a factor affecting the sensor's response, and the optimum sag has been studied. Further studies will be employing a distributed optical fiber vibration sensor to detect wave frequency in a fully distributed manner along the fiber link. Such a distributed sensor will be particularly useful for water wave measurements in field conditions or three-dimensional wave basins, where diffraction and reflection of waves can create spatially complex wave environments.

Acknowledgements

Financial support from the Natural Sciences and Engineering Research Council (NSERC) of Canada and the Canadian Networks of Centers of Excellence: CIPI, GEOIDE is greatly appreciated. We also like to thank Audur Atladottir, Shalini Kashyap, and Ryan Bolen for their help during the experimental program.

References

[1] W.S. Burdic, Underwater Acoustic System Analysis, 2nd ed., Prentice-Hall, Englewood Cliffs, New Jersey, 2003.
[2] G.A. Cranch, P.J. Nash, C.K. Kirkendall, IEEE Sensor. J. 3 (2003) 19.
[3] G.A. Cranch, R. Crickmore, C.K. Kirkendall, A. Bautista, K. Daley, S. Motley, J. Salzano, J. Latchem, P.J. Nash, J. Acoust. Soc. Am. 115 (6) (2004) 2848.
[4] Ziyi Zhang, Xiaoyi Bao, Qinrong Yu, Liang Chen, Photon. Technol. Lett. 18 (9) (2006) 1034.
[5] Ziyi Zhang, Xiaoyi Bao, Qinrong Yu, Liang Chen, Opt. Fiber Technol. 13 (1) (2007) 62.
[6] Ziyi Zhang, Xiaoyi Bao, Opt. Express 16 (2008) 10240.
[7] Ziyi Zhang, Xiaoyi Bao, IEEE J. Lightwave Technol. 26 (7) (2008) 852.

Reproduced with permission of the copyright owner. Further reproduction prohibited without permission.

Concrete pavement vibration monitoring due to the car passing using optical fiber sensor

Ziyi Zhang*, Samuel LeBlanc, Xiaoyi Bao*
Physics Department, University of Ottawa, 150 Louis Pasteur, Ottawa, ON, K1N6N5, Canada

ABSTRACT

An optical fiber vibration/acoustic sensor based on polarization diversity scheme has been developed to study the vibration of the highway pavement slabs with vehicles passing. This process induced the birefringence change in a 50m sensing fiber embedded along the FRP bars. The damping of the impact in time domain and a 2Hz vibration frequency are observed.

Keywords: fiber-reinforced polymers; impact monitoring; polarization

1. Introduction

Fiber-reinforced polymers (FRP) have been used for constructing civil structures, such as buildings, bridges and highway pavements. The combination of high-strength, high-stiffness structural fibers with low-cost, light-weight, environmentally resistant polymers made it attractive than steel structures[1]. However, one concern using FRP laminates in structures is their susceptibility to delamination cracking under transverse impact loading, which greatly degrades FRP stiffness, strength and durability[2]. Therefore, it is crucial to monitor the response of FRP under impact wave and detect damage at the earliest possible stage. The health monitoring system for FRP structures should provide time domain signal under impact events for the vibration frequency in real time. This can be used as indication of the mechanical condition when the structure degradation occurs.

The accelerometer, the most conventional vibration sensor was used to study the dynamic properties of highway bridges under traffic loads[3]. Although it is accurate, it suffers from covering a relative small area and the difficulty of electrical isolation. Recently, a fiber Bragg grating (FBG) system was developed to detect impact damage in carbon FRP, which is only able to monitor a limited region due to the nature of a point sensor[4].

This paper presents an optical fiber vibration/acoustic sensor based on polarization diversity scheme to monitor the impact wave on structures in presence of external disturbances. Benefited from its high SNR (>37dB) without signal averaging, this sensor is capable of detecting impact events with frequency range of sub-Hz to 16kHz in real time. It can detect the decay time of the structures and frequency spectrum with large fiber covering area. We also demonstrate a real time impact monitoring due to the high speed (~100km/hour) vehicles passing on pavement slabs with a 50m sensing fiber embedded along the FRP bars. Most vibration frequencies are within the low range (<20Hz) with a main peak at 2Hz. The field test data is crucial to study the slab's dynamic properties under impact wave. And this sensor could be used to find potential problems in the structure.

2. Experimental setup

The birefringence property of single mode fibers (SMF) is due to the asymmetry of the fiber core induced by fiber drawing and cabling processes. As a result, two orthogonally polarized components of light experience slightly different refractive indexes, causing a phase shift between the fields in two axes. The phase shift is susceptible to external disturbances applied on the fiber, such as: impact, strain, acoustic wave, temperature, etc, leading to the changes of output state of polarization (SOP). Since the temperature is a slow process, for the purpose of impact detection, it could be neglected. Our vibration/acoustic sensor is based on monitoring the optical power of polarized light changes at the fiber end, which provides both time and frequency information about the structure's response under the impact wave.

*zzhan089@uottawa.ca, *xbao@uottawa.ca; phone 1-613-562-5800 ext 6911; fax 1-613-562-5190

19th International Conference on Optical Fibre Sensors, edited by David Sampson, Stephen Collins, Kyunghwan Oh, Ryozo Yamauchi, Proc. of SPIE Vol. 7004, 70041U, (2008) 0277-786X/08/$18 doi: 10.1117/12.785876

Reproduced with permission of the copyright owner. Further reproduction prohibited without permission.

Figure 1 describes the configuration of the optical fiber vibration/acoustic sensor. A linearly polarized light from a DFB laser source passing through a polarization controller launches into a sensing fiber. At the other end of the sensing fiber, a polarization beam splitter (PBS) is positioned to separate the input light into two orthogonal polarized beams, which are detected by two photodetectors with 16kHz bandwidth low noise amplifiers to minimize the noises and to enhance the sensitivity. The two output beams from PBS will encounter relative π phase shift when two beams are balanced, as illustrated in figure 1 both outputs consist of a small AC component plus a large DC portion. Thus by subtracting the two signals, we are able to enhance the AC signal by 3dB and remove the DC portion as only AC signals include vibration information under external perturbations. This kind of polarization diversity scheme benefits not only from minimizing the noises induced by the laser source and enhancing the signal, but also from avoiding AC coupling at the digitizer end, which usually leads a cutoff frequency around 10Hz. As a result, our sensor is capable of measuring sub-Hz to a few kHz disturbances with dynamic range >37dB.

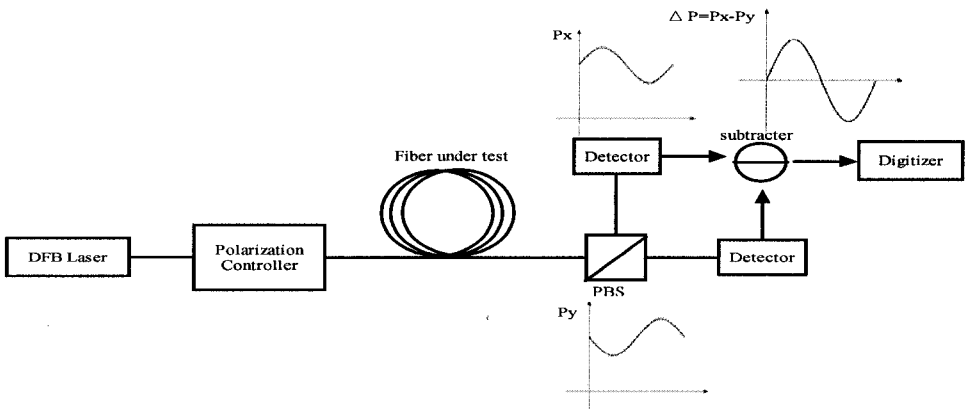

Fig. 1. Experimental setup of optical fiber diversity vibration/acoustic sensor

3. Comparison of optical fiber sensor and accelerometer

An experiment on a cantilever beam was performed in lab environment to compare our optical fiber sensor with a commercial accelerometer. The cantilever beam was made of spring steel with dimension 320*40*0.9mm (L*W*H), and one end was clamped on a stage. As shown in figure 2, its shape was designed to be isosceles trapezoid, which would have uniform strength along the beam under impact wave. An accelerometer with response of 1-10kHz was glued at the fixed end (marked as a dot at in Fig. 2) to reduce its weight effect on the whole beam, while the bare fiber (SMF-28) was taped by clear lightweight scotch tape on the beam with total length of 60cm. Impact wave was induced by the tip of a bent nose pliers at the fixed end. A slightly taping on the cantilever beam is applied to minimize the overall oscillations. Signals from optical fiber sensor and accelerometer were recorded simultaneously at the sampling rate of 2 kHz.

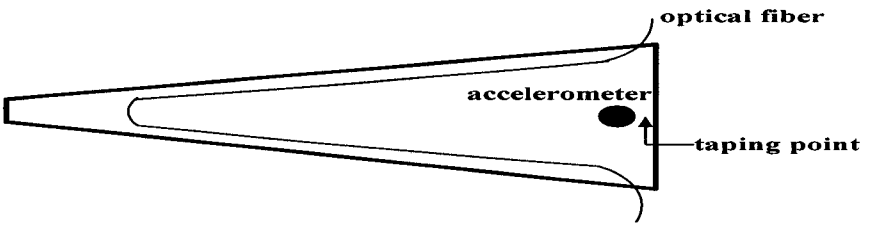

Fig. 2. Top view of the cantilever beam with an accelerometer (black dot) and optical fiber (solid line)

Figure 3(a) shows the response of our optical fiber sensor and accelerometer after a single hit, both of which have clear damped trends in time domain. The result is obtained with no averaging or filtering. After the first 0.2s, the accelerometer decay to zero. While the optical fiber sensor still shows some small oscillations due to its long length coverage over the entire beam. In order to compare their frequency components, fast Fourier transform is computed and the power spectrum is depicted in figure 3(b). All five main peaks appear at the same frequencies: 113.75Hz; 235Hz;

Reproduced with permission of the copyright owner. Further reproduction prohibited without permission.

362.5Hz; 535Hz and 742.5Hz, respectively, which represent different excited modes within the cantilever beam because of the strength of the initial hit. We also notice the tendency that the amplitude of accelerometer in power spectrum is lower than that of the fiber sensor. This is caused by a lower sensitivity of the accelerometer in the low frequency range. This accelerator is designed to detect higher frequency components above a few hundred Hz. For low frequency vibration/acoustic measurements, velocity or displacement transducers work more efficiently than accelerometers. Apparently the fiber sensor has the ability to detect wider frequency range to accurately measure dynamic property of the structures under impact wave in real time.

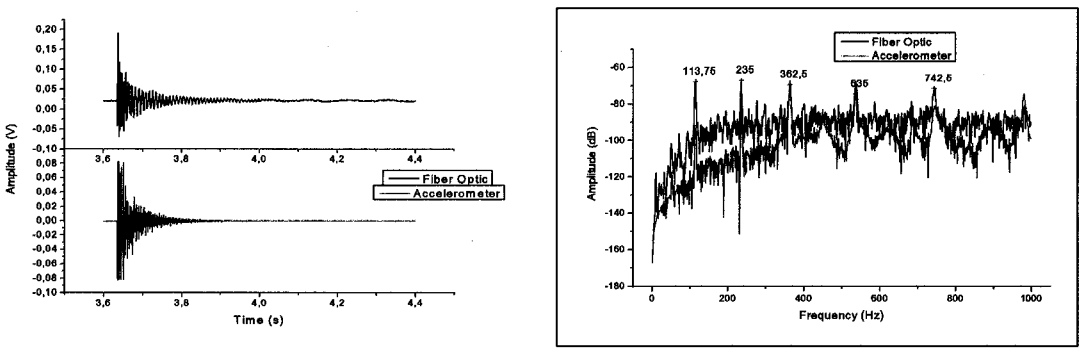

Fig. 3. Impact detection of a cantilever beam with optical fiber sensor (black) and accelerometer (red): (a) time trace; (b) normalized power spectrum

4. Field test results

The field test of traffic induced impact on concrete slab was carried out on Highway 40 East of Montréal, Canada. Highway 40 consists of three lanes with 3.7m wide each as seen in figure 4(a). Eighteen full-scale continuous reinforced concrete pavement (CRCP) slabs were constructed using glass fiber reinforced polymer (GFRP) bars. Each slab in the test section is 25m long and 3.7 wide, so the total test section is 150m long. The 50m sensing fiber for impact wave detection was attached on longitudinal GFRPs (as shown in figure 4(b)) under two CRCP slabs only (E2 and E1) in Lane3. This is a right lane with most of fully loaded trucks at high speed (~100km/hour) passing by.

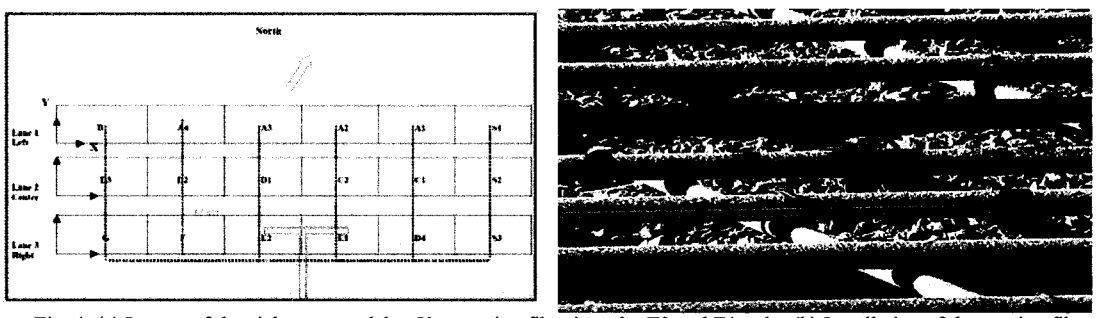

Fig. 4. (a) Layout of the eighteen test slabs, 50m sensing fiber is under E2 and E1 only; (b) Installation of the sensing fiber along with longitudinal GFRPs

The dynamic data was collected when cars and trucks are passing on the concrete slabs reinforced by GFRP bars, hence the birefringence of the optical fiber attached to them would be affected. The sampling rate of our sensor was set to be 1 kHz as the frequencies of interest should be fairly low. Figure 5(a) represents a typical power spectrum of the testing signal from 50m sensing with the main frequency components below 20Hz. This matches the previous research on dynamic testing of Highway Bridge using traffic loads[3]. The first peak locates at 2Hz, about 18dB higher than the second peak at 12.5Hz and the third peak at 18Hz. These three frequencies should correspond to the natural frequencies of the whole test slabs' structure. We believe these particular frequencies and their amplitudes on spectrum depend on many

Reproduced with permission of the copyright owner. Further reproduction prohibited without permission.

parameters, including the size, type and boundary conditions of the slabs; the size, load and speed of the cars or trucks; the way of optical fiber attached to GFRP bars; etc.

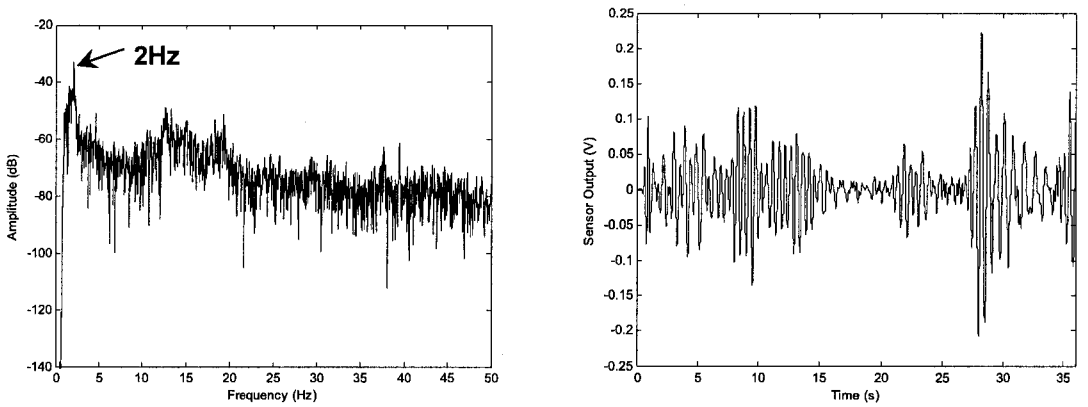

Fig. 5. Field test of traffic impact monitoring: (a) Power spectrum up to 50Hz of the raw data after 1Hz highpass filter; (b) Time trace of the signal around 2Hz, after 1Hz-5Hz bandpass filter

A bandpass filter (1Hz - 5Hz) is applied on one set of the raw data to retrieve the signal around 2Hz as plotted in figure 5(b) within 36 seconds. During this time period, more than five cars and trucks passing on those two slabs were observed visually. Each vehicle represents one oscillation profile. In the first 15 seconds, it seems two or more impact events overlapping each other, as the damping time of the slab is much longer than the spacing time between cars. The maximum amplitude is at 28th second, corresponding to a loaded truck passing by, and the damping time is for 6 seconds till the next impact event occurs. The weight of the car may be identified by damping time, if the calibration of the car weight and decay time is characterized. Through this field test, the frequency response and the damping time of the pavement slabs have been successfully obtained with the optical fiber diversity sensor.

5. Conclusions

We have demonstrated a polarization based optical fiber sensor for traffic induced impact on highway pavement slabs reinforced by the FRP bars. This sensor system provides the response of the structure over a relatively large area under external disturbances by extracting the frequency information and damping trend as accurately as a commercial accelerometer. Further studies will be focused on utilizing Rayleigh backscattering to indicate the impact location in a fully distributed fashion. Some initial results have been obtained along a 1km fiber in the lab and more experiments to simulate the field environment will be further investigated.

Acknowledgements

Authors acknowledge the support from the Canadian Network of Centers of Excellence ISIS Canada. And we would like to thank M. Eisa, S. El-Gamal and B. Benmokrane from University of Sherbrooke, Canada.

REFERENCES

[1] C.E.Bakis et. al., "Fiber-reinforced polymer composites for construction---state-of-the-art review," J. Compos. for Constr. **6(2),** 73-87 (2002).

[2] A.P.Mouritz, "Comment on the impact damage tolerance of stitched composites," J. Mater. Sci. Lett. **22(7),** 519-521 (2003).

[3] P.Paultre,"Dynamic testing procedures for highway bridges using traffic loads," J. Struct. Eng.**121(2),** 362-376 (1995).

[4] H.Tsuda et.al., "Impact damage detection in CFRP using fiber Gragg gratings", Smart Mater. Struct. **13,** 719-724, (2004).

Reproduced with permission of the copyright owner. Further reproduction prohibited without permission.

The mass loading effect on lightweight cantilever mode frequency measurement by optical fiber sensor

Ziyi Zhang[a], Pingyu Zhu[b], Xiaoyi Bao*[a]

[a]Physics Department, University of Ottawa, 150 Louis Pasteur, Ottawa, ON, K1N6N5, Canada

[b]Provincial Key Lab of Hunan Province Health Maintenance for Mechanical Equipment, Hunan University of Science and Technology, Xiangtan 411201, China

*email: xbao@uottawa.ca

ABSTRACT

Dynamic response of lightweight structures is affected by the mass of a transducer. The additional mass of the transducer is defined as a mass loading for the system, which is comparable to the weight of the structures, such as composites and thin cantilever beam/bar. In this paper, we measure the bending and torsion mode frequencies with and without mass loading to the lightweight structures by using lightweight optical fiber sensor (OFS) and conventional accelerometer. The frequency difference is verified by the finite element method using ANSYS software. The OFS, benefited to its lightweight, has shown the advantage of measuring vibration frequency accurately without affecting the dynamic response of the structure.

Keywords: loading mass; vibration frequency measurement; light weight cantilever structure; optical fiber sensing

Reproduced with permission of the copyright owner. Further reproduction prohibited without permission.

I. Introduction

Vibration measurement is considered as an important mean to evaluate dynamic characteristics of a structure. Contacting transducers such as accelerometers and force gauges have been used as conventional vibration sensors [1-2]. In most light weight structures, the measured vibration frequencies may deviate from their true values due to the mass of the transducer, which is attached to the test structure [3-4]. The prediction and assessment of mass loading effects have been studied previously [3-5] and up to now, this effect on frequency response functions (FRFs) can be only corrected by certain formulas for a rectangular cantilever plate [5]. However, those algorithms require complicated boundary conditions for every specific structure.

With the recent advances in demodulation technology and smart material systems (SMS), fiber based vibration sensors have been developed and successfully applied to structures health monitoring [6]. Kim et al. proposed an optical fiber accelerometer based on an integration of the Moiré fringe phenomenon to measure natural frequency and damping ratio of the single-degree-of-freedom system [7]. A sensor head made by optical fiber cantilever beam has been constructed and applied on the vibration monitoring of a rotating machine [8]. Despite of optical sensor's superiority compared to the conventional vibration sensors, they still added considerable masses on the test structure since the sensor head containing optical grating has been packaged by metal enclosures. The size of those enclosures is even bigger than a conventional transducer, because those sensors are designed for structure health monitoring (SHM) or large-size machine, not for the purpose of vibration measurement of light weight structures.

Reproduced with permission of the copyright owner. Further reproduction prohibited without permission.

Fiber Bragg grating (FBG) has been reported to measure dynamic strain up to several kHz [9]. However, since it is essentially a point sensor as an accelerometer, it is impossible for one FBG to measure various mode frequencies of a lightweight structure. To the best of our knowledge, so far no report on using a lightweight sensor to measure the unaltered bending and torsion vibration frequencies to study the mass loading effect on a lightweight structure. As it has been known that one-axis can only measure the bending mode frequency, not the torsion mode; triaxial accelerometer should be applied to torsion mode detection. However, since triaxial accelerometer is much heavier than one-axis one, it has more tendency to prevent the torsion mode to happen for lightweight structure.

In this paper, a simple optical fiber sensor based on polarization change of single mode fiber (SMF) has been implemented to accurately measure natural vibration frequencies of a lightweight structure for both bending and torsion mode. A bare optical fiber with less than milligram mass serves as a sensor head in order to eliminate the mass loading effect on vibration frequencies of a lightweight cantilever bar. We focus on the different frequencies detecting from the optical fiber sensor with and without the mass loading, caused by a piezoelectric accelerometer attached at various positions on the bar. Both the bending mode and torsion mode frequencies are measured for the first time to check the mass loading effect on a cantilever bar. The simple numerical example using finite element (FE) analysis is also presented as a reference for experimental results.

Reproduced with permission of the copyright owner. Further reproduction prohibited without permission.

II. Theoretical analysis

2.1 Theoretical frequencies for the cantilevered structures

2.1.1. First Bending modes of a cantilever bar

Beam theory considers the mass of the bar only while neglects the effect of shear deformation and rotary inertia, then the fundamental frequency is calculated as shown below [10]

$$\omega = \sqrt{k / m} \tag{1}$$

Where m is the equivalent mass; k, for a horizontal vibrating bar can be calculated by elastic modulus of the bar E_{bar} and the moment of inertia I_{bar} : $k = 3E_{bar}I_{bar} / L_{bar}^3$. While spring theory only considers the mass added at the free end of the bar, the frequency is calculated by $\omega = \sqrt{k / m_{added}}$; m_{added} is the loading mass. Combing both spring theory and beam theory, an experiential formula was developed to compute the frequency taking into account both the mass of the bar and the loading mass [10].

$$\omega = \sqrt{\frac{3E_{bar}I_{bar}}{L_{bar}^3 \cdot \left(m_{added} + \frac{1}{4} \cdot m_{bar}\right)}} \tag{2}$$

When the loading mass is neglected, the formula becomes

$$\omega = \sqrt{\frac{3E_{bar}I_{bar}}{L_{bar}^3 \cdot (0.25 m_{bar})}} \tag{3}$$

2.1.2. Torsional modes of a cantilever bar

Consider a rectangular bar clamped at one end and free at the other end. When the ratio of its width to thickness is greater than six, the frequencies of its torsional modes may be approximated by [11].

Reproduced with permission of the copyright owner. Further reproduction prohibited without permission.

$$f_n = \frac{2n-1}{4L_{bar}} \cdot \frac{2h_{bar}}{W_{bar}} \sqrt{\frac{G}{\rho_{bar}}} \quad (n=1,2,3...) \tag{4}$$

Where, G is the shear modulus of the bar, h_{bar} is the thickness, L_{bar} is the length, W_{bar} is the width, and ρ_{bar} is the density. The shear modulus is related to Young's modulus of the cantilever.

$$G = E_{bar} / 2(1+\mu) \tag{5}$$

Where, E_{bar} is the elastic modulus of the bar, μ is Poisson's ratio. Substituting parameters into equation (4) and equation (5), the torsional frequencies of the cantilever bar can be calculated.

2.2 Finite element model and results

Finite element analysis gives a computational solution for the vibration of a complex structure by separating the structure into finite elements with a defined mesh connection. Before the experiment section, numerical results are presented to provide references for identifying the natural frequencies. Although the structures have infinite degrees of freedom and modes, the limited sensors can only tested certain modes depending on sensor location.

A modal analysis is carried out by the finite element simulator ANSYS, version 10.0 A (Swanson Analysis Systems, Inc.). A rectangular bar with uniform rectangle cross-section clamped at one end and free at the other end is a simple vibrating system that can be solved analytically. The cantilever bar's properties are listed in Table 1. To simulate experimental data, a fine FE model with 80 ×11 nodes is constructed by ANSYS software as shown in Fig.1. It is assumed that out-of-plane (Y-direction) vibrations are simulated

Reproduced with permission of the copyright owner. Further reproduction prohibited without permission.

with shell module of the software. First four mode shapes of the bar from the initial FE model are plotted in Fig.2.

Table 1. Physical properties of the cantilever beam

Material	**Steel**
Length (L_{bar})	0.32m
Width (W_{bar})	0.04m
Thickness (h_{bar})	0.0009m
Density (ρ_{bar})	$7870 kgm^{-3}$
Young's modulus (E_{bar})	$207 \times 10^{9} Nm^{-2}$
Poisson's ratio (μ)	0.33

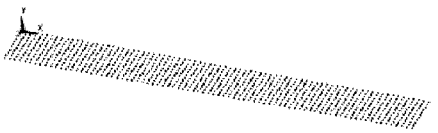

Fig. 1. Fine FE model (880 nodes)

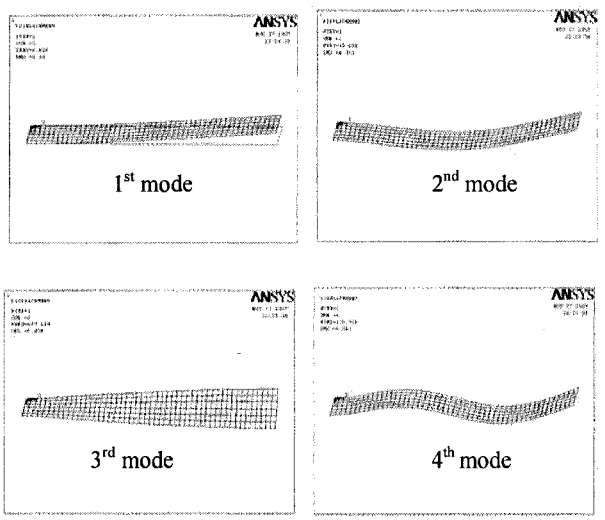

Fig.2 Mode shapes of the cantilever bar from the initial FE model

Reproduced with permission of the copyright owner. Further reproduction prohibited without permission.

The modal values are: 1st is 6.82 Hz, 2nd is 42.69Hz, 3rd is 107.18Hz, 4th is 119.73Hz.

The first bending mode frequency is at 7.18Hz (equation (3)) and 6.82Hz (FE method), respectively. According to equation (2), this frequency will shift to 6.11Hz when an 8.6g accelerometer attached to the free end of the bar.

As the ratio of the cantilever's width to thickness 0.04/0.0009=44.44 is larger than 6, torsion modes arise as shown in Fig 2. The fundamental torsion frequency of this cantilever bar is 107.18Hz (FE method) compared to 111.35Hz using equation (4).

III. Experimental verification

In order to verify the calculated results, both accelerometer and optical fiber sensor are employed during the measurement of the cantilever bar. For a small structure, experimental modal analysis rarely uses multi-sensors, leading to limited test results. Since the available transducers have hardware limited frequency ranges, it is quite difficult for an accelerometer to have a wide dynamic range with high sensitivity. While optical fiber sensor can cover large area structures without adding additional mass and has wider frequency range compared to the accelerometer.

3.1 Experimental setup

The experiment setup and instruments for modal testing as shown in Fig.3 are:

- A hammer with a rubber tip is used to produce the driving signal, thus the response of the cantilever bar would remain in low frequency range (below 200Hz) as we focus on the mass loading effect on the first natural frequency. The frequency range of excitation

Reproduced with permission of the copyright owner. Further reproduction prohibited without permission.

provided by a hammer is determined by the stiffness of the hammer-structure contact surface and the mass of the hammer head.

• An accelerometer B&K 4513-B has frequency response of 1-10 kHz and mounted resonance frequency is 32 kHz. The mass of the sensor head is about 8.6g. The accelerometer is fixed by a thin layer of wax to the surface of the tested bar.

• Optical fiber sensing system Bare optical fiber is attached to the top of the tested bar by transparent tape in order to monitor the dynamic response of the structure. The lead fibers were taped down to the optical table to eliminate noises.

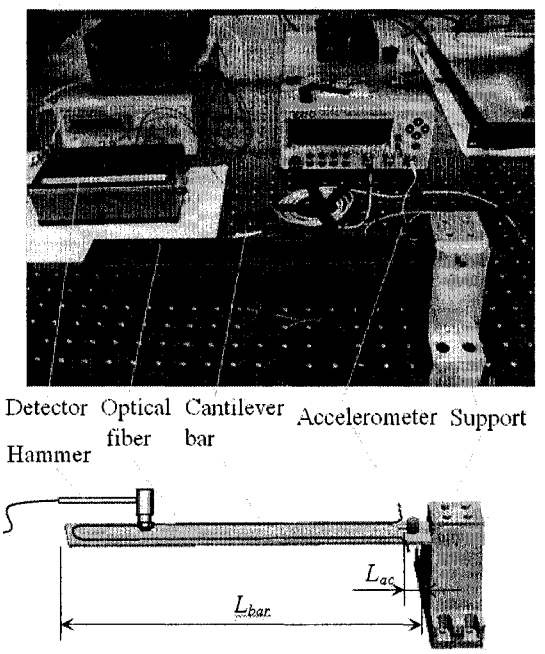

Fig.3 Experimental setup of the cantilever bar
(The accelerometer is close to the clamped end, Lac=10mm)

3.2 Principle of optical fiber sensing system

Our optical fiber vibration sensor is based on birefringence properties of SMF. It is known that in single mode fiber, some random imperfections breaks the circular

Reproduced with permission of the copyright owner. Further reproduction prohibited without permission.

symmetry of the fiber core, causing two orthogonally polarized components of light to travel with different velocities. The birefringence in fiber varies with many physical parameters such as: strain, temperature, pressure wave, ultrasonic fields, etc, leading to changes in the phase shift between two polarization eigenmodes. Thus the output state of polarization (SOP) changes at the fiber end. According to the field test result of buried [12], aerial [13] and submarine [14] fiber, the evolution of SOP due to environmental effects is in the order of several seconds, which is a relatively slow process compared to the frequency of our target impact wave (from a few Hz to several kHz). Hence, those effects can be neglected in this dynamic response measurement. By monitoring the power change of the polarized light in time and frequency domain, one can detect the impact wave as well as the vibration frequency in real time.

As shown in Fig.4, a linearly polarized light from a DFB laser source passing through a polarization controller launches into a few meters long sensing fiber. At the other end of the sensing fiber, a polarization beam splitter (PBS) is positioned to separate the input light into two orthogonally polarized beams, which are detected by two photodetectors with 16 kHz bandwidth low noise amplifiers to minimize the noises and to enhance the sensitivity. The two output beams from PBS will have the same DC offset and encounter relative π phase shift when two beams are balanced, as illustrated in Fig.4 both outputs consist of a small AC component plus a large DC portion. Thus by subtracting the two signals, we are able to enhance the AC signal by 3dB and remove the DC portion as only AC signals include vibration information under external perturbations. The signal is amplified before digitized and displayed on the computer.

Reproduced with permission of the copyright owner. Further reproduction prohibited without permission.

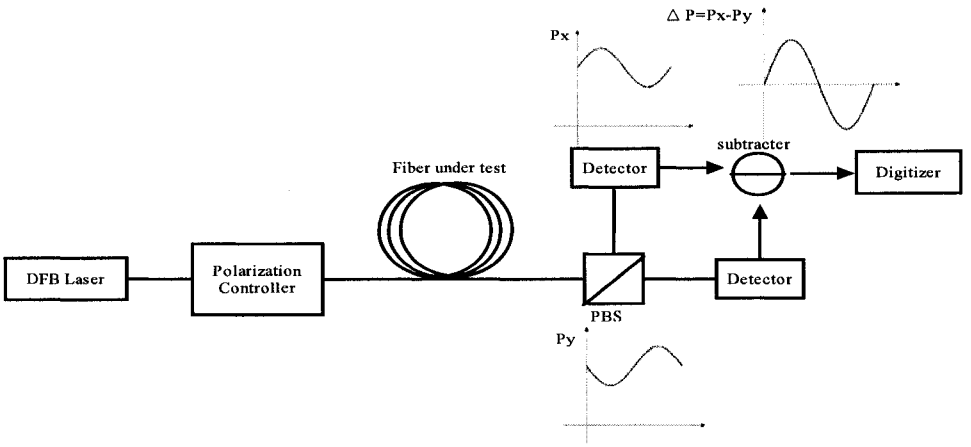

Fig.4 Schematic diagram of the optical fiber sensing system

3.3 Experiments of a cantilever bar

3.3.1. Case 1: the accelerometer is set at the fixed end of the cantilever bar

In order to demonstrate optical fiber sensor's ability of vibration detection, the accelerometer was first installed at 10mm away from the clamped end. According to section 2 theory, an additional mass at the fixed end should have the least effect on the natural frequency of the lightweight structure. The vibration induced by the impact will cause maximum strain at the fixed end while maximum displacement at the free end. The driving point, i.e. the impact point by the hammer is near the middle of the bar.

Fig.5 (a) plots the time trace signals from both optical fiber and accelerometer after the hammer impact. The accelerometer's signal is damped quickly while optical fiber has more oscillations, which is due to the fact that the former acts like a point sensor while the latter's result is superimposed by signals from every position along the bar. The power spectrum is computed after fast Fourier transform (FFT) of the time domain signal. From both the optical fiber and accelerometer, the first and second bending mode frequency appears at 7.0Hz and 43.4Hz respectively, as shown in Fig.5 (b). The

Reproduced with permission of the copyright owner. Further reproduction prohibited without permission.

uncertainty of the testing frequency is 0.2Hz for both fiber sensor and accelerometer, caused by the sampling rate and test duration. The experimental result, 7.0Hz, is in the middle of 7.18Hz (equation (3)) and 6.82Hz (FE). The first mode frequency from optical fiber is more obvious to observe than that from the accelerometer due to high signal to noise ratio (SNR) of the fiber sensor.

From Fig.5(c), optical fiber is capable of measuring the fundamental torsional frequency, appearing at 108.4Hz , which is very close to both the FE simulation result 107.18Hz and the calculated value 111.35Hz in section 2. While this type of accelerometer we used is only for one axis, thus, it is not sensitive to the torsional mode.

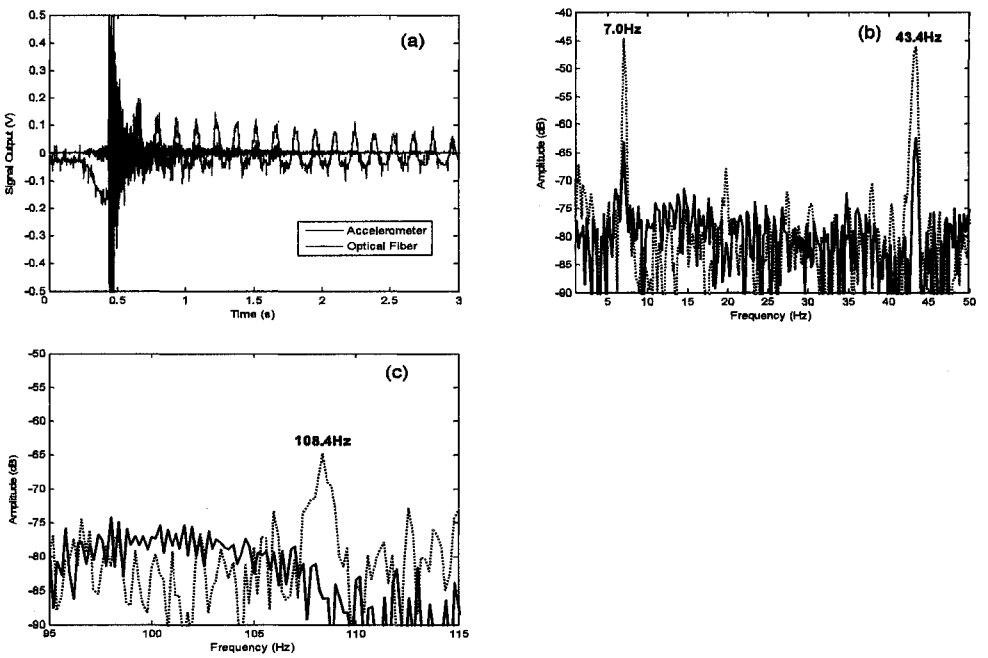

Fig.5 Experiment results in the case of accelerometer close to the fixed end: (a) time domain signals of optical fiber (red) and the accelerometer (blue); (b) power spectrum around the first and second bending mode frequency; (c) power spectrum around the torsional frequency.

3.3.2. Case 2: the accelerometer is set at the free end of the cantilever bar

Reproduced with permission of the copyright owner. Further reproduction prohibited without permission.

We then move the accelerometer to the free end of the cantilever bar. This time the accelerometer becomes more sensitive due to large displacement. The same procedure is conducted and the experimental results are shown in Fig.6.

The results from optical fiber and accelerometer match very well. We notice that the first and the second bending mode frequencies have shifted to 6.0Hz and 39.0Hz, respectively. Therefore, by setting the accelerometer close to the free end of a lightweight cantilever bar, the additional mass loading will affect the natural frequencies of the whole structure. The experimental result of first mode, 6.00Hz, is close to the calculated result by equation (2), 6.11Hz.

We also noticed that the fundamental torsional mode could not be detected by optical fiber in this case as the additional mass on the free end prevents the torsional modes to occur.

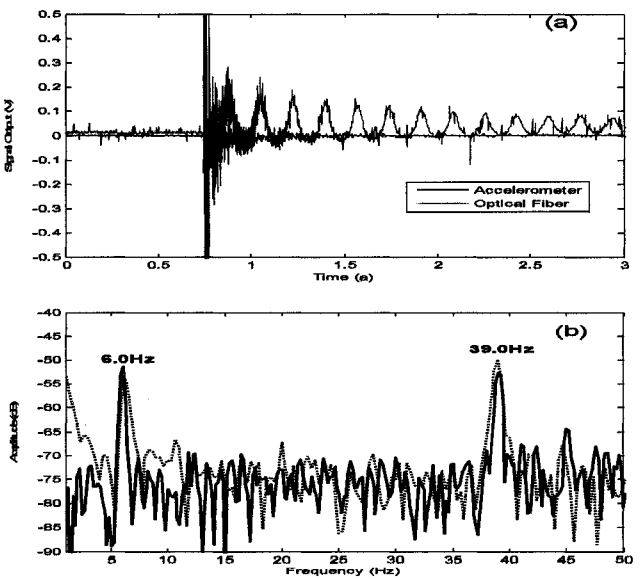

Fig.6 Experiment results in the case of accelerometer at the free end: (a) time domain signals of optical fiber (red) and the accelerometer (blue); (b) power spectrum around the first and second bending mode frequency; the fundamental torsion mode could not be detected in this case.

Reproduced with permission of the copyright owner. Further reproduction prohibited without permission.

3.3.3. Case 3: Only optical fiber sensor is used

To obtain the fundamental frequency of the bar without any loading mass effect, the accelerometer is taken away from the bar. Fig.7 (a) shows the first and second bending mode tested by optical fiber is 7.0Hz and 43.0Hz, respectively. Considering the 0.2Hz uncertainty in the power spectrum peak reading, those results are very close to case one. Therefore the difference in the vibration frequencies depends on the position of the accelerometer.

The fundamental torsion frequency detected by optical fiber appears at 107.6Hz, comparable to 108.4Hz in case one. Thus, based on the results from case one and case three, the loading mass at the fixed end has less effect on the vibration frequency of the structure.

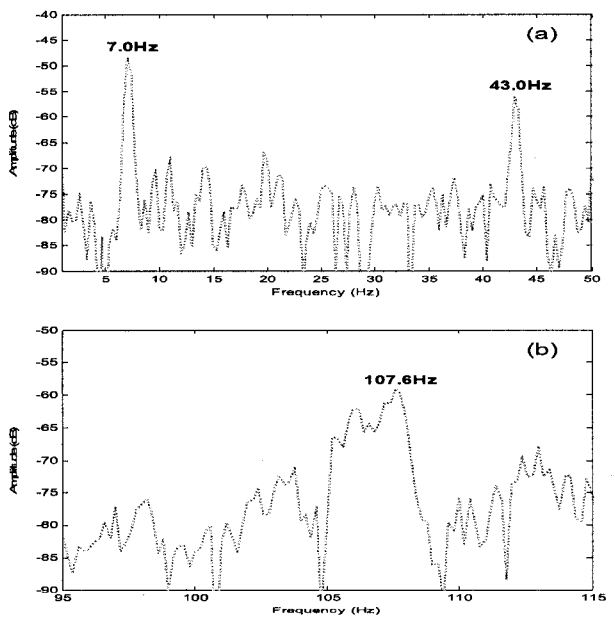

Fig.7 Experiment results in the case of no accelerometer: (a) power spectrum around the first and second bending mode frequency; (b) power spectrum around the torsion frequency

Reproduced with permission of the copyright owner. Further reproduction prohibited without permission.

3.3.4. Case 4: the accelerometer is in the middle of the cantilever bar

In order to qualitatively study the dependence of the vibration frequencies on the position of the accelerometer, the accelerometer has been attached on the bar 12cm away from the free end. As shown in Fig.8 (a), the first and second mode frequency in this case become 6.7Hz and 41.6Hz, which are smaller than case one or case three (accelerometer set at the fixed end or no accelerometer) but larger than case two (accelerometer set at the free end). Hence, the closer the additional mass to the free end of the cantilever bar, the larger difference in bending mode frequencies one would get from the no loading mass condition.

Also, the torsion frequency has shifted down to 103.2Hz from 107.6Hz as in Fig8(b), which illustrates that the location of the loading mass affects not only the bending mode but also torsion mode frequencies.

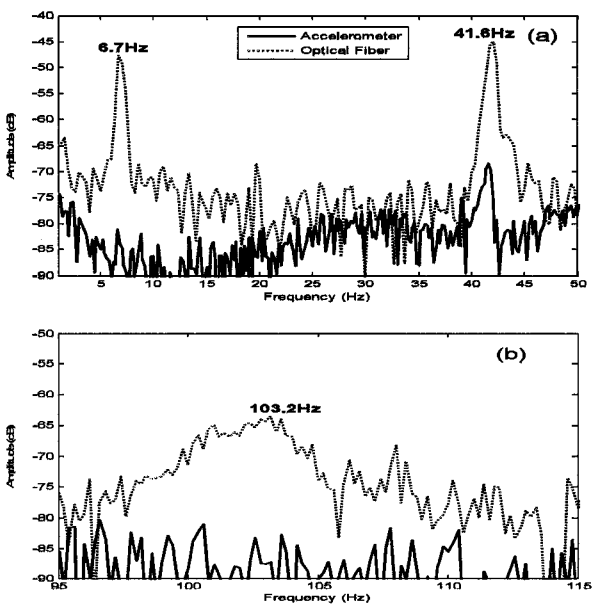

Fig.8 Experiment results in the case of accelerometer in the middle of the bar: (a) power spectrum around the first and second bending mode frequency; (b) power spectrum around the torsion frequency

Reproduced with permission of the copyright owner. Further reproduction prohibited without permission.

Table 2 summaries the results obtained from theoretical calculations, simulations and measurements. The differences between the testing results and calculation or simulation of the two bending modes are within the frequency uncertainty 0.2Hz.

Apparently, depending on the position of one-axis accelerometer it sometimes could not give correct vibration frequencies, and it fails to provide the torsion mode frequency. For example, if the accelerometer is used and placed at the free end of the bar, then the tested first bending frequency is 6Hz which deviates from the true value (~7Hz); and it also prevents the torsion mode to happen. While optical fiber sensor doesn't have such problem due to its lightweight sensor head.

Table 2. Compare the vibration frequencies (in the unit of Hz)

	mass condition	**Formula**	**FE**	**Accelerometer**	**Fiber**
first bending mode	mass at the fixed end			7.0	7.0
	mass at the free end	6.11		6.0	6.0
	No mass	7.18	6.82	N.A	7.0
	mass in the middle			N.A	6.7
second bending mode	mass at the fixed end			43.4	43.4
	mass at the free end			39.0	39.0
	No mass		42.69	N.A	43.0
	mass in the middle			41.6	41.6
first torsion mode	mass at the fixed end			Undetectable	108.4
	mass at the free end				N.A
	No mass	111.35	107.18		107.6
	mass in the middle				103.2

IV. Conclusion

This paper demonstrates that both bending mode and torsion mode frequencies of a cantilever bar change with respect to the position of a loading mass, such as an

Reproduced with permission of the copyright owner. Further reproduction prohibited without permission.

accelerometer. The theoretical and experimental results show that the influence of a loading mass should not be neglected in experimental modal analysis for lightweight cantilever structures. Also, optical fiber benefited to its lightweight has been demonstrated to detect impact/vibration accurately without adding additional mass, thus the dynamic feature of lightweight structures could be measured directly rather than corrected by certain formulas. The proposed sensing system can be easily extended to capture other transient responses of a vibration system, such as abrupt fault diagnosis.

Acknowledgements

The authors would like to acknowledge the financial support from the ISIS Canada and GEOIDE, NSERC Discovery Grant.

REFERENCES

[1] B T Wang and C C Wang, "Feasibility analysis of using piezoceramic transducers for cantilever beam modal test", Smart Mater. Struct. **6,** 106-16 (1997).

[2] C R Fuller, S J Elliott and P A Nelson, "Active control of vibration", San Diego, CA92101, Academic Press, (1996).

[3] O Dossing, "Prediction of transducer mass-loading effects and identification of dynamic mass, *Proceedings of the 9th International Modal Analysis Conference* 579-85, (1991)

[4] J M M Silva, N M M Maia and A M R Ribeiro, "Some applications of coupling/uncoupling techniques in structural dynamics-Part 1: solving the mass cancellation problem", *Proceedings of the 15th International Modal Analysis*

Reproduced with permission of the copyright owner. Further reproduction prohibited without permission.

Conference, 1431-39, (1997).

[5] O Cakar and K Y Sanliturk, "Elimination of transducer mass loading effects from frequency response functions", *Mechanical Systems and Signal Processing* **19** 87–104, (2005).

[6] H N Li, D S Li, and G B Song, "Recent applications of fiber optic sensors to health monitoring in civil engineering", *Eng. Struct.* **26** 1647–57, (2004).

[7] D H Kim and M Q Feng, "Real-Time structural health monitoring using a novel fiber-optic accelerometer system", *IEEE Sensors Journal* **7** 536-43, (2007).

[8] J M López-Higuera, M A Morante and A Cobo, "Simple low-frequency optical fiber accelerometer with large rotating machine monitoring applications", *Journal of Lightwave Technology* **15** 1120-30, (1997).

[9] M.A.Davis, A.D.Kersey, T.A.Berkoff and R.T.Jones, "Dynamic Strain Monitoring of an In-Use Interstate Bridge using Fiber Bragg Grating Sensors", *Smart Mater. Struct.* 3043 87-95, (1997).

[10] Milivoje Kostic, Introduction to Oscilloscope and Vibration Measurement of a Cantilever Beam, Northern Illinois University, http://www.kostic.niu.edu/ScopeDemo.html, (2001).

[11] L E Kinsler, A R Frey, A B Coppens and J V Sanders 1982 Fundamentals of Acoustic New York : Wiley

[12] J. Cameron, L. Chen, X. Bao, and J. Stears, "Time evolution of polarization mode dispersion in optical fibers", IEEE *Photon. Technol. Lett.*, **10**,1265-1267 (1998).

[13] D. Waddy, P. Lu, L. Chen, and X. Bao, "Fast state of polarization changes in aerial fiber under different climatic conditions," *IEEE Photon. Technol. Lett.*, **13**(9), 1035–

Reproduced with permission of the copyright owner. Further reproduction prohibited without permission.

1037 (2001).

[14] Z. Zhang, X. Bao, Q. Yu and L. Chen, "Fast state of polarization and PMD drift in submarine fibers," *IEEE Photon. Technol. Lett.*, **18**(9), 1034–1036 (2006).

Reproduced with permission of the copyright owner. Further reproduction prohibited without permission.

Chapter 10

Conclusion

10.1 Thesis outcomes

Through this thesis, my work has focused on the polarization effects in optical fiber communication systems, i.e. PMD and PDL, as well as in distributed vibration sensing systems.

We have proposed a new PDL vector measurement based on the equation of motion in Stokes space, which has been verified by both numerical simulation and experiment. Compared with the well known Jones Matrix method, it requires less measurement steps to retrieve the PDL vectors as a function of wavelength. Since the measured accuracy is limited by the wavelength resolution, and the minimum step which can be achieved by the tunable laser in our lab is 10pm, the obtained results agree well with the Jones Matrix method within ~0.5nm. Therefore, in order to apply our approach, we have shown that one needs to first determine the initial PDL vectors at some coarse wavelength steps and then compute PDL vectors between those coarse steps by numerical integration. As the testing speed is critical in dynamic PMD and PDL monitoring, our new method has advantages over other available techniques for polarization mitigation applications in high bit-rate communication systems.

For the first time we have performed a fast PMD test for three pairs of 240km submarine fibers under the Caribbean Sea at the Bahamas Islands. The long measurement

Reproduced with permission of the copyright owner. Further reproduction prohibited without permission.

durations (26h for one pair of fiber) with 15s intervals has allowed us to conduct a detailed study of PMD fluctuations as well as study the correlation between polarization and environmental effects. Temporal drift time of both DGD and SOP in submarine fibers is on the order of a few minutes, which is shorter than buried fibers but longer than aerial fibers. Based on the experimental autocorrelation functions we further found that the faster change in DGD and SOP is less than 15s, limited by the testing speed. Moreover, the weather data (such as temperature, wind, tide) during field tests has been recorded and correlated with DGD test data. The DGD reaches two peak values at the moment of maximum water current speed due to the semidiurnal tide, which makes us to believe that submarine fibers are affected by deep-ocean current induced tensions.

From the submarine field test, it is evident that the polarization effects vary with respect to environmental conditions. In other words, polarization change should be able to monitor external disturbances, which inspires us to build a polarization based optical fiber vibration sensor. The development of such a sensor involves two phases. First, we have constructed a vibration sensor using either continuous transmission or backscattered light for measuring small vibration in real-time without any averaging or signal filtering. Continuous and damped vibrations, generated by a piezo fiber stretcher and a cantilever beam respectively, have been successfully demonstrated, and the obtained results are in agreement with a commercial polarization analyzer. It is worth mentioning that although the first phase gives vibration frequency information and damping trends, it could not resolve the disturbance location. Therefore our second phase has addressed this issue by launching pulsed light instead of continuous light. Currently available distributed optical fiber sensors mainly deal with various types of static measurements. Distributed dynamic

Reproduced with permission of the copyright owner. Further reproduction prohibited without permission.

measurements are considered quite difficult to achieve because one needs to average over a large number of waveforms in order to increase signal to noise ratio and cancel out polarization effects induced signal fluctuation. For the first time, we have developed a Polarization-OTDR system to fully realize distributed dynamic measurements along a 1km fiber link with 10m spatial resolution. What's more, with our proposed spectrum analysis we have shown its ability to resolve double events happening simultaneously with the same vibration frequency up to 5kHz. We believe this distributed vibration sensor is greatly in demand for the field application of intrusion sensing and structural health monitoring.

Various lab and field tests were conducted using the transmission setup which was built in our first phase of research. These test results are summarized in the following. 1) A characterized frequency distribution of regular as well as irregular water waves in a flume was accomplished and also confirmed by a wave gauge. 2) A real-time impact monitoring on highway pavement slabs due to high speed vehicles passing was demonstrated. A 2Hz natural frequency of the slabs has been clearly observed. 3) Both bending and torsion mode frequencies of a lightweight structure were studied. Unlike a conventional accelerometer, an optical fiber sensor is able to accurately measure those frequencies without altering the structural dynamic feature.

10.2 Future work

Some possible future directions are presented here.

As seen in submarine fiber tests (Chapter 5 and Chapter 6), the state-of-the-art polarization analyzer took 15s to measure and calculate DGD values at steps between

Reproduced with permission of the copyright owner. Further reproduction prohibited without permission.

1520-1580nm. Before this field test was carried out, according to other publications polarization had been "expected" to vary slowly as comparable to buried fibers. However, as the results have shown, polarization effects in submarine fiber fluctuated in the order of few minutes, much faster than that in buried fiber (hours or days). The fastest change occurred within 15s, which is limited by the test interval. In order to further study this issue it will be interesting to collect SOP at a fixed wavelength with another polarization analyzer at the same duration of DGD measurement. Since the test speed of SOP at a fixed wavelength can easily reach ~ms, i.e. ~kHz, it should be sufficient to track faster polarization effects in submarine fibers.

In the distributed vibration sensor developed in our lab, a digitizer card (DAQ card) and a desktop computer were employed to process the data. As stated in Chapter 8 the signals had been processed in the following way:. "*First, one Polarization-OTDR curve is stored onto the on-board memory of the DAQ card every 0.1ms, corresponding to a 10kHz repetition rate. Once the memory is filled up, all of thousands of curves will be transferred to computer to be further analyzed*". For our demonstration of 1km total sensing length with 10m spatial resolution and 10kHz pulse repetition rate, the on-board memory was filled up in 1.5s. It needs another 4s to transfer the signals to the desktop computer and do data analysis. The problem is during the 4s data transferring time, the DAQ card is idling, and consequently the signals would be lost. We believe that this could be solved by custom designing a micro-processor and FPGA (Field-programmable gate array), so that the signal averaging and processing can be performed directly on board. In this way the sensor system will provide real-time information rather than post-test data process, which is highly desirable for field applications.

Reproduced with permission of the copyright owner. Further reproduction prohibited without permission.

Another possible improvement for our current system is to avoid "dead points", which refers to a few positions along the sensing fiber that are not sensitive to vibration detection with only one input SOP. This problem was mentioned in section 3.3 of Chapter 8. Although it is not severe for 10m spatial resolution as the uncertainty caused by "dead points" is on the order of a few meters, it will become a concern for shorter resolution. One straightforward solution is to use two or more polarizers/detectors at the detection end, but it would decrease the maximum detectable frequency. Here we propose a new approach to solve this problem without sacrificing the testing speed. A double pulse containing slightly different SOPs could be generated and launched to the sensing fiber while all the detection end data processing keep the same as before.

Reproduced with permission of the copyright owner. Further reproduction prohibited without permission.

Bibliography

[Agilent 2002] "Polarization Measurements of Signals and Components," Product Note 8509-1, http://cp.literature.agilent.com/litweb/pdf/5091-2879E.pdf, (2002).

[Agrawal 2002] G. P. Agrawal, *Fiber-Optic Communication Systems*, 3rd ed., John Wiley & Sons, Inc. (2002).

[Alasaarela 2002] I. Alasaarela, P. Karioja, and H. Kopola, "Comparison of distributed fiber optic sensing methods for location and quantity information measurements," *Optical Engineering,* 41, 181-189 (2002).

[Allen 2003] C. Allen, P. Kondamuri, D. Richards, and D. Hague, "Measured temporal and spectral PMD characteristics and their implications for network-level mitigation approaches," *Journal of Lightwave Technology,* 21, 79–86 (2003).

[Bao 2004] X. Bao, Q. Yu, and L. Chen, "Simultaneous strain and temperature measurements with polarization-maintaining fibers and their error analysis by use of a distributed Brillouin loss system," *Optics Letters,* 29,1342-1344 (2004).

[Bao 2008] X. Bao, W. Li, C. Zhang, M. Eisa, S. El-Gamal, B. Benmokrane, "Monitoring the distributed impact wave on concrete slab due to the traffics based on polarization dependence on the stimulated Brillouin scattering," *Smart Materials and Structures,* 17, 015003-015008 (2008).

[Barnoski 1976] J. K. Barnoski and S. M.Jensen, "Fiber waveguides: A novel technique for investigation attenuation characteristics," *Applied Optics,* 15, 2112-2115 (1976).

[Bergh 1981] R. A. Bergh, H. C. Lefevre, and H. J.Shaw, "All-single-mode fiber-optic gyroscope," *Optics Letters,* 6, 198-200 (1981).

[Berkoff 1996] T. A. Berkoff and A. D. Kersey, "Experimental demonstration of a fiber Bragg grating accelerometer," *IEEE Photonics Technology Letters,* 8, 1677 - 1679 (1996).

[Beltrame 2000] D. Beltrame, F. Matera, M. Settembre, A. Galtarossa, A. Pizzinat, F. Favre, D. Le Guen, and M. Henry, "Impact of Polarization Mode Dispersion on the Statistics of Q factor in Optical Transmission Systems," *Electronics Letters,* 36, 1400-1401 (2000).

[Bisby 2004] L. A. Bisby, "ISIS educational module 5: an Introduction to structural

Reproduced with permission of the copyright owner. Further reproduction prohibited without permission.

health monitoring," ISIS Canada, (2004).

[Born 1999] M. Born and E. Wolf, *Principles of Optics,* 7th ed., Cambridge University Press, New York, (1999).

[Cameron 1998] J. Cameron, L. Chen, X. Bao, and J. Stears, "Time evolution of polarization mode dispersion in optical fibers," *IEEE Photonics Technology Letters,* 10, 1265–1267 (1998).

[Chausse 1995] E. Chausse, N. Gisin, and Ch. Zimmer, "POTDR, depolarization and detection of sections with large PMD," presented at *Optical Fiber Measurement Conference (OFMC)'95,* Liege, Belgium, (1995).

[Chen 2004] L. Chen, O. Chen, S. Hadjifaradji, X. Bao, "Polarization-mode dispersion measurement in a system with polarization-dependent loss or gain," *IEEE Photonics Technology Letters,* 16, 206–207 (2004).

[Curti 1990] F. Curti, B. Daino, G. De Marchis, and F. Matero, "Statistical treatment of the evolution of the principal states of polarization in single-mode fibers," *IEEE Journal of Lightwave Technology,* 8, 1162-1166 (1990).

[DeMerchant 2000] M. DeMerchant, "Distributed Strain Sensing for Civil Engineering Applications," Ph.D Thesis, University of New Brunswick (2000).

[Derickson 1998] D. Derickson, *Fiber Optic Tests and Measurements*, Prentice Hall, (1998).

[Digonnet 2004] M. J. F. Digonnet, B. J. Vakoc, C. W. Hodgson and G. S. Kino, "Acoustic fiber sensor arrays", Second European Workshop on Optical Fibre Sensors, *Proceedings of SPIE,* 5502, (2004).

[Doebling 1996] S. W. Doebling, C. R. Farrar, M. B. Prime, and D. W. Shevitz, "Damage identification and health monitoring of structural and mechanical systems from changes in their vibration characteristics: A literature review," Los Alamos National Laboratory, Tech. Rep. LA-13070-MS (1996)

[Ellison 1998] J. G. Ellison and A. S. Siddiqui, "A Fully Polarimetric Optical Time-Domain Reflectometer," *IEEE Photonics Technology Letters,* 10, 246-248 (1998).

[Fomitchov 2000] P. A. Fomitchov, S. Krishnaswamy, J. D. Achenbach, "Extrinsic and intrinsic fiber optic Sagnac ultrasound sensors", *Optical Engineering,* 39, 1972-1984 (2000).

[Galtarossa 2000] A. Galtarossa and L. Palmieri, A. Pizzinat, M. Schiano, and T. Tambosso, "Measurement of local beat length and differential group delay in installed single-mode fibers," *IEEE Journal of Lightwave Technology,* 18, 1389-1394 (2000).

Reproduced with permission of the copyright owner. Further reproduction prohibited without permission.

[Galtarossa 2004] A. Galtarossa and L. Palmieri, "Spatially Resolved PMD Measurements," *IEEE Journal of Lightwave Technology,* 22, 1103-1115 (2004).

[Gangopadhyay 1999] T. K. Gangopadhyay and P. J. Henderson, "Vibration: history and measurement with an extrinsic Fabry-Perot sensor with solid-state laser interferometry," *Applied Optics,* 38, 2471-2477 (1999).

[Gisin 1991a] N. Gisin, "Solutions of the dynamical equation for polarization dispersion," *Optics Communications,* 86, 371-373 (1991).

[Gisin 1991b] N. Gisin, R. Passy, B. Perny, A. Galtarossa, C. Someda, F. Bergamin, M. Schiano, and F. Matera, "Experimental comparison between two different methods for measuring polarization mode dispersion in singlemode fibres," *Electronics Letters,* 27, 2292-2293 (1991).

[Gisin 1992] N. Gisin, and J. P. Pellaux, "Polarization Mode Dispersion: Time versus Frequency Domains," *Optics Communications,* 89, 316-323 (1992).

[Gisin 1994] N. Gisin, "Polarization mode dispersion: definitions, measurements and statistics," *Proceedings of Symposium Optical Fiber Measurements, SOFM'94,* 149-153 (1994).

[Gisin 1997] N. Gisin and B. Huttner, "Combined Effects of Polarization Mode Dispersion and Polarization Dependent Loss in Optical Fibers," *Optics Communications,* 142, 119-125 (1997).

[Gordon 2000] J. P. Gordon and H. Kogelnik, "PMD fundamentals: Polarization mode dispersion in optical fibers," *Proceedings of the National Academy of Sciences,* 97, 4541-4550 (2000).

[Granch 2003] G. A. Cranch, P. J. Nash and C. K. Kirkendall, "Large-scale remotely interrogated arrays of fiber-optics interferometric sensors for underwater acoustic applications", *IEEE Sensors Journal,* 3, 19-30 (2003).

[Grattan 2000a] K. T. V. Grattan and B. T. Meggitt, *Optical Fiber Sensor Technology: Fundamentals,* Kluwer Academic Publishers, (2000).

[Grattan 2000b] K. T. V. Grattan and B. T. Meggitt, *Optical Fiber Sensor Technology: Advanced Applications-Bragg Gratings and Distributed Sensors,* Kluwer Academic Publishers, (2000).

[Hartog 1983] A. H. Hartog, "A distributed temperature sensor based on a liquid-core optical fibre," *Journal of Lightwave Technology,* 1, 498-509 (1983).

[Hathaway 1999] M. W. Hathaway, N. E. Fisher, D. J. Webb, C. N. Pannell, D. A.

Reproduced with permission of the copyright owner. Further reproduction prohibited without permission.

Jackson, L. R. Gavrilov, J. W. Hand, L. Zhang, and I. Bennion, "Combined ultrasound and temperature sensor using a fiber Bragg grating," *Optics Communications*, 171, 225 - 231 (1999).

[Heffner 1992a] B. L. Heffner, "Automated measurement of polarization mode dispersion using Jones matrix eigenanalysis," *IEEE Photonics Technology Letters,* 4, 1066-1069 (1992).

[Heffner 1992b] B. L. Heffner, "Deterministic, analytically complete measurement of polarization dependent transmission through optical devices," *IEEE Photonics Technology Letters,* 4, 451-454 (1992).

[Hentschel 1989] C. Hentschel, *Fiber optic handbook,* Hewlett-Packard (1989).

[Horiguchi 1989] T. Horiguchi and M. Tateda, "BOTDA-nondestructive measurement of single-mode optical fiber attenuation characteristics using Brillouin interaction: Theory," *IEEE Journal of Lightwave Technology,* 7, 1170-1 176 (1989).

[Hunttner 1999] B. Hunttner, B. Gisin, and N. Gisin, "Distributed PMD measurement with a Polarization-OTDR in optical fibers," *IEEE Journal of Lightwave Technology,* 17, 1843-1848 (1999).

[Huttner 2000] B. Huttner, C. Geiser, and N. Gisin, "Polarization-Induced Distortion in Optical Fiber Networks with Polarization-Mode Dispersion and Polarization-Dependent Losses," *IEEE Journal of Selected Topics in Quantum Electronics,* 6, 317-329 (2000).

[Jasenek] J. Jasenek, "The theory and application of fiber optic sensors with spread parameters," http://www.eaeeie.org/theiere_bratislava/index.html

[Jones 1941] R. C. Jones, "A New Calculus for the Treatment of Optical Systems," *Journal of the Optical Society of America,* 31, 488-493 (1941).

[Juarez 2005] J. C. Juarez, E. W. Maier, C. Kyoo Nam, and H. F. Taylor, "Distributed fiber-optic intrusion sensor system," *Journal of Lightwave Technology,* 23, 2081-2087 (2005).

[Kampion 1997] D. Kampion, *Stoked! A History of Surf Culture,* Stoddart, (1997).

[Kapounek 2001] F. Kapounek and M. Maki, "IntelliFIBER - The Next Generation Fiber Optic Fence Sensor," *International Carnahan Conference on Security Technology,* 128-135 (2001)

[Karlsson 2000] M. Karlsson, J. Brentel, and P. Andrekson, "Long-term measurement of PMD and polarization drift in installed fibers," *Journal of Lightwave Technology,* 18, 941–951 (2000).

Reproduced with permission of the copyright owner. Further reproduction prohibited without permission.

[Kee 2000] H. H. Kee, G. P. Lees and T. P. Newson, "Technique for measuring distributed temperature with 35 cm spatial resolution utilizing the Landau–Placzek ratio," *IEEE Photonics Technology Letters,* 12, 873–875 (2000).

[Kogelnik 2002] H. Kogelnik, R. M. Jopson, and L. E. Nelson, "Polarization-Mode Dispersion," Chapter 15 of *Optical fiber telecommunications IV B: Systems and impairments,* edited by I. Kaminow and T. Li, Academic press, (2002)

[Li 2003a] Y. Li, F. Zhang, and T. Yoshino, "Wide temperature-range Brillouin and Rayleigh optical-time-domain reflectometry in a dispersion-shifted fiber," *Applied Optics,* 42, 3772-3775 (2003).

[Li 2003b] Y. Li, F. Zhang, and T. Yoshino, "Wide-Range Temperature Dependence of Brillouin Shift in a Dispersion-Shifted Fiber and Its Annealing Effect," *Journal Lightwave Technologies,* 21, 1663-1667 (2003).

[Liu 1999] K. Liu, S. M. Ferguson and R. M. Measures, "Fiber-optic interferometric sensor for the detection of acoustic emission within composite materials", *Optics Letters,* 15, 1255-1257 (1999).

[Lu 2001] P. Lu, Ph.D. thesis, "Characterization and application of optical fibers: 1. Application of optical fibers in gas concentration and radiation dose measurements; 2. Polarization effects in fiber communication systems," (2001).

[MacDonald 1981] R. I. MacDonald, "Frequency domain optical reflector," *Applied Optics,* 20, 1840–1844 (1981).

[Murphy 1992] K. A. Murphy, M. F. Gunther, A. M. Vengsarkar, and R.O. Claus, "Fabry-Perot fiber-optic sensors in full-scale fatigue testing on an F-15 aircraft," *Applied Optics,* 31 431-433 (1992).

[Nakazawa 1981] M. Nakazawa, T. Horiguchi, M. Tokuda, and N. Uchida, "Measurement and analysis on polarization properties of backward Rayleigh scattering for single-mode optical fibers," *IEEE Journal of Quantum Electronics,* 17, 2326-2334 (1981).

[Nakazawa 1983] M. Nakazawa, "Theory of backward Rayleigh scattering in polarization-maintaining single-mode fibers and its application to polarization optical time domain reflectometry," *IEEE Journal of Quantum Electronics,* 19, 854-861 (1983).

[Nelson 2004] L. E. Nelson and R. M. Jopson, "Introduction to polarization mode dispersion in optical systems," *Journal of Optical and Fiber Communications Reports,* 1, 312-344 (2004).

Reproduced with permission of the copyright owner. Further reproduction prohibited without permission.

[Neumann 1980] E.G.Neumann, "Analysis of the backscattering method for testing optical fiber cables," *AEÜ Journal of Electronics and Communications,* 34, 157-160 (1980).

[Omega Literature] "Introduction to Accelerometers," http://www.omega.com/prodinfo/accelerometers.html

[Patrick 2007] W. L. Patrick, "The History of the Accelerometer 1920's -1996 Prologue and Epilogue," *Sound and Vibration,* 40th anniversary issue, 84-92 (2007).

[Poincaré 1892] H. Poincaré, *Théorie Mathématique de la Lumière*, Guathiers-Villars, Paris, Vol.2 Chap.12. (1892).

[Poole 1986] C. D. Poole and R. E. Wagner, "Phenomenological Approach to Polarization Dispersion in Long Single-Mode Fibers," *Electronics Letters,* 22, 1029-1030 (1986)

[Poole 1997] C. D. Poole and J. A.Nagel, *Optical Fiber Telecommunications,* Vol IIIA I. P. Kaminow and T. L. Koch, Eds., Academic Press, San Diego, CA (1997).

[Rao 1997] Y. J. Rao, P. J. Henderson, D. A. Jackson, L. Zhang, and I. Bennion, "Simulations strain, temperature and vibration measurement using a multiplexed in-fibre Bragg grating/fibre-Fabry - Perot sensor system," *Electronics Letters,* 33, 2063 - 2064 (1997).

[Rogers 1981] A. J. Rogers, "Polarization-optical time domain reflectometry: A technique for the measurement of field distributions," *Applied Optics,* 20, 1060-1074 (1981).

[Rogers 2005] A. J. Rogers, S. V. Shatalin, S. E. Kanellopoulos, "Optical fibre backscatter polarimetry for the distributed measurement of full strain fields," *Proceedings of SPIE,* 6004, 600404, 1-14 (2005).

[Shurcliff 1962] W. A. Shurcliff, *Polarized Light,* Harvard University Press, Cambridge (1962).

[Sischka 1988] F. Sischka, F. Newton, S. A. Nazarathy, *H&P Journal,* 14-21, Dec. (1988).

[Smith 1999] J. Smith, A. Brown, M. DeMerchant, and X. Bao, "Simultaneous distributed strain and temperature measurement," *Applied Optics,* 38, 5372-5377 (1999).

[Soller 2005] B. J. Soller, D. K. Gifford, M. S.Wolfe and M. E. Froggatt, "High resolution optical frequency domain reflectometry for characterization of components and assemblies," *Optics Express* 13, 666-674 (2005).

Reproduced with permission of the copyright owner. Further reproduction prohibited without permission.

[Stallings 2000] J. M. Stallings, J. W. Tedesco, M. El-Mihilmy, and M. McCauley, "Field performance of FRP bridge repairs," *Journal of Bridge Engineering,* 5, 107-113 (2000).

[Takahashi 1993] T. Takahashi, T. Imai, and M. Aiki, "Time evolution of polarization mode dispersion in 120 km installed optical submarine cable," *Electronics Letters,* 29, 1605–1606 (1993).

[Udd 1991] E. Udd, *Fiber Optic Sensors, An Introduction for Engineers and Scientists,* John Wiely & Sons, Inc. (1991).

[Waddy 2001] D. Waddy, P. Lu, L. Chen, and X. Bao, "Fast state of polarization changes in aerial fiber under different climatic conditions," *IEEE Photonics Technology Letters,* 13, 1035–1037 (2001).

[Wikipedia Caribbean] http://en.wikipedia.org/wiki/Caribbean_Sea

[Williams 2004] P. Williams, "PMD measurement techniques and how to avoid the pitfalls," *Journal of Optical and Fiber Communications Reports,* 1, 84-105 (2004).

[Wuttke 2003] J. Wuttke, P. Krummrich, and J. Rosch, "Polarization oscillations in aerial fiber caused by wind and power-line current," *IEEE Photonics Technology Letters,* 15, 882–884 (2003).

[Yang 2002] Y. C. Yang and K. S. Han, " Damage monitoring and impact detection using optical fiber vibration sensors," *Smart Materials and Structures,* 11, 337-345 (2002).

[Yokosuka 2005] H. Yokosuka, S. Tanaka and N. Takahashi, "Time-division multiplexing operation of temperature-compensated fiber Bragg grating underwater acoustic sensor array with feedback control," *Acoustical Science and Technology,* 26, 456-458 (2005).

[Yu 2002] F. T. S. Yu and S. Yin, *Fiber Optic Sensors,* New York: Marcel Dekker (2002).

Reproduced with permission of the copyright owner. Further reproduction prohibited without permission.

Curriculum Vita

Full name Ziyi Zhang

Education

Ph.D 2003 – 2009
Department of Physics, University of Ottawa, Canada
Supervisors: Dr. Xiaoyi Bao and Dr. Liang Chen

B.Eng. 1999 – 2003
Department of Optoelectronic Engineering
Huazhong University of Sci. & Tech., China

List of publications

Journal Papers

Ziyi Zhang, Xiaoyi Bao, Colin D. Rennie, Ioan Nistor, Andrew Cornett, "Water Wave Frequency Detection by Optical Fiber Sensor," *Optics Communications,* 281, 6011-6015 (2008)

Ziyi Zhang and Xiaoyi Bao, "Distributed optical fiber vibration sensor based on spectrum analysis of Polarization-OTDR system," *Optics Express* 16, 10240-10247 (2008)

Ziyi Zhang and Xiaoyi Bao, "Continuous and Damped Vibration Detection Based on Fiber Diversity Detection Sensor by Rayleigh Backscattering," *Journal of Lightwave Technology, IEEE,* 26, 852-838 (2008)

Ziyi Zhang, Xiaoyi Bao, Qinrong Yu and Liang Chen, "Time evolution of PMD due to tides and sun radiation on submarine fibers," *Optical Fiber Technology,* 13, 62-66 (2007)

Ziyi Zhang, Xiaoyi Bao, Qinrong Yu and Liang Chen, "Fast state of polarization and PMD drift in submarine fibers," *Photonics Technology Letters, IEEE,* 18, 1034 –1036 (2006)

Liang Chen, **Ziyi Zhang** and Xiaoyi Bao, "Polarization dependent loss vector measurement in a system with polarization mode dispersion," *Optical Fiber Technology,* 12, 251-254 (2006)

Reproduced with permission of the copyright owner. Further reproduction prohibited without permission.

Conference Presentations

Ziyi Zhang, Pingyu Zhu, Xiaoyi Bao, "The mass loading effect on lightweight cantilever mode frequency measurement by optical fiber sensor", Photonic North, oral presentation, Montreal, Canada, June 2008

Ziyi Zhang, Ryan Bolen, Xiaoyi Bao, "Detection of the pipe thickness and wave frequency by optical fiber sensor", GEOIDE, oral presentation, Niagara Falls, Canada, May 2008

Ziyi Zhang, Samuel LeBlanc, Xiaoyi Bao, "Concrete pavement vibration monitoring due to the car passing using optical fiber sensor", Optical Fiber Sensor, poster presentation, Perth, Australia, April 2008

Jeff Snoddy, Yun Li, **Ziyi Zhang**, Wenhai Li, Xiaoyi Bao, "Polarization based fiber optic vibration sensor for structural health monitoring of civil structures", ISIS, poster presentation, Newfoundland, Canada, May 2007

Saeed Hadjifaradji, **Ziyi Zhang**, Liang Chen, and Xiaoyi Bao, "The effect of amplifier noise on eye diagram for communication systems having PMD, PDL and CD", AAPN (Agile All-Photonic Networks), poster presentation, Ottawa, Canada, June 2006

Liang Chen, **Ziyi Zhang**, Xiaoyi Bao, "Polarization dependent loss vector measurement in a system with polarization mode dispersion", Photonics North, oral presentation, Toronto, Canada, Sept. 2005

Ziyi Zhang, Evgueni Ponomarev, Liang Chen, Xiaoyi Bao "Polarization mode dispersion and chromatic dispersion field test for submarine fibers", AAPN (Agile All-Photonic Networks), poster presentation, Ottawa, Canada, June 2005

Ziyi Zhang, Xiaoyi Bao, Liang Chen, "A broadband real time PMD measurement set", AAPN (Agile All-Photonic Networks), oral presentation, Kingston, Canada, May 2004

Reproduced with permission of the copyright owner. Further reproduction prohibited without permission.